DISSERTATION

A RESILIENCE-BASED DECISION FRAMEWORK TO DETERMINE PERFORMANCE TARGETS FOR THE BUILT ENVIRONMENT

Submitted by

Hassan Masoomi

Department of Civil and Environmental Engineering

In partial fulfillment of the requirements

For the Degree of Doctor of Philosophy

Colorado State University

Fort Collins, Colorado

Spring 2018

Doctoral Committee:

Advisor: John W. van de Lindt

Bruce R. Ellingwood
Hussam N. Mahmoud
Bolivar Senior

ABSTRACT

A RESILIENCE-BASED DECISION FRAMEWORK TO DETERMINE PERFORMANCE TARGETS FOR THE BUILT ENVIRONMENT

Current design codes and standards focus on the design of individual facilities. A typical building is designed with the objective of the life safety of occupants. Even performance-based design approaches assess the required physical performance of an individual structure in order to satisfy prescribed criteria for that structure individually. Thus, even these performance objectives are likely not sufficient for a broad view of community-resilience goals. A modern community is made up of highly coupled networks, and disruptions within one or more networks may lead to disruptions to other networks. If a large number of buildings within a community become non-functional for a long time following an event, either because of physical damage or loss of utilities such as electric power and/or water, the consequences may affect other parts of the community such that, eventually, significant socioeconomic losses occur. Therefore, the current approach for designing individual physical components within a community can be reimagined such that it not only takes into account the performance of a component individually after a catastrophic event but also considers the consequences its design has on a community. The main purpose of this dissertation is to develop a methodology that links the performance of components within the built environment to community-level resilience goals by considering the dependencies and cross-dependencies between components and networks. Therefore, ultimately, this methodology enables disaggregation of the community-level objectives into a set of performance targets for the components of the built environment, which leads itself to the needs of policymakers and community leaders in order to make long-term planning decisions for a community.

DEDICATION

To my beloved parents

ACKNOWLEDGEMENTS

I would like to express my sincere gratitude and appreciation to my advisor, Professor John van de Lindt, for his guidance, support, insights, and constant encouragement throughout my Ph.D. studies. He gave me this valuable opportunity to explore interesting topics and develop my research with the freedom and enthusiasm along with his thoughtful guidance and support. I would also like to thank and recognize the other members of my doctoral committee, Dr. Bruce Ellingwood, Dr. Hussam Mahmoud, and Dr. Bolivar Senior, for providing me with additional guidance, valuable ideas, and critique. Additionally, I would like to thank Dr. Lori Peek for her help, contribution, and feedback on my work.

This work was funded by the National Science Foundation (NSF) under Grant No. CMMI-1452725. This support is greatly appreciated. Moreover, I was honored to be a recipient of the 2015-2016 and 2017-2018 Jack E. Cermak Wind Engineering Graduate Fellowship and would like to take this opportunity to thank the selection committee for choosing me for this prestigious award as well as to thank Ms. Gloria E. Garza for her generosity and kind spirit in providing this fellowship. I would also like to acknowledge the Department of Civil and Environmental Engineering at Colorado State University for providing the teaching opportunity for me in summer 2017.

I am very thankful to my fellow graduate students at Colorado State University for their support, encouragement, and friendship. I would like to extend many thanks to my parents and family for their unconditional love, sacrifice, guidance, support, and encouragement; without them, I wouldn't be able to accomplish this great milestone in my life.

TABLE OF CONTENTS

LIST OF TABLES

LIST OF FIGURES

CHAPTER 1: INTRODUCTION

COMMUNITY RESILIENCE

Modern communities depend on critical infrastructure systems such as electric power networks, telecommunication systems, water and wastewater systems, and transportation systems; which have historically been vulnerable to disruptive events including natural disasters (e.g., Hurricane Maria in 2017; Joplin Missouri tornado in 2011; and Japan Earthquake and Tsunami of 2011), malicious attacks (e.g., the 2001 World Trade Center Attack), and accidents (e.g., the 2003 North America Blackout). Thus, studying the resilience of critical infrastructure systems has been in the engineering research spotlight over the past decade. A resilient community has been defined as one that has planned for potential hazards in order to be able to resist, absorb, and adjust to changing conditions as well as to return to a level of normalcy within a reasonable time following a disaster (Alexander, 2013; Bruneau et al., 2003; Platt et al., 2016; PPD-21, 2013).

The word resilience stems from the Latin word "resiliere" which means "to jump back". Resilience has been used, defined, and evolved in various disciplines. Bhamra et al. (2011) as well as Martin-Breen and Anderies (2011) reviewed the concept, literature, and evolution of resilience as an increasingly popular term used in many disciplines including ecology, psychology, sociology, engineering, and economics. Hosseini et al. (2016) reviewed the definition of resilience and the metrics used to quantify it throughout the articles published over the last two decades in various disciplines. They categorized the definitions of resilience into four domains: organizational (e.g., Vogus and Sutcliffe, 2007; Patterson et al., 2007), social (e.g., Adger, 2000; Keck and Sakdapolrak, 2013; Pfefferbaum et al., 2008), economic (e.g., Rose, 2007; Rose and Liao, 2005; Martin, 2011), and engineering (e.g., Bruneau et al., 2003; Hollnagel et al., 2007; Youn et al.,

2011). They also reviewed and classified the resilience assessment approaches into qualitative (e.g., Cutter et al., 2008; Kahan et al., 2009; Vlacheas et al., 2013) and quantitative (e.g., Ayyub, 2014; Bruneau et al., 2003; Chang and Shinozuka, 2004; Henry and Ramirez-Marquez, 2012) approaches each of which was categorized into several sub-categories. Koliou et al. (2018) reviewed the previous community resilience studies with a focus on the effects of natural hazards on the built environment as well as social and economic systems within a community. They also discussed the critical gaps that are needed to be filled to enhance the available community-level resilience assessment methodologies. An example of these critical paucities in the literature is considering the dependencies and cross-dependencies across community components and networks to study a community-level resilience methodology that links the physical, social, and economic systems within the community. More recently, Mahmoud and Chulahwat (2017) studied the interaction of physical, social, and economic systems within a community through a dynamic framework.

Bruneau et al. (2003) defined a conceptual framework of community resilience and proposed a quantitative measure for infrastructure resilience which is well-known as the resilience triangle model. They introduced four properties of resilience in their definition which are well-known as the four R's: (i) Robustness which is the strength or ability of a system to resist any disruptive event or accident to prevent losing functionality, (ii) Redundancy which is the extent of substitutable components or systems that are capable of satisfying functionality requirements in the presence of disruption, (iii) Resourcefulness which is the ability to recognize and manage problems in a case of emergency or disaster by defining priorities and allocating material (i.e., monetary, information, technological, physical) and human resources to achieve predefined goals,

and (iv) Rapidity which is the speed or rate of system restoration to meet an acceptable level of functionality after a disaster.

Chang and Shinozuka (2004) proposed a probabilistic approach to measure community resilience by comparing initial performance loss in a system and the recovery length to a predefined standard for each (i.e., system performance and recovery length). In their study, predefined standards were defined for four dimensions of community resilience, which were previously proposed by Bruneau et al. (2003): technical, organizational, social, and economic dimensions. Chang and Shinozuka (2004) illustrated their proposed measurement framework by assessing seismic resilience of the water delivery system in Memphis, Tennessee, for two retrofit strategies.

Miles and Chang (2003, 2004, and 2006) established a conceptual model for recovery after disasters in order to study community resilience. The model was conceptualized on the basis of imperative relationships among a community's households, businesses, critical infrastructure, and neighborhoods. Five primary interrelated factors that affect recovery (and, therefore, community resilience) were proposed to build the model: (1) time, (2) space, (3) agents attributes, (4) interactions, and (5) policy. Temporal (i.e., dynamic) effects represent the changes in the condition of a system over time. Spatial effects represent the importance of the topology of community components. For example, households and businesses are affected by the availability of water and electric power, transportation conditions, or local employment opportunities which have different states/performance in different locations within the community. An example for the agent-attribute effects is the type of demand for the businesses. Businesses with local demands are affected by the local transportation conditions and the recovery of households in the neighborhood while these local variables do not significantly affect the businesses that export their products. Interaction effects represent the dependencies, cross-dependencies, and interdependencies across community

components and networks. For example, electric power is needed for the pumping stations in the water supply systems. Any disruption in transportation system may impede the access of inspection and repair crews for repairing the damaged components in, for example, the electric power network. Households affect the business sector in that they provide employees and are the consumer of their products and, on the other hand, businesses affect households since they satisfy the households' demand. Finally, policy (i.e., decision) effects stem from the organizational decisions such as mitigation strategies and emergency planning before the event or restoration prioritization and resource (e.g., material, labor, and budget) allocation after the event.

Cavalieri et al. (2012) developed a model to estimate the number of displaced people after a seismic event as a metric that is advantageous to emergency managers for planning an emergency response after an earthquake. The model considers the interactions of residential buildings, the electric power network, and the water supply network to investigate the inhabitability (i.e., functionality) of a building after a seismic event. However, it does not consider the effects of the restoration processes in the estimation of the metric. Therefore, while useful to some degree, this metric is not necessarily representative of community resilience (i.e., although it is a community-level metric, it is not a community-resilience metric) because the model involves robustness (as one of the resilience properties) in the metric formulation, but it neglects the other three properties of resilience, i.e., rapidity, resourcefulness, and redundancy.

Lin et al. (2016) presented a disaggregation framework through an optimization problem, which seeks design performance objectives for individual buildings that satisfy a predefined community-level goal based on the percentage of the buildings in a community that become unsafe to occupy after a particular hazard. The framework is a step forward from the current performance-based design (PBD) toward a community-level (or building-portfolio-level) performance-based design.

The PBD approach assesses and, then, adjusts the physical performance of an individual structure through an iterative process to meet a prescribed criteria. However, the functionality of an individual structure is not governed only by its own physical performance, but also by the performance/functionality of other entities within the community. For example, a hospital in a community is non-functional without electric power and/or water even if the structure itself is physically intact. Reinhorn and Cimellaro (2014) and Cimellaro et al. (2015) proposed the concepts and a general formulation for resilience-based design (RBD) as an extension of performance-based design (PBD). RBD considers the interaction of all structures (i.e., components) and networks within a community to assess a community-level resilience metric which is required to be satisfied by the performance of individual structures/components within the community.

Regarding the efforts to change direction of the current modern design approaches that consider the structures (i.e., components) individually within the built environment of a community, Mieler et al. (2015) introduced a conceptual framework that disaggregates community-level resilience goals to specific performance targets for the networks and components within the community. They illustrated the methodology by disaggregating the community-level resilience goal of less than 1% probability of significant outmigration after an earthquake with a 500-year return period to a performance target for new residential building construction. The results required new residential buildings to have less than a 5% probability of being unsafe to occupy following the event in order to satisfy the specified community-resilience objective. As was noted in their paper, the example was only a simplified and generalized illustration of the concepts of the framework without any detail.

Community resilience works on the premise that some level of failure is inevitable but can be mitigated as well as planned for in order to minimize the socioeconomic consequences after a disaster by satisfying community-level resilience objectives. In this regard, a resilience assessment methodology needs a model that involves not only the components and networks within a community but also their interactions, their spatiotemporal properties, and policies in order to enable considering all four properties of resilience (i.e., robustness, redundancy, resourcefulness, and rapidity) in the proposed methodology.

TORNADO HAZARD

Policymakers, community leaders, engineers, and researchers have expressed growing concern for extreme natural hazard events and the resulting loss of life, property, and economic vitality. One such hazard is supercell-spawned tornadoes that can be in excess of 1 km (0.62 miles) wide and often have long tracks that can pass through an entire community. Recent examples of such events include the Tuscaloosa, Alabama (2011), Joplin, Missouri (2011), and Moore, Oklahoma (2013) tornadoes.

The occurrence rate of tornadoes is higher in the U.S. than in any other country. More than 1200 tornadoes touch down every year in the United States, which is approximately four times the amount reported in Europe (Heidorn, 2007; Bluestein, 2006). Many states throughout the United States, especially those located east of the Rocky Mountains, are prone to tornadoes (Boruff et al., 2003), but the probability of a tornado striking any particular community in any given year is quite low. This low probability of occurrence of tornadoes have prevented their consideration in modern building codes, but this is changing as a result of deadly and damaging tornadoes in recent years. For example, in the wake of the devastating tornadoes in Moore, Oklahoma (e.g., an F5 tornado in

1999, an F4 tornado in 2003, and an EF5 tornado in 2013), the city voted to modify their building code such that the residential buildings in their community could resist the wind speeds associated with an EF2 tornado (i.e. 60 m/s or 135 mph) (Ramseyer et al., 2015). Considering EF2 intensity for the design process was likely considered reasonable because (i) it can be accomplished with standard construction methods (Amini and van de Lindt, 2013) and (ii) historically more than 97% of all recorded tornadoes are rated as EF2 or lower (FEMA, 2009a). Moreover, even in higher-intensity tornadoes, the majority of the affected area is associated with EF2 level intensity or below (Standohar-Alfano and van de Lindt, 2014).

When considering natural hazards in the United States over the last 25 years, tornadoes have caused the third highest number of fatalities, only surpassed by floods and lightning; and the third highest in total dollar losses, just after floods and hurricanes (Boruff et al., 2003; NOAA, 2017a). A number of studies have reported a significant decrease in the number of fatalities and injuries associated with tornadoes during the past decades as a consequence of improvements in detection and warning technology, an increase in community awareness, and enhancements in the delivery of information (Brooks and Doswell, 2002; Boruff et al., 2003; Simmons and Sutter, 2008). In contrast to injuries and fatalities, property damage has increased as a function of several factors, including but not limited to growing populations, rising property prices, and demographic shifts (Brooks and Doswell, 2001 and 2002). For example, the Joplin, Missouri, tornado (May 22, 2011), the Tuscaloosa, Alabama, tornado (April 27, 2011), and the Moore, Oklahoma, tornado (May 20, 2013) are the top three costliest U.S. tornadoes since 1950 (NOAA, 2017b). Moreover, the tornado in Joplin on May 22, 2011, is among the top ten deadliest U.S. tornadoes ever and the deadliest since 1950 (NOAA, 2017c), which underscores the destructive and deadly impact of tornadoes, particularly when they hit urban areas. That being said, although the probability that a tornado

strikes a particular area of a community is quite low, the consequences can be severe and result in indirect economic losses and population outmigration, two key metrics in assessing the resilience of a community following a disaster; which if significant and long-lasting, can further exacerbate indirect losses over time.

OVERVIEW OF DISSERTATION

In this dissertation, a methodology will be presented for community-resilience-based design (CRBD). Indeed, performing community-level analyses is a fundamental part of CRBD, which was investigated thoroughly in several steps throughout this dissertation. In this regard, a community including households, businesses, schools, and several critical infrastructure systems was modeled with enough detail such that it enables considering the five primary interrelated parameters that affect community restoration, proposed by Miles and Chang (2003, 2004, and 2006), in the resilience assessment. As mentioned before, these parameters are time, space, agents attribute, interactions, and policy effects. Therefore, all four properties of resilience (i.e., robustness, redundancy, resourcefulness, and rapidity) are effective in the resilience assessment methodology in this dissertation. Moreover, modeling a community with enough detail facilitates studying the disaggregation of a community-level resilience goal to a performance target for the components of the built environment through an inverse problem or an optimization problem. Moreover, tornado hazard was investigated in this dissertation in that there exist no community-level studies to date for this hazard in the literature yet it has been among the deadliest and costliest natural hazards in the United States. A brief overview of the remaining chapters of this dissertation is summarized below.

Chapter 2 describes the different layers (i.e., sectors and networks) of the illustrative community modeled and utilized in this dissertation. It discusses the topology and structure of each layer as well as the cross-dependencies considered across the layers of the community. Although only the residential sector, business sector, electric power network, water supply network, and school network were modeled in this dissertation; other critical infrastructure systems such as transportation, telecommunication, natural gas and oil, banking and finance, and emergency services can be modeled and integrated into the current model in future studies.

Chapter 3 discusses the community components properties which, in this dissertation, are the performance of the components under the tornado hazard and the repair time associated with the component's level of damage following a hazard event. A tornado fragility methodology was described in this chapter to develop a model for the performance of community components when subjected to a simulated tornado. As a result, a set of tornado fragility curves were generated corresponding to four prescribed damage states for the community components.

Chapter 4 presents a methodology to simulate a tornado path in order to perform community-level analyses. In this regard, the statistical parameters for the tornado path length and width were studied for each EF-scale tornado based on the historical data. Moreover, simulating spatial damage over the community when subjected to a tornado hazard was discussed to be employed further in the restoration analysis (i.e., Chapter 5).

Chapter 5 offers a community restoration methodology that enables spatial and temporal depiction of the restoration process such that one can assess restoration curve/time for each region of the community besides estimating only one curve/time for the entire community or network. Moreover, the methodology allows consideration of the effect of cascading failures in the restoration analysis such that a component remains non-functional until all its suppliers are

recovered and functional even if the component itself has been repaired physically or has no damage. This is because the dependencies and cross-dependencies across components and networks were modeled in the community modeling. It is also worth mentioning that the proposed restoration methodology considers the effects of policy and decisions such that it allows considering different types of prioritization rules and different policies for resource allocation (e.g., the number of available recovery resource units for each network/sector and mutual aid agreements among utility companies).

Chapter 6 presents a socioeconomic resilience metric, population outmigration, and a methodology to quantify this metric. The methodology considers the spatiotemporal effects of school closure, job loss, non-functional residential buildings, as well as loss of electric power and water for the end users in order to quantify population outmigration. This allows the methodology to be flexible enough to assess population outmigration spatially and temporally at any level from the household level to the community level. Furthermore, the effects of different parameters in the quantification of population outmigration were discussed through sensitivity analysis.

Chapter 7 offers several models to predict the number of casualties (i.e., fatalities and injuries) resulting from a tornado event. Over the last 10 years, tornadoes have caused the highest number of fatalities among natural hazards in the United States. Therefore, in order to study the resilience of a community, a community-level life-safety constraint should be satisfied along with other community-resilience metrics. In this regard, the United States census database at the block level and the United States tornado database were employed in a methodology presented in this chapter to provide a dataset for a multi-variate regression model which predicts the expected number of injuries and fatalities caused by a tornado.

Chapter 8 presents a methodology for community-resilience-based design of the components of the built environment within a community by defining community-level objectives based on, for example, the socioeconomic-resilience metric and the life-safety metric developed in Chapter 6 and Chapter 7, respectively. This methodology aims to disaggregate several community-level goals into the required performance targets for the components of the built environment.

Finally, the overall summary of the conclusions, the anticipated contribution to the profession, and the recommendations for future research studies are provided in Chapter 9 of this dissertation.

CHAPTER 2: TESTBED COMMUNITY MODELING

INTRODUCTION

Modern communities rely significantly on critical infrastructure systems (CISs) in order to provide services that support their economy and provide for the well-being of their residents. Several modeling and simulation approaches have been developed and utilized over the last decades to capture the behavior of CISs and to analyze their dependencies, cross-dependencies, and vulnerabilities. Ouyang (2014) reviewed these modeling approaches and categorized them into several types: empirical approaches, agent based approaches, system dynamics based approaches, economic theory based approaches, network based approaches, the hierarchical holographic modeling approach, the high level architecture based approach, the petri-net based approach, the dynamic control system theory based approach, and the Bayesian network based approach.

The network based approaches (e.g., Dueñas-Osorio et al., 2007; Guidotti et al., 2016; Masoomi and van de Lindt, 2018a; Masoomi et al., 2017b; Ouyang et al., 2012; Unnikrishnan and van de Lindt, 2016) are employed to describe CISs by modeling CIS components as nodes and the physical and relational connections among them as links. These approaches model single CISs by networks and apply the interdependencies by inter-links. For information regarding the other approaches as well as the comparison of different approaches refer to Ouyang (2014) and other review references (e.g., Eusgeld et al., 2008; Griot, 2010; Pederson et al., 2006; Satumtira and Dueñas-Osorio, 2010).

A community as a complex system includes highly coupled networks. Any malfunction in a network or one or more of its components could result in a cascading failure, which, in turn, can cause a loss of functionality in all or part of the system. Therefore, in order to perform risk and

resilience assessment at the community level, the topology of relevant community components needs to be modeled with a representative level of dependencies and cross-dependencies across components and networks to capture these cascading failures. In this dissertation, the network based approach was employed to model an illustrative community after Norman, Oklahoma. The residential sector, the business sector, the school network, the water supply network, and the electric power network were considered in the model. Since the modeled community does not take into account all details of a community, it is not strictly representative of Norman, OK, and therefore, has been termed pseudo-Norman in this dissertation. Other CISs such as transportation, telecommunication, natural gas and oil, banking and finance, and emergency services can be modeled and attached to the model used in this dissertation for future studies. The pseudo-Norman model, employed in this dissertation, is described below.

RESIDENTIAL SECTOR

The western part of Norman, OK, with an area of 14.5 km by 12.9 km (9 miles by 8 miles) was studied herein as pseudo-Norman and includes more than 90% of Norman's population. Pseudo-Norman and the corresponding area of Norman, OK, are shown in Figure 2-1. This area was divided into 0.16 square kilometer (one-sixteenth square mile) grids in order to define the properties of residential and business sectors in pseudo-Norman with enough detail to still perform the analyses effectively. The number of houses in each grid was counted using Google Maps (or it can be estimated by using GIS shapefiles of the US Census database), and the results are shown in Figure 2-2 (a) as a heat map. Pseudo-Norman was estimated to have 41,254 houses which are comparable to 41,813 houses based on the census data in 2013 (City-Data, 2016). Then, the number of occupied and unoccupied houses, population, median house value, median household income, median family income, the percentage of unemployment, as well as the number of students

in each school level were derived from census data (City-Data, 2016) for each grid within the entire city. Thus, 37,785 occupied houses, 3,469 unoccupied houses, 4,829 elementary school students, 3,671 middle school students, 3,460 high school students, and a total population of 110,844 make up the community of pseudo-Norman. As will be discussed later, each residential grid (RG) is supplied by specific business grids, school buildings, water tower(s), and an electric power distribution substation. Therefore, the residential sector (RS) is cross-dependent on the business sector (BS), the school network, the water supply network, and the electric power network in this dissertation.

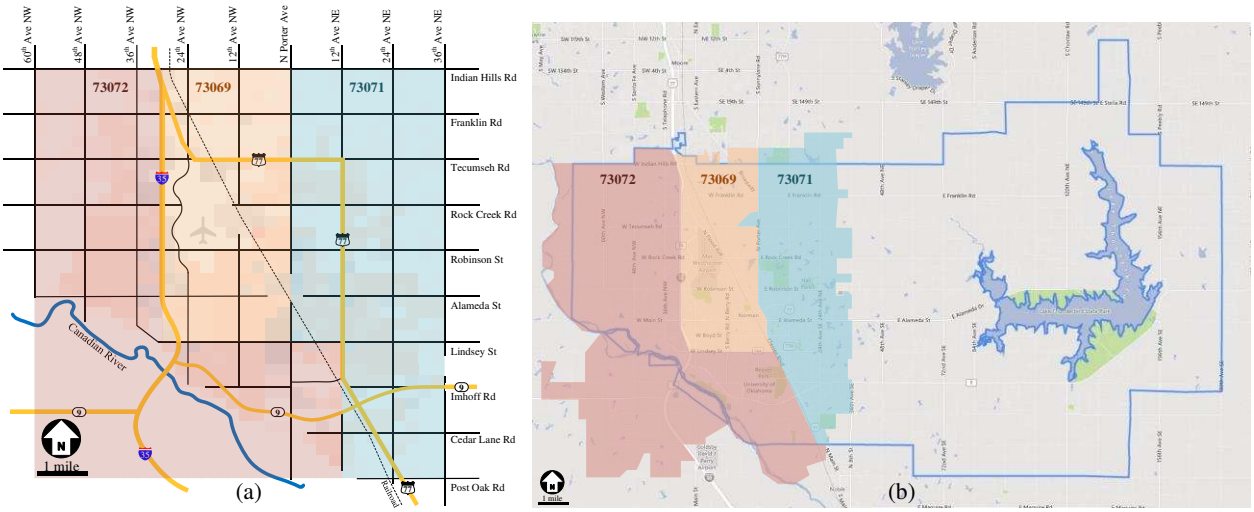

Figure 2-1. (a) Pseudo-Norman and (b) the corresponding area in Norman, OK, modeled in this dissertation. The numbers on the maps are the corresponding ZIP codes for this area

BUSINESS SECTOR

The number of workplace buildings (i.e., the buildings where people work) in each grid was also approximately counted using Google Maps. For each workplace building, a number of employees was assumed based on the size and type of business and, finally, the number of employees for each business grid (BG) was estimated which is depicted in Figure 2-2 (b). In total, 53,890 people work in pseudo-Norman, among which, 49,848 employees live in the city and the rest (i.e., 4,042

employees) live outside of pseudo-Norman. Each business grid is supplied by specific residential grids, water tower(s), and an electric power distribution substation. Therefore, the business sector (BS) is cross-dependent on the residential sector, the water supply network, and the electric power network. It is worth mentioning that some of the important workplaces in pseudo-Norman (such as hospitals, fire departments, police departments, Walmart, shopping centers, and the airport) were modeled as nodes to enable future economic studies.

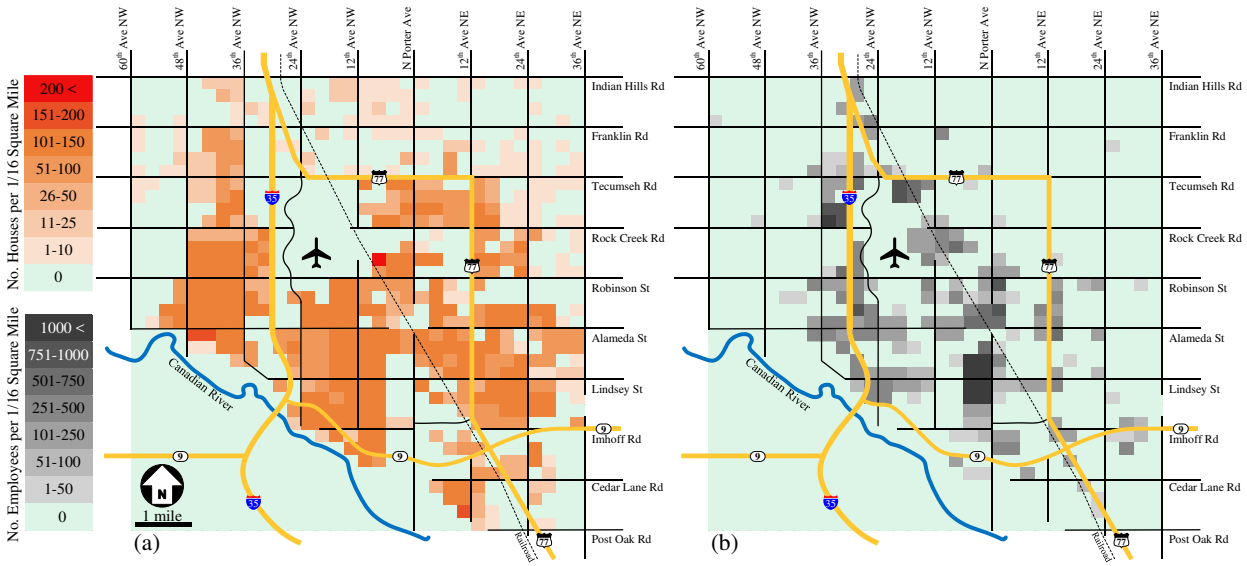

Figure 2-2. Pseudo-Norman map showing (a) the density of residential buildings in the residential sector and (b) the number of employees in the business sector

RESIDENCE-BUSINESS CROSS-DEPENDENCY

In order to link the residential sector to business sector, the employees who live in each residential grid must be associated with a workplace in a business grid. It was assumed that each occupied house in the city has two people who are eligible to work, which means that, in total, 75,570 people who live in the city can be an employee. However, based on the census (City-Data, 2016), there is some percentage of unemployment for each grid, which results in 71,198 employees who live in pseudo-Norman. Yet, in the census (City-Data, 2016), only 70% of these employees (i.e., 49,848

employees) work in pseudo-Norman and the rest have a job outside of the city. For each residential grid, those employees who work in the city were divided into 10 groups, and each group was assigned to a business grid.

Figure 2-3 sheds light on the cross-dependencies between the residential sector and business sector. For example, 70% of the employees whose houses are located in the residential grid marked with a black star in Figure 2-3 (a) work in a workplace located in the business grids marked with white stars in Figure 2-3 (b), and the other 30% work outside of the city. Moreover, the employees who work in the business grid marked with a white circle in Figure 2-3 (b) live in a house located in the residential grids marked with black circles in Figure 2-3 (a). It should be noted that some of the employees who work in a business grid may live outside of the city. The cross-dependencies between the residential sector and business sector will be used to consider the influence of affected businesses on the households and vice versa as will be discussed later.

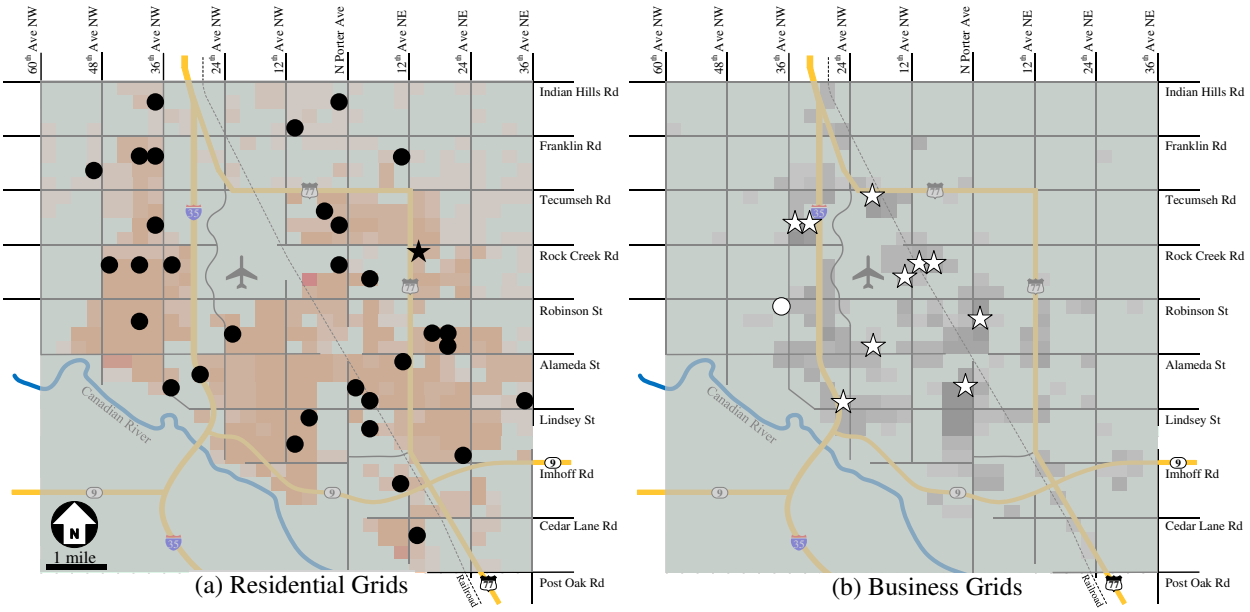

Figure 2-3. An example of cross-dependencies between the residential sector and business sector

Finally, it is worth mentioning that the purpose of using grids for modeling residences and workplaces in pseudo-Norman was to reduce the complexity of the model by narrowing the heterogeneity and cross-dependencies. However, during the analyses (e.g., population outmigration analysis), every single building was analyzed through the process, if needed, (e.g., every single household in a residential grid was analyzed in population outmigration analysis and then the results were integrated at the grids level and the community level).

ELECTRIC POWER NETWORK

The electric power network (EPN) plays a key role in the functionality of a community in that almost all other lifeline networks operate using some level of electric power. Therefore, power outages can result in substantial economic loss and social disruption. However, in general, these are short-term disruptions since the restoration of an electric power network following a natural disaster becomes a priority and is typically restored within hours, days, or in severe cases, after several weeks (NIST, 2016). Generally, an EPN consists of power stations, which generate electricity, transmission system, which carries the generated electric power to substations, and distribution system, which provides the electric power to nearby end-users. Distribution lines can be constructed using above ground poles or buried underground. However, providing underground systems for transmission is quite costly and a more recent addition to physical infrastructure systems.

Google maps of the city of Norman were used to model the EPN in this dissertation. The EPN in pseudo-Norman includes 4 transmission substations (TSS), 18 distribution substations (DSS), 123 transmission towers, and 1,393 sub-transmission towers. Transmission and sub-transmission towers are spaced at 310 m and 110 m, respectively. It is worth mentioning that buried underground

distribution lines were considered for the EPN in pseudo-Norman, which transfer the electric power to the end users from distribution substations. The EPN is depicted in Figure 2-4. The transmission lines transfer the electric power to the transmission substations near the point of consumption, where the power is regulated to sub-transmission voltages. Sub-transmission lines transmit this electric power to distribution substations, which reduce the voltage further to distribution voltage levels. Finally, the electric power is distributed through buried underground distribution lines to the end-users. Coverage zones for electric power distribution substations were defined such that an area is supplied by only one distribution substation. In other words, although there might be redundancy in providing electricity for a DSS, i.e., several (sub-)transmission lines to a DSS, there is no redundant DSS for end-users.

WATER SUPPLY NETWORK

A community relies on its water supply network (WSN), which is essential for life, public health, firefighting, and industrial processes (NIST, 2016). A typical water network consists of supply, storage, transmission, and distribution components. These components can be classified into generating components including reservoirs, water treatment plants, storage tanks, and pumping stations; and distribution components including pipelines, junctions, and fire hydrants.

In this dissertation, however, a simplified water supply network, including six water towers (WT) with different capacities and one water treatment plant (WTP), was considered for pseudo-Norman. The location and the number of WTs, WTP, and fire departments were extracted from the website of the Utilities Department of the city of Norman. Figure 2-4 shows the components of water supply network as well as fire departments in the city. A coverage zone was assumed for each water tower such that an area may be covered by more than one water tower. The functionality

of each WT depends not only on its physical performance but also on the functionality of the electric power distribution substation that provides electricity for the pumping station of the WT as well as on the functionality of the water treatment plant. Therefore, the WSN is cross-dependent on the EPN. In the case of tornadoes, uprooted trees may cause damages to underground electric power distribution lines or pipelines of the water supply network; however, that effect was neglected in the analyses in this dissertation.

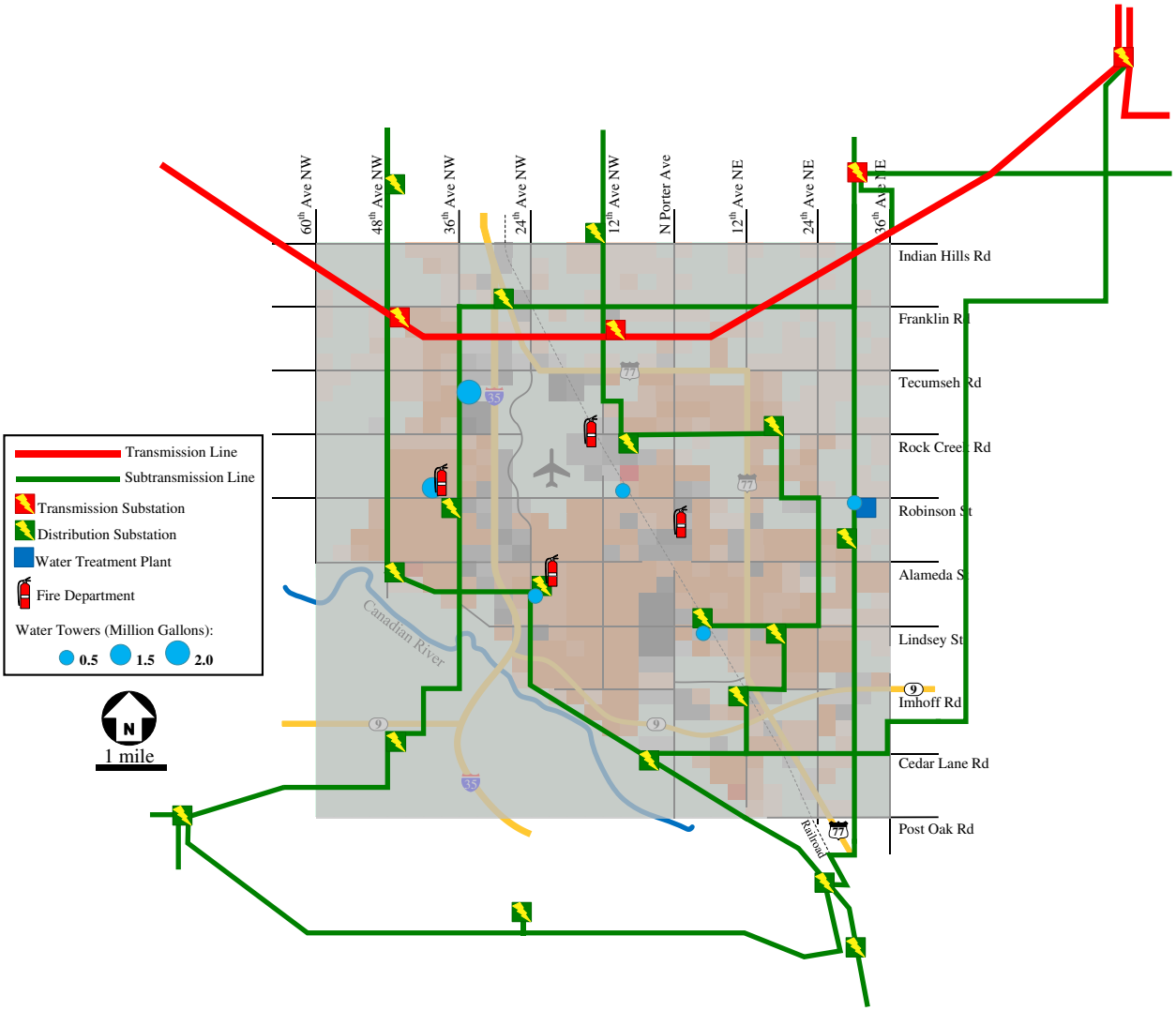

Figure 2-4. Electric Power network and water supply network in pseudo-Norman

SCHOOL NETWORK

The school network (SN) within a community often captures the attention of residents because it hosts virtually all children within the community each day. Destruction of school buildings in natural disasters results in social disruption in addition to possible direct injuries and fatalities. Therefore, school buildings, as important community components, were included in the community modeling in this dissertation. As shown in Figure 2-5, fifteen elementary schools (ES), four middle schools (MS), and two high schools (HS) host pseudo-Norman students. The attendance boundary of school buildings is also shown in Figure 2-5 using different colors, which illustrates the cross-dependency of the residential sector with the school network. Each school building is supplied by specific water tower(s) and an electric power distribution substation. Therefore, the school network is cross-dependent on the WSN and EPN.

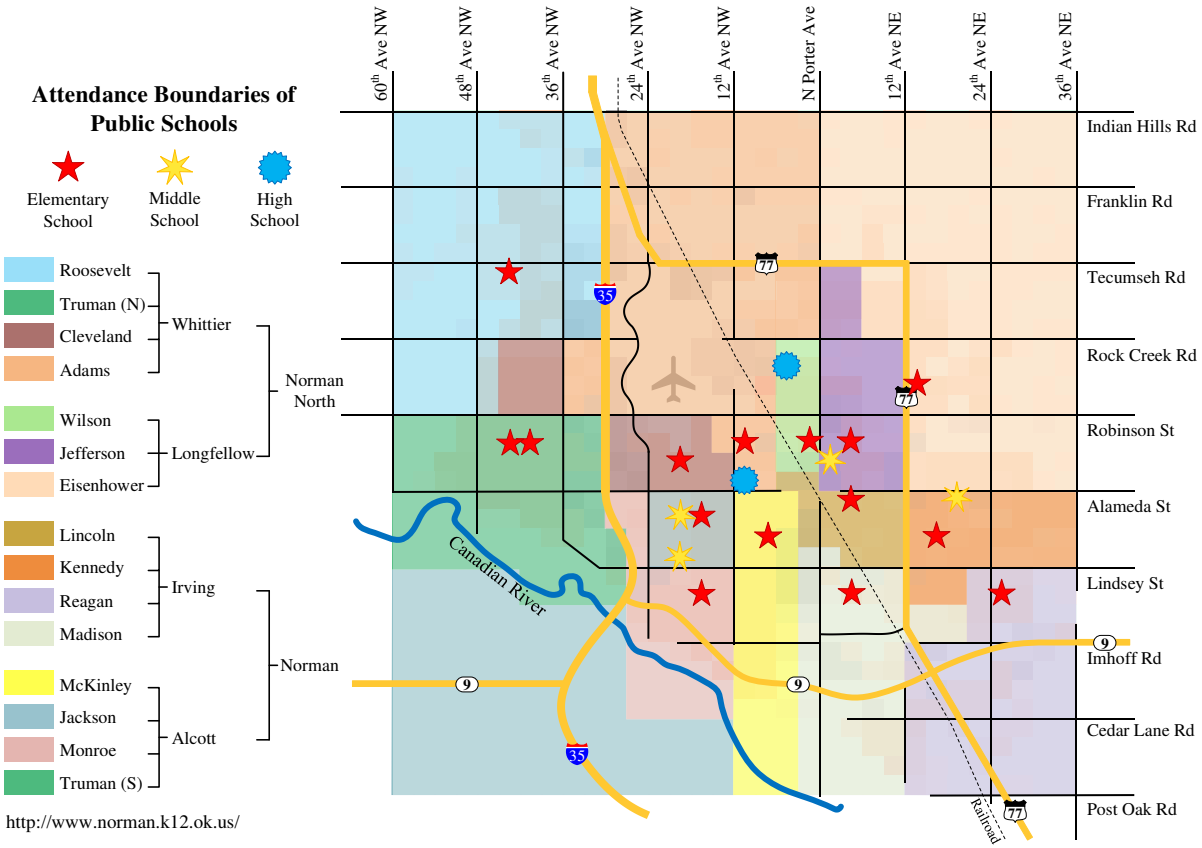

Figure 2-5. Public school network in pseudo-Norman

CROSS-DEPENDENCY MATRIX

For the purpose of the analyses in this dissertation, as illustrated in Figure 2-6, five networks were modeled for pseudo-Norman—the residential sector, the business sector, the electric power network, the water supply network, and the school network. The dependencies among the components of each network as well as the cross-dependencies among networks were modeled to capture the effects of cascading failure in the analyses. The cross-dependencies among networks are illustrated in Figure 2-6 and summarized in Table 2-1.

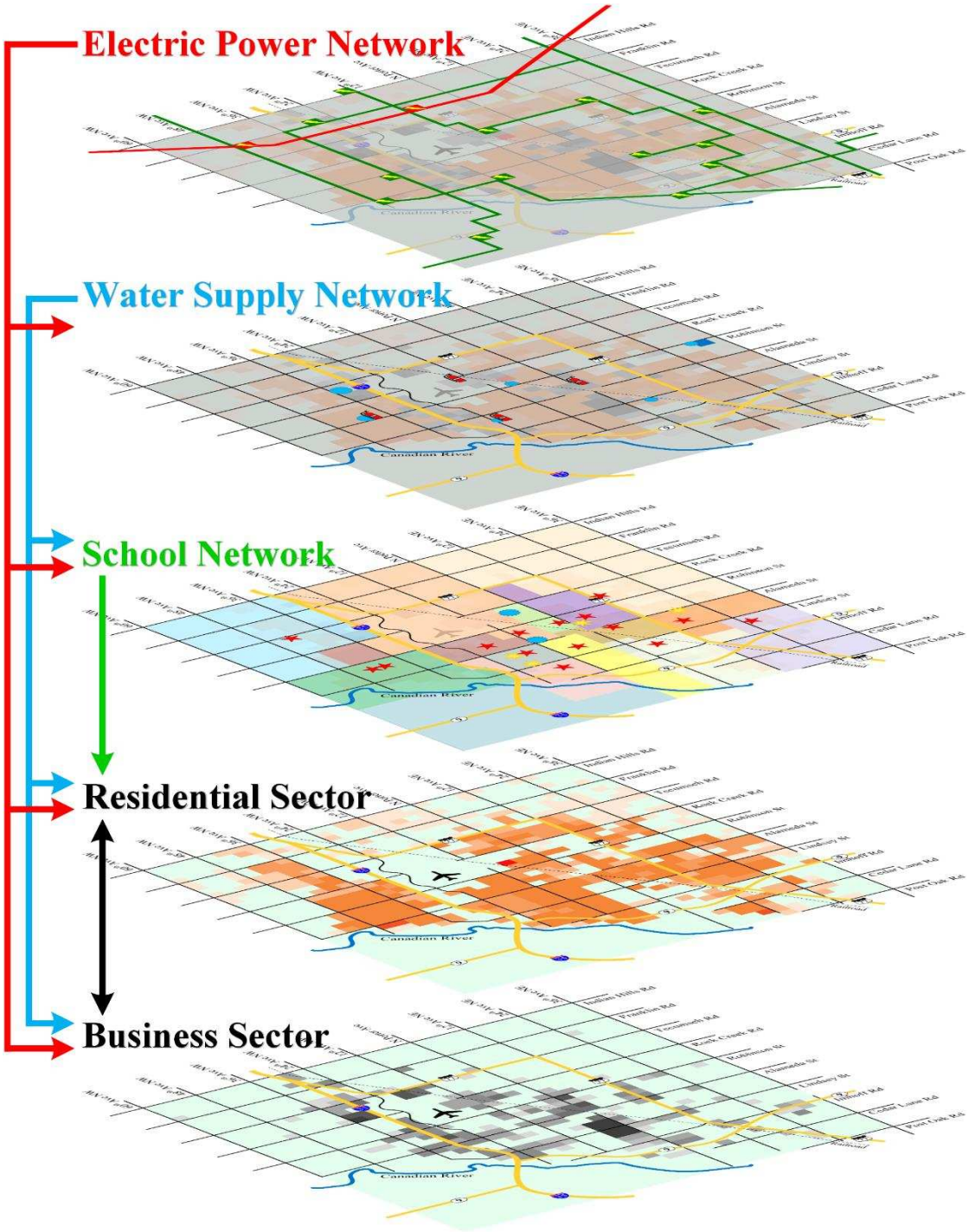

Figure 2-6. Pseudo-Norman networks and the corresponding cross-dependencies

Table 2-1. Cross-dependency matrix considered for modeling pseudo-Norman in this dissertation

Network	is cross-dependent on (i.e., is supplied by):				
	RS	BS	EPN	WSN	SN
Residential Sector (RS)		×	×	×	×
Business Sector (BS)	×		×	×	
Electric Power Network (EPN)					
Water supply Network (WSN)			×		
School Network (SN)			×	×	

CHAPTER 3: COMMUNITY COMPONENTS PROPERTIES

INTRODUCTION

After modeling the topology of community components, the dependencies among components, and the cross-dependencies between networks; the component properties that are required for the damage simulation under a hazard and for the restoration process need to be assigned to each community component in the model. These properties are the performance of the component under the hazard and the repair time associated with the component's level of damage following the hazard event. The performance of community components when subjected to a simulated tornado were investigated through fragility analysis. A set of tornado fragility curves were developed corresponding to four prescribed damage states. Additionally, a repair time associated with each damage state was assigned to each community component for investigating the restoration process following a simulated tornado event.

TORNADO FRAGILITY METHODOLOGY[1]

Tornado Load Modeling

The low probability of occurrence of tornadoes has prevented consideration of tornado loads in modern building codes, but this is changing as a result of deadly and damaging tornadoes over the last five years (Tuscaloosa, 2011; Joplin, 2011; Moore, 2013). Several experimental studies have been completed that focused on understanding tornado-induced loads on building surfaces (Haan et al., 2010; Letchford et al., 2015; Refan et al., 2014). As a result of the study by Haan et al.

[1] This section is based on the paper: Masoomi, H., and van de Lindt, J.W. (2016). "Tornado fragility and risk assessment of an archetype masonry school building." *Engineering Structures*, 128, 26-43.

(2010), a tornado load coefficient was proposed by van de Lindt et al. (2013) which implicitly considers the pressure deficit in tornado load calculation. On the other hand, Kikitsu et al. (2011) modified the formula for tornado-induced pressure calculation, proposed by Simiu and Scanlan (1996), to explicitly consider the effect of pressure deficit on internal pressure. The latter proposed approach provides a more detailed model for tornado-induced load calculation, but a lack of information on building leakage and statistics for model parameters still persists. In another study, Masoomi and van de Lindt (2017) modified the formula proposed by Simiu and Scanlan (1996) and developed two Rankine-vortex-based methods to generate tornado fragility surfaces. Their tornado fragility methodology considered not only the effects of pressure deficit but also the location of building in terms of the distance from the tornado center line. Their methodology results in tornado fragility surfaces that can be applied for tornado-induced damage prediction spatially over a community.

In this dissertation, two ASCE-7-based methods were developed to generate tornado fragility curves. The procedure discussed in ASCE 7-10 (2010) for calculation of wind forces resulting from straight-line winds have been extensively studied, and the equation for calculating velocity pressure is:

$$q_z = 0.613 K_z K_{zt} K_d V^2 \qquad (\text{N/m}^2;\ V \text{ in m/s}) \qquad \textit{Equation 3-1}$$

$$q_z = 0.00256 K_z K_{zt} K_d V^2 \qquad (\text{lb/ft}^2;\ V \text{ in mph})$$

where, K_z = velocity pressure exposure coefficient, K_{zt} = topographic factor, K_d = wind directionality factor, V = basic wind speed, q_z = velocity pressure calculated at height z, and q_h = velocity pressure calculated at mean roof height h.

Wind pressure for the main wind force resisting system (MWFRS) is then calculated as:

$$p = qGC_p - q_i(\mathrm{GC}_{pi}) \qquad (\mathrm{lb/ft^2})\ (\mathrm{N/m^2}) \qquad \textit{Equation 3-2}$$

where, q and q_i are velocity pressure calculated at height z or h, G = gust-effect factor, C_p = external pressure coefficient, and GC_{pi} = internal pressure coefficient.

For components and cladding (C&C) wind pressure is determined as:

$$p = q_h\left[\left(GC_p\right) - \left(GC_{pi}\right)\right] \qquad (\mathrm{lb/ft^2})\ (\mathrm{N/m^2}) \qquad \textit{Equation 3-3}$$

where, q_h = velocity pressure calculated at mean roof height h, (GC_p) = external pressure coefficients, and (GC_{pi}) = internal pressure coefficient.

The winds from a tornado extend 9,000 to 15,000 meters (30,000 to 50,000 feet) above the ground and are a turbulent phenomenon. In general, there are many key differences between tornadoes and straight-line wind. In this dissertation, certain modifications were applied to the ASCE 7-10 (2010) methodology for straight-line wind loads in order to obtain the tornado-induced forces.

The first modification is with regard to the directionality factor, K_d. Justification for using the directionality factor is mentioned in the ASCE 7-10 commentary (2010) as the following: "This factor accounts for two effects: (1) The reduced probability of maximum winds coming from any given direction and (2) the reduced probability of the maximum pressure coefficient occurring for any given wind direction." Indeed, these effects consider circumstances in which it is probable that the strongest winds come from a non-critical direction. All of these considerations deal with straight-line winds but the maximum wind speed can occur from any direction in tornadoes, which may exert a maximum pressure coefficient on buildings from any direction (Prevatt et al., 2013;

FEMA, 2015). Thus, the directionality factor is conservatively neglected in the tornado-induced load calculation and is set equal to 1.0 in the determination of tornadic loads.

The second consideration for wind loading is that different exposures in ASCE 7-10 (2010) result in a different coefficient for straight-line winds. Several studies have been completed regarding the effects of ground surface roughness in tornadoes (Dessens, 1972; Leslie, 1977; Liu and Ishihara, 2016; Natarajan and Hangan, 2009; Sabareesh et al., 2012 and 2013). Sabareesh et al. (2013) showed that, with the introduction of roughness, the internal pressures decrease in magnitude irrespective of swirl ratio, external pressures decrease in magnitude compared to internal pressures, and the net local roof wind force increases in magnitude. However, in this dissertation, regardless of the ground surface roughness and the fetch length of the surrounding terrain, the analysis is considered based on the Exposure C (ASCE 7-10, 2010).

Moreover, there is an ongoing debate related to the modification of pressure coefficients. Several studies have shown that tornadoes result in greater pressure on buildings than straight-line winds for the same reference wind speed (Alrasheedi and Selvam, 2011; Haan et al., 2010; Roueche et al., 2015; Sabareesh et al., 2012; Selvam and Millett, 2003; Sengupta et al., 2008). However, there is no consensus on the intensity of pressure that tornadoes can apply on building surfaces since tornado loading still possesses significant uncertainty primarily related to researchers understanding of the phenomena. Therefore, additional parameters are defined in this dissertation to modify pressure coefficients. The modification of the pressure coefficient is divided into two parameters to separate internal and external pressure coefficients which are different in ASCE 7-10 (2010). The first parameter is tornado external pressure adjustment, T_e, which is defined herein to modify the external pressure coefficients. The tornado external pressure adjustments are based on the study done by Haan et al. (2010). Note that Haan et al. (2010) used ASCE 7-05, but using

ASCE 7-10 (2010) does not alter the values since the external pressure coefficients are the same for both editions. The second coefficient is T_i, tornado internal pressure adjustment, which needs further investigation and is set to 0.0 or 1.0 in this dissertation as will be discussed later.

The modifications described above are applied to the method outlined in the wind provisions of ASCE 7-10 (2010) to assess wind loads from tornadoes in this dissertation. Moreover, the local topographic effect was neglected, i.e., K_{zt} is assumed to be 1.0, and all the analyses either for the main wind force resisting system (MWFRS) or for components and cladding (C&C) were determined based on velocity pressure calculated at mean roof height h, i.e., q_h. Since the near-surface wind flow in tornadoes is turbulent and has not been adequately studied, this assumption is felt to be rational. Thus, the tornado-induced wind load is calculated by the following equations:

$$q_h = 0.613 K_h K_{zt} V^2 \qquad (\text{N/m}^2);\ V \text{ in m/s} \qquad \textit{Equation 3-4}$$

$$q_h = 0.00256 K_h K_{zt} V^2 \qquad (\text{lb/ft}^2);\ V \text{ in mph}$$

$$p = q_h \left[T_e \left(GC_p \right) - T_i \left(GC_{pi} \right) \right] \qquad (\text{lb/ft}^2)\ (\text{N/m}^2) \qquad \textit{Equation 3-5}$$

where, K_h = velocity pressure exposure coefficient at mean roof height h, K_{zt} = topographic factor, V = 3-sec gust wind speed, and q_h = velocity pressure calculated at mean roof height h, G = gust-effect factor, C_p = external pressure coefficient, (GC_{pi}) = internal pressure coefficient, T_e = tornado external pressure adjustment, and T_i = tornado internal pressure adjustment.

In order to calculate tornado-induced wind loads by using Equation 3-5, two alternative approaches were proposed in this dissertation—namely Approach A and Approach B, which are as follows:

Approach A: Using the pressure coefficients per ASCE 7-10 (2010) along with tornado pressure adjustments derived based on the study done by Haan et al. (2010).

Haan et al. (2010) studied tornado-induced wind loads in a laboratory-simulated tornado on a 1:100 scale one-story gable roof building model with a 91 mm by 91 mm (3.6 in. by 3.6 in.) plan, an eave height of 36 mm (1.4 in), and roof angle of 35°. They compared the measured pressures with the ASCE 7-05 standard and found that external pressure coefficients appeared to be greater than those prescribed by ASCE 7-05 for straight-line winds over open terrain. Based on their study, the uplift pressure coefficients for the MWFRS and for C&C exceeded those from the ASCE 7-05 wind provisions by a factor of 1.8–3.2 and 1.4–2.4, respectively. They assumed a fully sealed building in their study, which negated the effect of internal pressure change on mitigating the static pressure drop caused by the tornado vortex. However, there exist openings and some level of leakage in typical buildings which could significantly decrease the effect of static pressure drop (Roueche et al., 2015). Therefore, using these coefficients as T_e in Equation 3-5 requires that T_i be set equal to zero since the internal pressure has already been considered inherently in coefficients identified by Haan et al. (2010). It is worth mentioning that although openings reduce the effect of the static pressure drop, at the same time they may cause notable internal pressure by letting wind flows into building (Kikitsu et al., 2011; Letchford et al, 2015). A similar observation was made for lateral pressure coefficients and revealed that the pressure coefficients ranged from 1.0 to 1.5 times larger than those coefficients in ASCE 7-05 for MWFRS and 1.2 to 1.5 times larger for C&C. Using the values obtained for adjusting the lateral pressure coefficients for C&C (i.e., T_e ranges between 1.2 and 1.5) in Equation 3-5, T_i should be set equal to zero for the same reason explained above for the MWFRS and C&C. However, lateral pressure coefficients for MWFRS were calculated by integrating the pressures over the model surface, which canceled out the static

pressures effect (internal pressure and pressure drop) only in this case (Haan et al., 2010). Therefore, using this T_e value for lateral pressure coefficients for MWFRS in Equation 3-5 should be done by setting T_i equal to 1.0.

Approach B: Using the pressure coefficients per ASCE 7-16 (2016) along with both T_e and T_i equal to 1.0.

The ASCE 7-16 (2016) coefficients for roof pressures are notably larger than the ASCE 7-10 (2010) based on recent wind tunnel test results and are believed to be derived from the best pressure measurements generated to date. Moreover, as discussed earlier, internal pressure is neglected in Approach A (except for estimating lateral pressures on MWFRS). However, in some cases, including internal pressure and using tornado pressure adjustments (i.e., T_e and T_i) equal to 1.0 in Equation 3-5 may result in a higher load than when using Approach A. In this regard, the alternative Approach B is defined by setting the tornado pressure adjustments (i.e., T_e and T_i) equal to 1.0 and using the pressure coefficients per ASCE 7-16 (2016) representing the best knowledge in pressure coefficients currently available for straight-line winds.

The differences between the Approach A and Approach B for calculating tornado-induced load by using Equation 3-5 are highlighted in Table 3-1.

Table 3-1. Difference between Approaches A and B for Calculating Tornado-induced Load

Parameters Description				Approach A	Approach B
Tornado Pressure Adjustment	Uplift Pressure	MWFRS	T_e	1.8 - 3.2	1.0
			T_i	0.0	
		C&C	T_e	1.4 - 2.4	
			T_i	0.0	
	Lateral Pressure	MWFRS	T_e	1.0 - 1.5	
			T_i	1.0	
		C&C	T_e	1.2 - 2.0	
			T_i	0.0	
External Pressure Coefficients, GC_p				ASCE 7-10	ASCE 7-16

The statistics for wind load parameters are summarized in Table 3-2. Since the illustrative building archetype provided in this chapter has a flat roof, the nominal values for GC_p for roof covering are based on the values for gable roofs with $\theta \leq 7°$ in ASCE 7-10 (2010) or ASCE 7-16 (2016). As mentioned before, the topographic factor, K_{zt}, is deterministic and set equal to 1.0. It is noted that the ASCE 7-16 (2016) parameters are the same as those in ASCE 7-10 (2010) except the external pressure coefficients for roof C&C.

Table 3-2. Wind Load Statistics

Parameters	Descriptions	Nominal	Mean	COV	Distribution	References
K_z	0 - 4.57 m (0 - 15 ft)	0.85	0.82	0.14		Lee and Rosowsky (2005)
	6.10 m (20 ft)	0.90	0.84	0.14		
	7.62 m (25 ft)	0.94	0.88	0.14		
	9.14 m (30 ft)	0.98	0.94	0.14		
	12.19 m (40 ft)	1.04	1.00	0.14		
G	-	-	0.82	0.10		Ellingwood and Tekie (1999)
GC_{pi}	Enclosed Buildings	0.18	0.15	0.33		
	Partially Enclosed Buildings	0.55	0.46	0.33		
C_p	Wall	0.80	0.69	0.15		
	Roof	-0.90	-0.81	0.15	Normal	
GC_p	Parapet	1.50	1.43	0.18		COV and Mean/Nominal: Ellingwood and Tekie (1999)
	Door	-0.86	-0.81	0.12		
	Window	-0.81	-0.77	0.12		
	Roof Cover- Zone 1	-1.00	-0.95	0.12		Nominal: ASCE 7-10 (2010) ASCE 7-16 (2016)
	Roof Cover- Zone 2	-1.80	-1.71	0.12		
	Roof Cover- Zone 3	-2.80	-2.66	0.12		
	Roof Cover- Zone 1’	-0.90	-0.86	0.12		
	Roof Cover- Zone 1	-1.70	-1.62	0.12		
	Roof Cover- Zone 2	-2.30	-2.19	0.12		
	Roof Cover- Zone 3	-3.20	-3.04	0.12		

Resistance Modeling

Over the years tornadoes have destroyed or severely damaged a significant number of schools, resulting in injuries and fatalities. One well-known case was Xenia senior high school in Xenia,

Ohio, in the United States, which was hit by an F5 tornado in 1974 (FEMA, 2009a). The school building is shown in Figure 3-1 before and after the tornado that passed directly over the school. The enclosure walls failed on the west and south sides; roofs collapsed over the three long spans—the auditorium, the boys' gym, and the girls' gym; and the lightweight roof was torn off by the extreme winds.

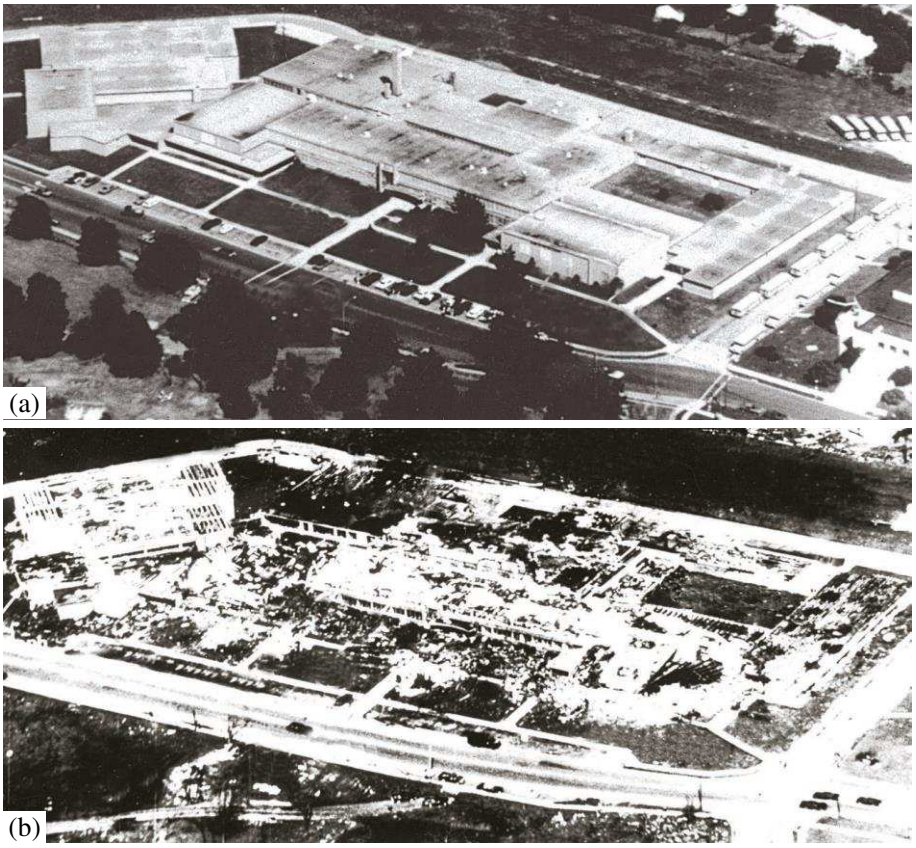

Figure 3-1. Xenia Senior High School, Xenia, Ohio: (a) before tornado, (b) after tornado (Excerpted from FEMA (2009a), photo credit: WERC, TEXAS TECH UNIVERSITY)

The floor plan for Xenia Senior High School, shown in Figure 3-2, was selected here to be studied as an illustrative archetype representing the school buildings within a community. The construction types for Xenia Senior High School varied among the main parts of the school—original building, and three additions; namely A, B, and C (FEMA, 2009a). The structural system for the original building and addition B was a lightweight steel frame with open-web steel joists. Addition A had

loadbearing masonry walls with hollow-core precast concrete roof planks, and addition C had precast concrete frames with concrete double-tee roof beams. Moreover, the girls' gym included loadbearing masonry walls with precast concrete tee beams while the auditorium and the boys' gym included loadbearing masonry walls with steel trusses. However, the archetype studied here is assumed to be a one story building with a structural system consisting of unreinforced masonry walls constructed of 0.2-meter (8-inch) concrete masonry units and 0.1-meter (4-inch) face bricks. The roof consists of hollow-core precast concrete roof planks (Figure 3-3). Moreover, this high school has three unreinforced masonry long-span rooms, i.e., two gymnasiums (girls' gym and boys' gym) and one auditorium, constructed of 0.3-meter (12-inch) concrete masonry units and 0.1-meter (4-inch) face bricks. The long-span rooms have roofs with precast concrete tee beams (Figure 3-3). Details for roofs and walls are summarized in Table 3-3, and the beam cross-sections used in the roof system of the main building and the girls' gym are shown in Figure 3-3.

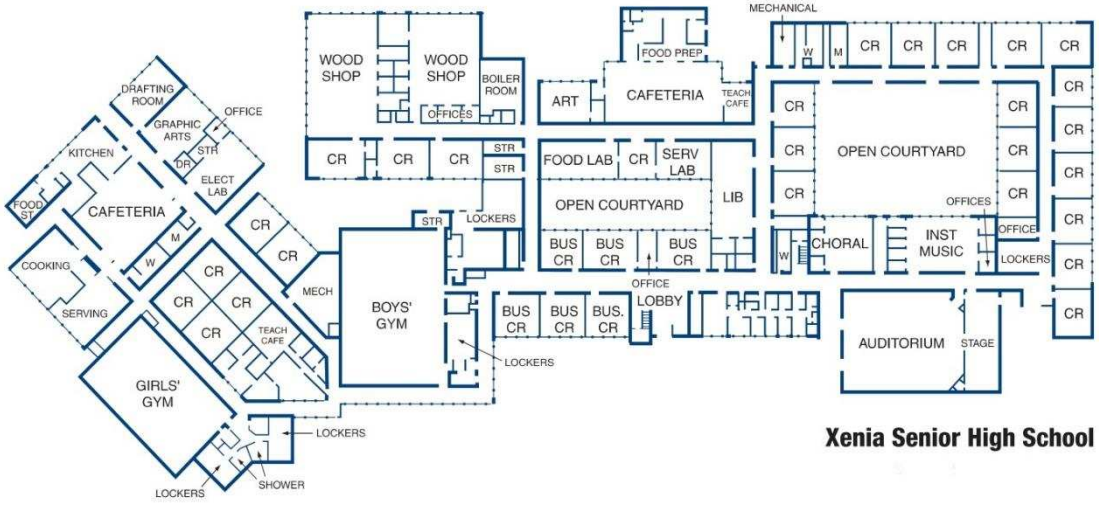

Figure 3-2. The High School Archetype Floor Plan, Excerpted from FEMA (2009a)

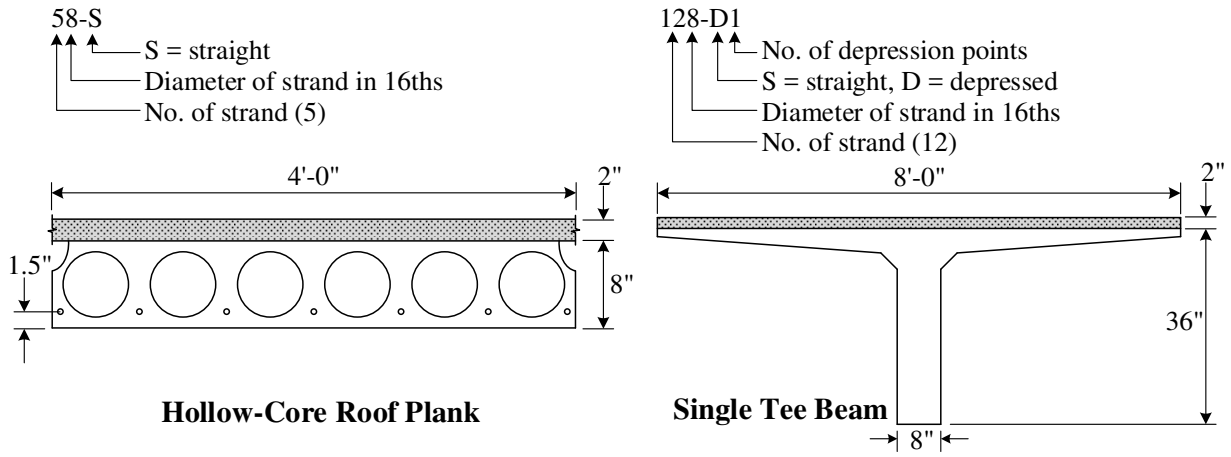

Figure 3-3. Cross-sections Used in the Roof System of the Main Building and the Girls' Gym.

Table 3-3. High School Building Construction Details

Building Part	Dimensions	Walls	Precast Concrete Roof System*		
			Beam Type	Name in PCI (1971)	Strand Pattern
Main	Walls Height = 4.3m (14ft) Parapets Height = 0.9m (3ft)	8' CMU	Hollow-Core	4HC8+2	58-S
Girls' Gym	39m × 24.5m × 8m (128ft × 80ft × 26ft)	12' CMU	Single Tee	8ST36+2	128-D1
Boys' Gym	43m × 30.5m × 9m (140ft × 100ft × 30ft)	12' CMU	Single Tee	10ST48+2	188-D1
Auditorium	44m × 27.5m × 9m (144ft × 90ft × 30ft)	12' CMU	Single Tee	10ST48+2	148-D1

* Roof details can be found in PCI (1971).

For edge-supported (by roof, floor, and adjacent walls, etc.) unreinforced masonry walls under uniform lateral pressure loading, the major failure mechanism is associated with cracking due to flexural tensile stress (FEMA, 2009b). Therefore, tensile strength is the most important failure metric in unreinforced masonry design, which is a function of several factors including tension direction, such as tension parallel to or perpendicular to the bed joint; type of units, i.e., solid units or hollow units; the unit grouting condition, i.e., ungrouted, partially grouted, or fully grouted; and the mortar type, such as Portland-Cement Lime mortar (PCL) or Masonry Cement (MC) mortar,

which can be type M, S, or N mortar. The out-of-plane modulus of rupture values in the strength provisions of the Masonry Standards Joint Committee code (MSJC, 2011) are approximately 1.9 times the allowable stress design values. Since no source data is available for partially grouted masonry, its values are determined on the basis of linear interpolation between fully grouted hollow units and ungrouted hollow units based on amount (percentage) of grouting (MSJC, 2011). In this dissertation, 25 percent of grouting was assumed as the definition of partially grouted masonry which would be consistent with grouting of cells at 1.53 to 1.83 meter (5 to 6 feet) on-center for reinforcement. Two types of concrete masonry units (12" CMU for gyms and auditoriums, and 8" CMU for the rest of the building) and five types of masonry material are considered here. A summary of the flexural tension values is given in Table 3-4; all the values are related to tension normal to bed joints in hollow units. The table gives the sample size, mean, and coefficient of variation of each masonry material type. Furthermore, the current allowable flexural tension stress and modulus of rupture in the MSJC code (2011), and the ratio of the mean flexural tension stress to allowable stress is highlighted in the aforementioned table. All flexural tension values given in Table 3-4 are based on net cross-sectional properties (Kim, 2002), and normal distributions were assigned for all of these materials.

Precast concrete single Tee beams and precast concrete hollow-core beams were selected for the roof system which is consistent with the roof system in the Xenia senior high school failure in 1974. In fact, prestressed concrete is a technique for overcoming concrete's weakness in tension so that it can be used in beams with a longer span. Conventionally, precast concrete beams are designed for the gravity loads, and not for the uplift loads. Hence, although prestressing removes a number of design limitations and has several advantages under normal loading conditions, it can be a disadvantage if the design engineer did not recognize the effects of wind uplift loads. Failure

of precast concrete beams occurred in several wind events (e.g., Typhoon Paka, Guam 1997; a tornado in Missouri, May 2003) (FEMA, 2010).

The statistics for negative moment resistance and material properties of precast concrete beams are provided in Table 3-5. The statistics for negative moment resistance of beams are calculated based on material properties and conventional procedures in precast concrete structural analysis. The section properties and strands pattern of each beam were determined using a PCI (1971) design manual. The old Xenia senior high school, which was destroyed in the 1974 tornado, had been built in 1957, but the archetype herein was designed to be representative of a 1970's school.

Moreover, the connections between the precast concrete decks and wall are not usually designed for uplift loads. Therefore, because the deck dead load itself is often inadequate to resist the tornado uplift, bolt break out can be another roof failure mode in this case. Bolt break out statistics are given in Table 3-6.

Table 3-4. Statistics of Masonry Flexural Tension- Normal to bed joints, Hollow units (Kim, 2002)

Type	Masonry and Mortar Types	Sample Size	Mean	COV	Modulus of Rupture in MSJC Code	Allowable Stress in MSJC Code	Ratio of Mean to Allowable Stress
M1	Fully Grouted, M/S, PCL	6	2.0 MPa (289.6 psi)	0.11	1.12 MPa (163 psi)	0.59 MPa (86 psi)	3.37
M2	Partially Grouted, M/S, PCL	-*	1.47 MPa (213.0 psi)	0.31	0.61 MPa (88 psi)	0.32 MPa (46 psi)	4.63
M3	Ungrouted, M/S, PCL	80	1.29 MPa (186.5 psi)	0.48	0.43 MPa (63 psi)	0.23 MPa (33 psi)	5.65
M4	Ungrouted, N, PCL	61	0.69 MPa (100.5 psi)	0.45	0.33 MPa (48 psi)	0.17 MPa (25 psi)	4.02
M5	Ungrouted, N, MC	17	0.36 MPa (52.7 psi)	0.45	0.16 MPa (23 psi)	0.08 MPa (12 psi)	4.39

* The values for partially grouted masonry are determined on the basis of linear interpolation between fully grouted hollow units and ungrouted hollow units.

Table 3-5. Summary of Statistics for Negative Moment Resistance and Material Properties of Roof Beams

Parameters Description		Mean	COV	Distribution	References
f_c (Concrete 28-day cylinder strengths)		45.85 MPa (6.65 ksi)	0.130	Normal	Unanwa and Mahan (2014)
f_y (Yield strength of reinforcement bars)		475.74 MPa (69 ksi)	0.073		Bournonville et al. (2004)
E_{ps} (Modulus of Elasticity of Grade 270 Strands)		195928 MPa (28417 ksi)	0.034		Hill (2006)
f_{pu} (Ultimate Strength of Grade 270 Strands)		1992.6 MPa (289 ksi)	0.087		Hill (2006)
Negative Moment Resistance	4HC8+2 With Strand Code 58-S	19.66 kN.m (174 kip.in)	0.086	Normal	Based on Calculation and PCI (1971)
	8ST36+2 With Strand Code 128-D1	221.56 kN.m (1961 kip.in)	0.076		
	10ST48+2 With Strand Code 148-D1	275.23 kN.m (2436 kip.in)	0.080		
	10ST48+2 With Strand Code 188-D1	265.06 kN.m (2346 kip.in)	0.095		

Table 3-6. Roof-to-Wall Connections Statistics

Description	Mean	COV	Distribution	References
Bolt #5; 8" CMU; Fully Grouted	49.73 kN (11.18 kip)	0.10	Normal	Cui (2007)
Bolt #5; 8" CMU; Partially Grouted	32.65 kN (7.34 kip)	0.12		
Bolt #5; 12" CMU; Fully Grouted	51.38 kN (11.55 kip)	0.15		
Bolt #5; 12" CMU; Partially Grouted	40.52 kN (9.11 kip)	0.10		

Roof covering damage is the most common type of wind damage. Built-up roof (BUR) covers and single-ply membrane (SPM) covers can be used as a roof covering system. Failure of the perimeter flashing is usually the first wind-induced failure for BUR covers, which then expedites peeling for the roof cover membrane at the newly exposed edge; the peeling failure can continue and result in extensive roof covering damage. Bubbling is another roof cover failure, where the roof cover is separated from the substrate by high wind uplift pressures. A bubbled part of the roof membrane may become breached by impact from flying debris or by tearing at the perimeter of the bubble, or it may expand to an area where the roof cover is torn and therefore that bubbled section can also

tear. Moreover, since BUR covers are often surfaced with gravel or slag, the loose aggregate of the built-up roof can blow off and cause damage to windows in nearby houses. Window and door damage is also among the most common wind damage. The importance of building envelope damage cannot be understated because of water intrusion into buildings at envelope breaches. The resistance statistics for the BUR roof cover, windows, and doors are shown in Table 3-7. Moreover, it is worth mentioning that dead loads have a beneficial effect in wind-induced fragility analysis since they resist uplift loading and must, therefore, be included in the analysis. Dead load statistics for precast concrete roofs and concrete masonry units are provided in Table 3-8.

Table 3-7. Resistance Statistics for Roof Cover, Window, and Door

Component		Mean	COV	Distribution	References
Built-up Roof Cover	Flashing Resistance	328.36 N/m (22.5 plf)	0.30	Normal	FEMA (2009b)
	Peeling Resistance	2.39 kPa (50 psf)	0.15		
	Bubbling Resistance	7.18 kPa (150 psf)	0.15		
Windows Resistance		1.92 kPa (40 psf)	0.20		
Doors Resistance		2.39 kPa (50 psf)	0.20		

Table 3-8. Dead Load Statistics

Element Type	Mean	COV	Distribution	Sources
Hollow-Core Beam (4'HC8'')	4.73 kN/m (324 plf)	0.1	Normal	COV and Distribution Type: Ellingwood et al. (2004); Mean Values: PCI (1971)
Single-Tee Beam (8'ST36'')	11.59 kN/m (794 plf)			
Single-Tee Beam (10'ST48'')	15.54 kN/m (1065 plf)			
CMU 8'	2.30 kPa (48 psf)	0.1	Normal	COV and Distribution Type: Ellingwood et al. (2004)
CMU 12'	3.54 kPa (74 psf)			

Damage States Definition

Vann and McDonald (1978) defined five damage classes for mobile homes from damage class 0 (i.e., no damage) to damage class 5 (i.e., destruction of the building) based on the building envelopes. This approach was used in HAZUS-MH-MR4 (FEMA, 2009b) for developing hurricane fragility curves. Damage states for the school building here were defined based on the approach proposed by Vann and McDonald (1978). The damage states used for the school building were defined in Table 3-9 and are governed by the performance of the building envelope, roof structure, and walls. Damage is classified into five states, varying between 0 and 4 for consistency with HAZUS-MH-MR4 (FEMA, 2009b):

Damage State 0 (*No Damage*): Little or no visible damage from the outside; No broken windows or doors; Minimal loss of roof covering, with no or very limited water penetration.

Damage State 1 (*Minor Damage*): Maximum of one or two broken windows or doors; Moderate roof covering loss that can be covered with a tarp to prevent additional water entering the building[1]; Marks or dents on walls requiring painting or patching for repair.

Damage State 2 (*Moderate Damage*): Still capable of being occupied; Major roof covering damage; Moderate window breakage; some resulting damage to interior of the building from water.

Damage State 3 (*Severe Damage*): Not able to be occupied, but repairable; Major roof covering loss; Major loss of windows and doors; Extensive damage to interior from water; Non-load-bearing wall failure.

[1] It should be noted that unlike hurricanes, not all tornadoes are accompanied by rainfall. One example is the 2011 EF4 Tuscaloosa tornado that had very little rainfall associated with it until later in the day from a second supercell that spawned tornadoes in different locations.

Damage State 4 (*Destruction*): Not able to be occupied and not repairable; Roof system failure; Load-bearing wall failure.

If any of the shaded damage indicators in a given row of Table 3-9 occur, the school building is considered to be in that damage state. For example, for a school to be considered to have sustained damage state 4 (Destruction), the building must have sustained either roof structural failure or load-bearing wall failure. It is worth mentioning that in damage state 4 the first four damage indicators will typically occur, which means that damage state 4 depends only on roof structural failure and load-bearing wall failure.

Table 3-9. Damage States for School Building

Damage State	Damage Indicators and the Corresponding Limit States					
	Roof Covering Failure	Window/Door Failure	Parapet Failure	Non-load-bearing Wall Failure	Roof Structural Failure	Load-bearing Wall Failure
0	≤ 2%	No	No	No	No	No
1	> 2% and ≤ 15%	1 or 2	No	No	No	No
2	> 15% and ≤ 50%	> 1 or 2 and ≤ 25%	No	No	No	No
3	> 50%	> 25%	Yes	Yes	No	No
4	Typically > 50%	Typically > 25%	Typically Yes	Typically Yes	Yes	Yes

* Each damage state is defined as occurrence of any of the shaded damage indicators in a given row.

Fragility Analysis

Fragility analysis is a common approach to evaluate the performance of a building or a component of a building (e.g., roof covering) under extreme loads by considering uncertainties in load calculation and resistance estimation. In order to develop fragility curves for a building under wind loads, as shown in Table 3-9, different limit states are considered for several building components each of which participates in constructing a damage state for the building. A fragility curve at the component level can be defined as the conditional probability of exceeding a limit state (LS) based

on a specified engineering demand parameter (EDP) under a given hazard intensity, and can be expressed mathematically as (Ellingwood et al., 2004):

$$\mathrm{Fr}(V) = \mathrm{P}\left[LS \geq ls_i \mid V = v\right] \qquad \textit{Equation 3-6}$$

At the building level, the fragility curve for damage state *j* is defined as the conditional probability of occurrence of any of the shaded damage indicators in the row *j* in Table 3-9 under a given hazard intensity, which can be expressed as:

$$\mathrm{Fr}(V) = \mathrm{P}\left[\bigcup_i (LS \geq ls_{ij}) \mid V = v\right] \qquad \textit{Equation 3-7}$$

Monte Carlo simulation (MCS) with 10,000 runs was conducted to develop fragility curves at the component level and building level for the school building archetype introduced earlier. The procedure is presented in flowchart form in Figure 3-4. For convenience and often a good statistical fit, a fragility curve can be presented by fitting a lognormal cumulative distribution function to the developed fragility curve in Monte Carlo simulation.

$$\mathrm{Fr}(V) = \Phi\left(\frac{\ln(v) - \lambda}{\zeta}\right) \qquad \textit{Equation 3-8}$$

where $\Phi(.)$ = standard normal cumulative distribution function, v = 3-sec gust wind speed, λ = the mean of $\ln(V)$, and ζ = the standard deviation of $\ln(V)$.

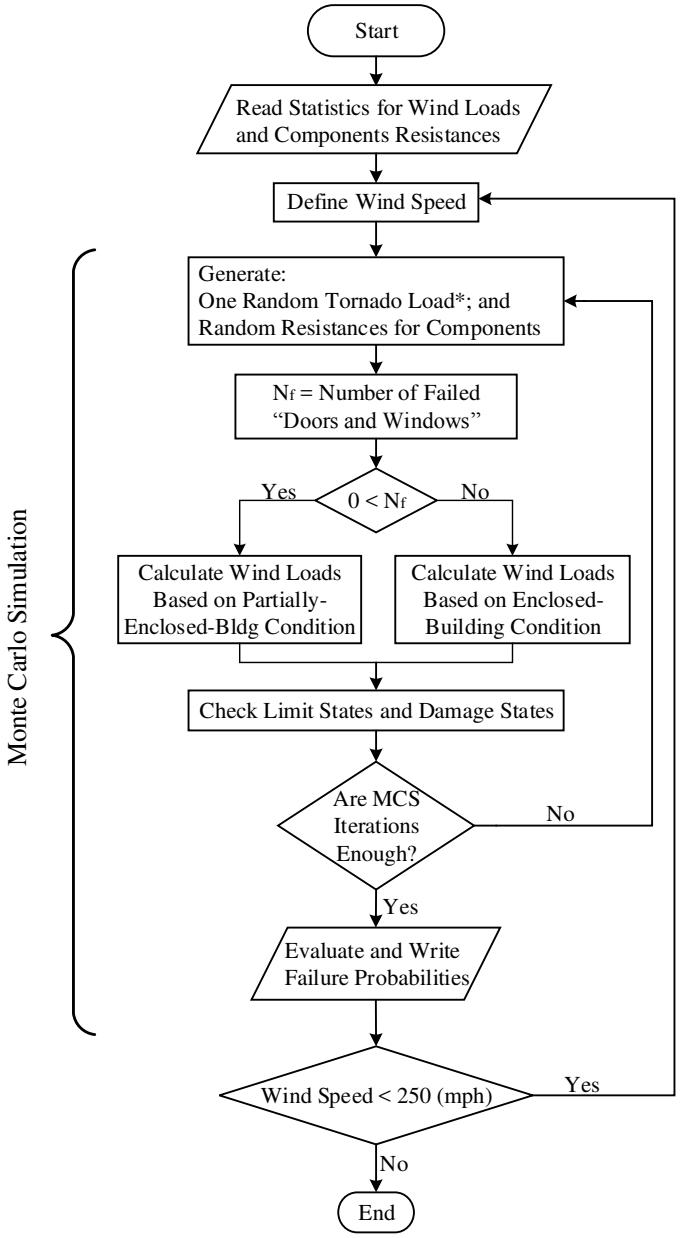

* It is noted that for a large building, loads may differ from one side of the building at a point in time. However, since the peak load from a 3-sec gust wind speed is used, i.e., a static analysis, the spatial effect across the building was neglected.

Figure 3-4. Flowchart for Developing Fragility Curves

Component-Level Fragility Curves

Based on the three limit states presented in Table 3-9 for doors and windows (the third column in the table), the fragility curves for this damage indicator were developed for both the enclosed and

partially enclosed building condition and are presented in Figure 3-5 as a function of 3-sec gust wind speed. As mentioned before, the enclosed or partially enclosed condition of a building has no effect on the wind load calculations in Approach A (except for calculating the lateral pressures on MWFRS), but they affect wind loads related to Approach B. A total of 120 doors and windows were considered in the analysis, specifically 20 doors and 100 windows.

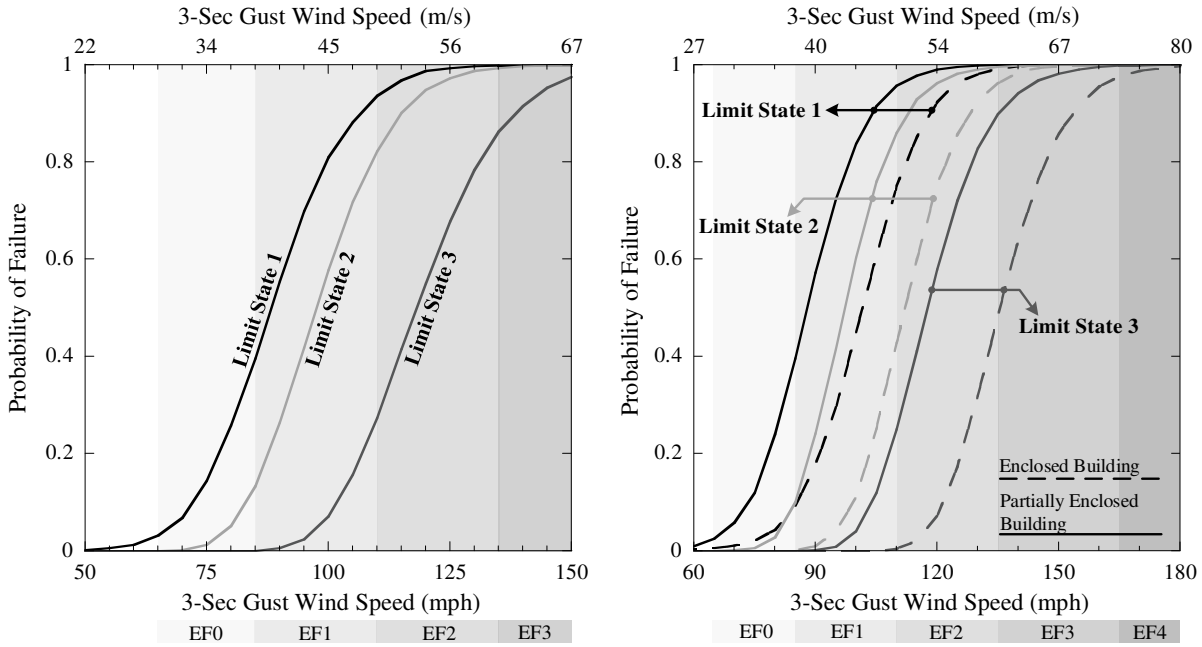

Figure 3-5. "Doors and Windows" Fragility Curves

Observations of roof covering damage in hurricanes have indicated that because of building aerodynamics the highest uplift pressures occur at roof corners, the second highest at the roof perimeter, and the remainder of the roof has even lower pressures (FEMA, 2010; van de Lindt et al., 2007). Investigation following tornadoes appears to be somewhat consistent (van de Lindt et al., 2013). Therefore, based on limited knowledge of tornado pressures compared to hurricanes at this stage there is no logical reason to use different pressure zones beyond those which are defined by ASCE 7-10 (2010) for roof wind load calculations. Figure 3-6 shows the failure probability of

roof perimeter flashing and the probability of peeling or bubbling for roof covering for the different zones indicated in this Figure. According to Figure 3-6, for Approach A fragilities, the roof covering has a 16% probability of peeling or bubbling for only a 45 m/s (100 mph) 3-sec gust wind speed in zone 1, and it has a significantly higher peeling or bubbling probability in zone 2 and 3, namely 85% and 100%, respectively. On the other hand, using Approach B will result in no failure in zone 1', and 5%, 35%, and 85% probability of failure respectively in zones 1 to 3 for peeling and bubbling of roof covering.

Roof covering fragility curves for the limit states defined in Table 3-9 (the second column in the table) are presented in Figure 3-7. In order to calculate the roof covering probability of failure, the roof area is divided into one-square-foot areas. Monte Carlo Simulation was implemented and the failure condition of each one-square-foot area was found by comparison of randomly generated values of resistance and load using roof covering resistance and wind loads statistics. It is worth mentioning that, although areas are considered to be statistically independent with respect to roof covering resistance, they are dependent on their exposure to wind loads. Therefore, in order to find the binary failure condition for the areas, all randomly generated resistances were compared to a single random demand (i.e., equal velocity pressure, q_h, for all the roof area in each run, but different wind pressure, p, for different zones) in each MCS run.

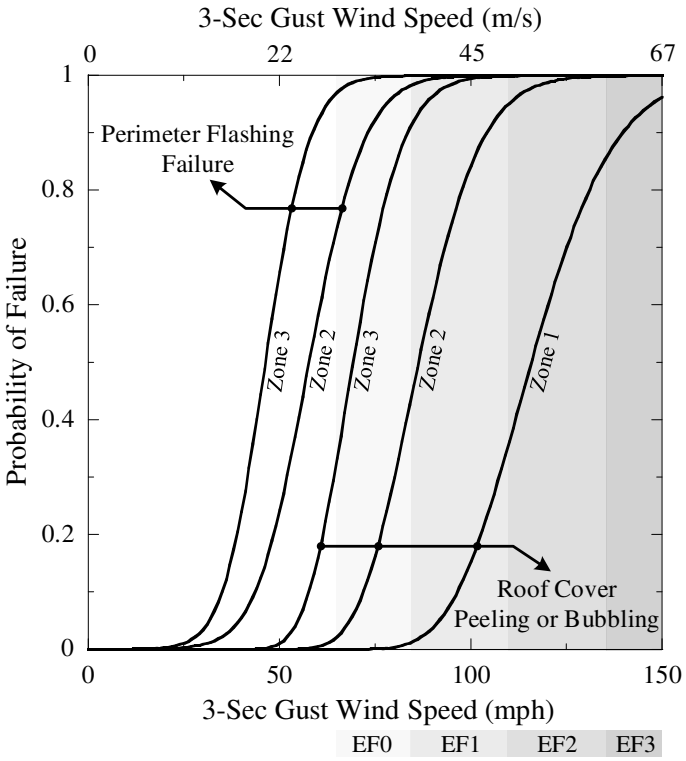

(a) Approach A Fragilities

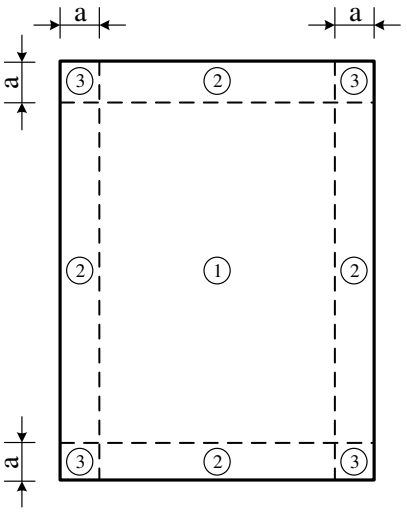

Three zones defined in ASCE 7-10 (2010) in order to find external pressure coefficients, GC_p, on components and cladding of flat roofs.

a: 10% of least horizontal dimension or 0.4h, whichever is smaller, but not less than either 4% of least horizontal dimension or 0.9 m (3 ft).

h: Eave height.

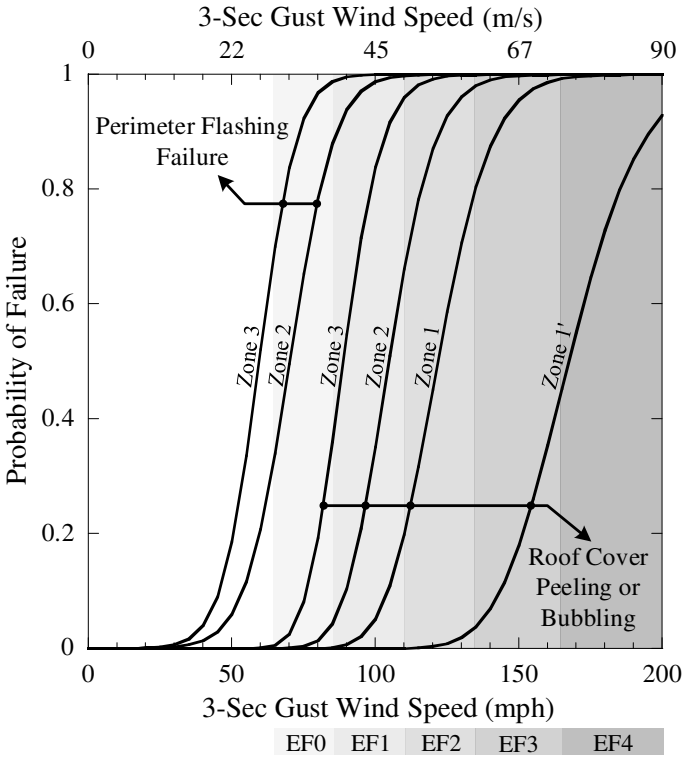

(b) Approach B Fragilities

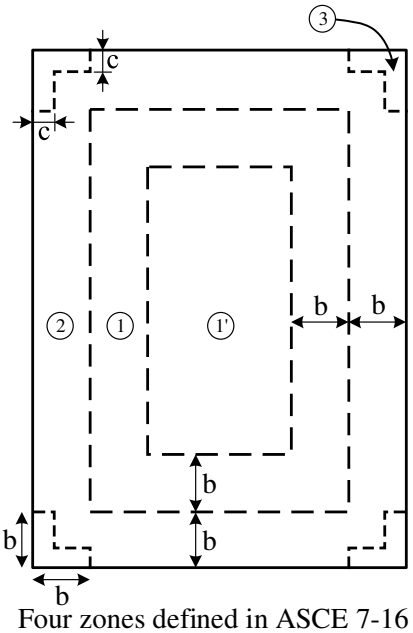

Four zones defined in ASCE 7-16 (2016) for finding external pressure coefficients, GC_p, on C&C of flat roofs .

b = 0.6h; c = 0.2h

h: Eave height.

Figure 3-6. Built-Up Roof (BUR) Covers Probability of Failure

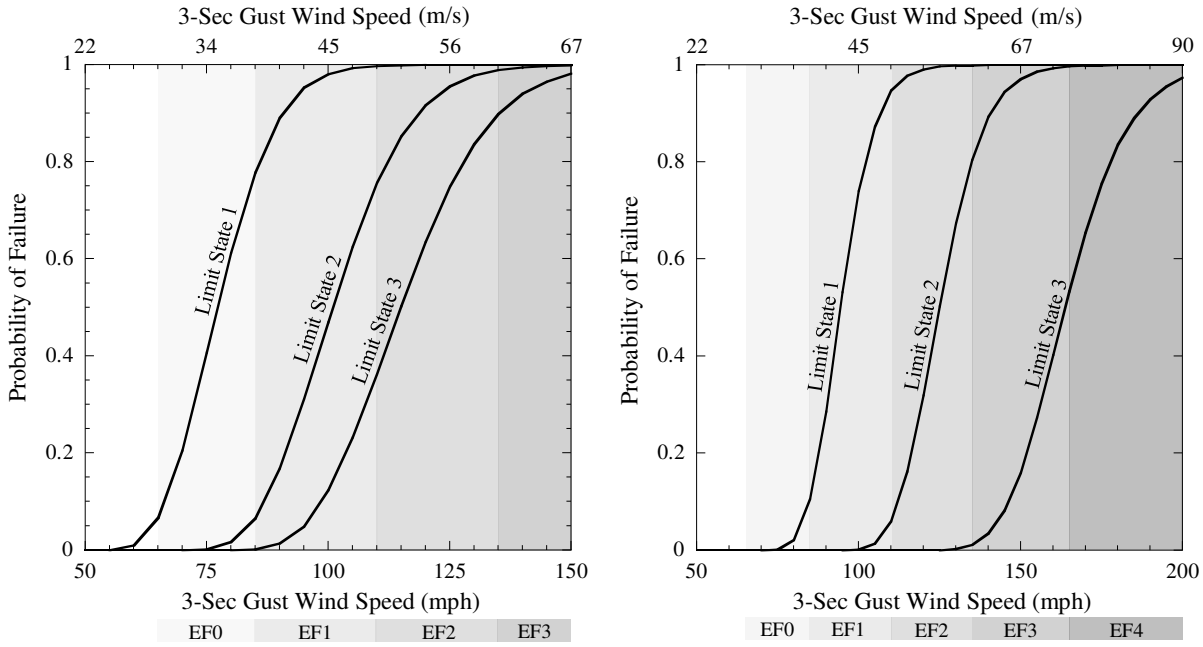

(a) Approach A Fragilities (b) Approach B Fragilities

Figure 3-7. Built-Up Roof Covers Fragility Curves

Although the external pressure coefficients for roof C&C were increased for zones 1 to 3 in ASCE 7-16 (2016), the fragilities for roof covering based on ASCE 7-16 (2016) are not necessarily greater than those based on ASCE 7-10 (2010) since a new zone (i.e., zone 1') was defined in ASCE 7-16 (2016) which has lower external pressure coefficient than the three zones in ASCE 7-10 (2010). Buildings with the smaller horizontal dimension less than 2.4h do not include zone 1', therefore their fragilities are shifted left when ASCE 7-16 (2016) coefficients are used. However, in a building which major part of the roof is zone 1', although limit state 1 and 2 may have a higher failure probability based on ASCE 7-16 (2016) coefficients, they might have a lower probability for limit state 3 since zone 1' has a significant contribution to this limit state (i.e., more than 50% of the roof covering fails).

During intense tornadoes, roofs can be lifted off and can re-settle often collapsing as the result of significant wind uplift pressure. The weight of building components (e.g., roof precast concrete

beams) helps resist uplift loads. Consequently, these components usually survive extreme winds if they are also well tied to all other building components. However, concrete roof panels that are not properly connected or reinforced have failed during severe winds. Conventionally, precast concrete beams are designed for gravity loads (i.e., positive moment), but not for the uplift loads (i.e., negative moment). Hence, the combined effects of large wind uplift forces and the beams own pre-stressing forces can result in lifting of the panels and thus negative bending failure.

Two modes were considered here for roof panel failure, which include the roof-to-wall connection failure and the bending failure of the roof deck under negative moment. The roof structural failure probability, P_{rsf}, was evaluated based on the union of these two failure modes defined as:

$$P_{rsf} = P[F_c \cup F_b] \qquad \textit{Equation 3-9}$$

where, F_c is roof-to-wall connections failure, and F_b is bending failure of the roof beam. These two events are not statistically independent since they are subjected to the same wind uplift pressure.

MCS were utilized to evaluate survivability of a beam in bending and connections, and subsequently the survivability of the roof (or the probability of roof failure). Structural analyses were conducted under the assumption of a simply supported beam (i.e., simply supported single tee beams for the boys and girls gymnasiums as well as auditorium, and simply supported hollow-core roof panels for the rest of the building) in order to find demand forces. Figure 3-8 shows probability of roof-to-wall connections failure, P_{cf}, probability of bending failure of the roof beam, P_{bf}, and probability of roof structural failure, P_{rsf}, as a function of 3-sec gust wind speed for the boys' gymnasium roof. As indicated in Figure 3-8, the fragility curves for the union of bending

failure and connection failure lies on the fragilities of bending failure, which reveals the fact that these two events are statistically dependent.

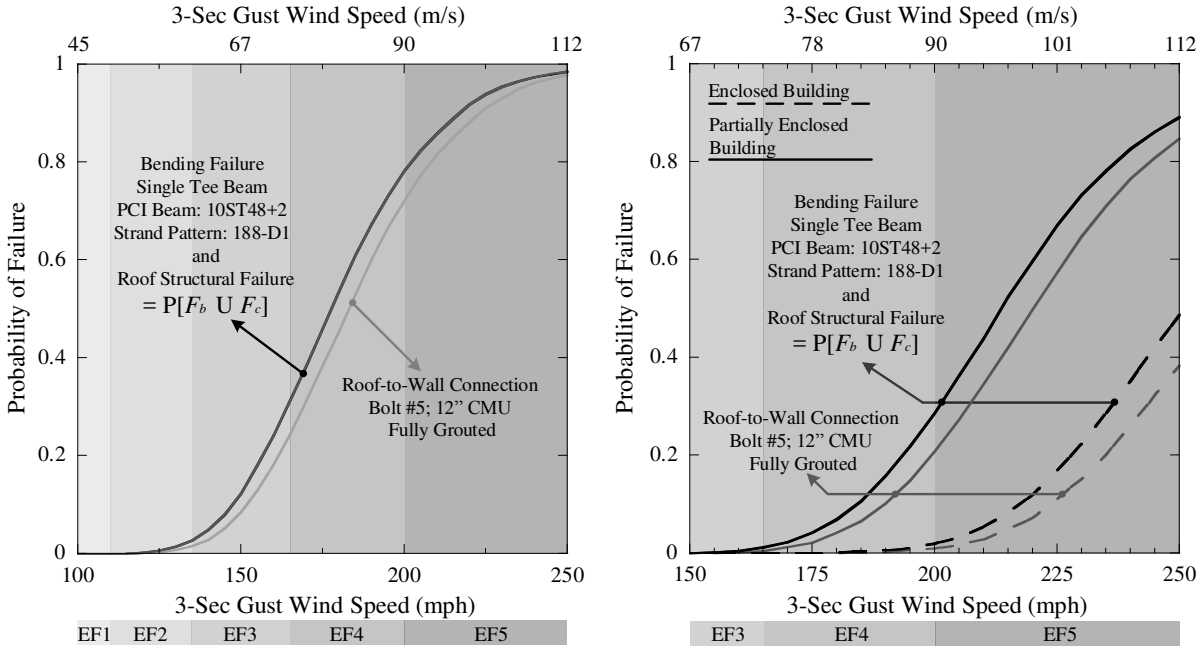

Figure 3-8. Structural Roof Fragility Curves for the Boys' Gymnasium

The main point here is that all single beams constructed in a roof are somewhat tied together such that they cannot be assumed to be statistically independent. Thus, the influence of all the roof beams is inherently applied as a simply supported beam assumption with bending failure at midspan. In other words, the curves in Figure 3-8 were based on a single tee beam, but these curves were considered to be representative of the failure probability of the roof. During the analyses for the school building here, four separate roof portions were assumed, including the boys' gym roof, girls' gym roof, auditorium roof, and the roof for the rest of the building. The total probability of roof structural failure for the school was calculated by the union of roof structural failure for these four parts which are stochastically dependent as discussed before. Figure 3-9 shows the roof structural fragilities for the school building.

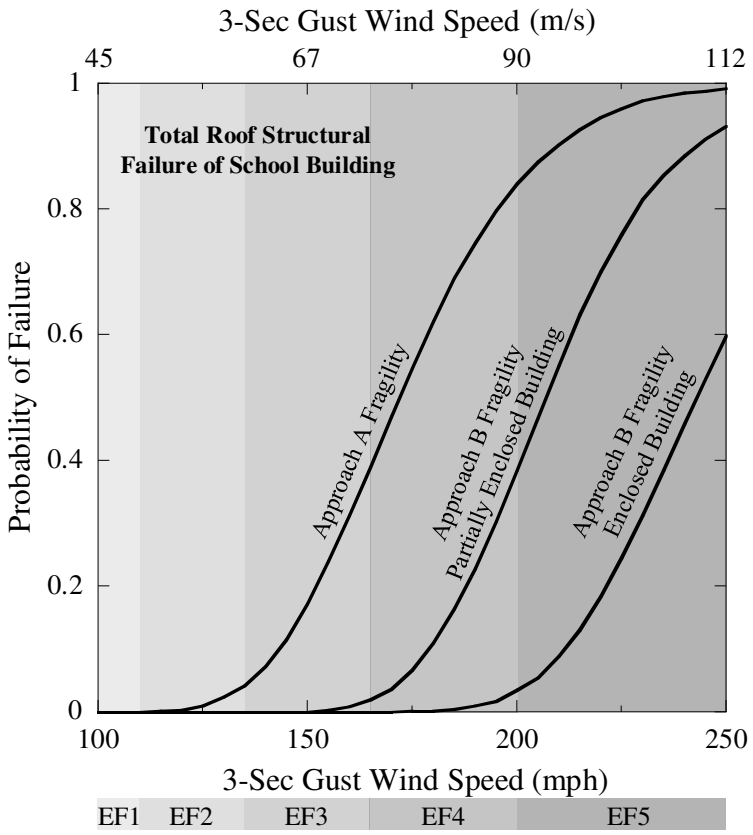

Figure 3-9. Roof Structural Fragility Curve for School Building

As mentioned before, five types of masonry construction, labeled URM1 to URM5, (with material properties summarized in Table 3-4) were considered in order to provide applicability across the range of masonry construction seen in the United States. In order to analyze masonry walls subjected to tornado wind loads, a 0.3 m (1 ft.) strip of wall was assumed as a simply supported beam typical to what is done conventionally in design to wind load for masonry walls. Four representative models were considered here for each non-load-bearing wall and load-bearing wall corresponding to each part of the school (i.e., boys' gym, girls' gym, auditorium, and the rest of the building). The school building fragilities for each non-load-bearing wall and load-bearing wall were calculated by the union of the failure of these parts. Fragility curves for the unreinforced

masonry load-bearing wall for the boys' gym are shown in Figure 3-10 for the five masonry construction types.

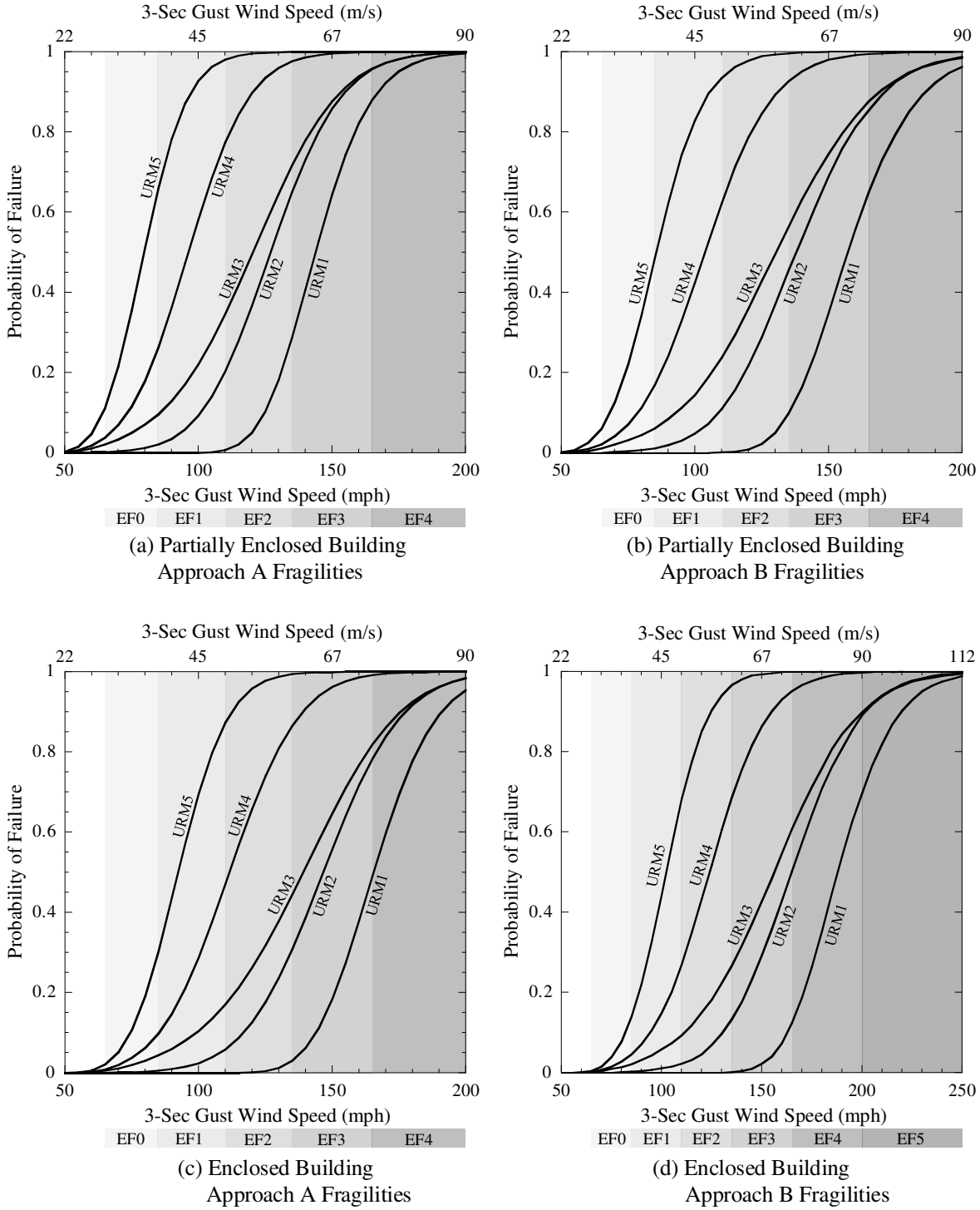

Figure 3-10. Unreinforced Masonry Load-Bearing Wall Fragility Curves for the Boys' Gymnasium (5 Different Material Assumptions)

Building-Level Fragility Curves

For the component-level fragility curves, the failure probabilities were provided for both an enclosed building and partially enclosed building conditions. Internal pressure in a building during a tornado is affected by two phenomena, wind flow into the building and static pressure drop caused by the tornado vortex. Although the latter phenomenon was not explicitly considered in tornado wind load calculations here, the effect of wind flow on internal pressure was included by considering different values for the internal pressure coefficient. If doors and windows on all sides of the building remain undamaged and closed during a tornado, wind flow into the building will be minor. However, once there is a breach in the building envelope from the failure of a door or a window, or penetration of the roof or walls, the wind pressure in the building increases. Therefore, for generating building-level fragility curves, it was assumed that any failure of doors or windows results in a partially enclosed building condition.

The building-level fragility curves for the school building with masonry construction types URM1 (i.e., fully grouted masonry construction) and URM3 (i.e., ungrouted masonry construction) are shown in Figure 3-11 based on Approach A and in Figure 3-12 based on Approach B. Since the prescribed damage states 1 and 2 in Table 3-9 are not dependent on the masonry construction type, they are the same for all construction types (i.e., URM1-URM5). On the other hand, damage states 3 and 4 have the non-load-bearing wall and load-bearing wall as one of their damage indicators; therefore, fragility curves related to these damage states are dependent on the masonry construction type, and any changes in masonry material statistics result in a change in their fragility curves. As a result, the fragility curves can cross each other when the masonry construction does not perform as well as the other damage indicators, e.g., roof covering. When a higher damage state curve (e.g., DS4) crosses a lower damage state curve (e.g., DS2) at a wind speed, it indicates that the lower

damage state is governed by the higher damage state and, therefore, does not occur at that wind speed. This type of damage has been observed in the field when, in a residential building, the roof-to-wall connection was weak and the entire roof detached prior to losing much (or any) sheathing panels (van de Lindt et al., 2012). In seismic fragility analysis, this phenomenon will typically not occur since, usually, only one engineering demand parameter is used to define damage states (e.g., inter-story drift ratio).

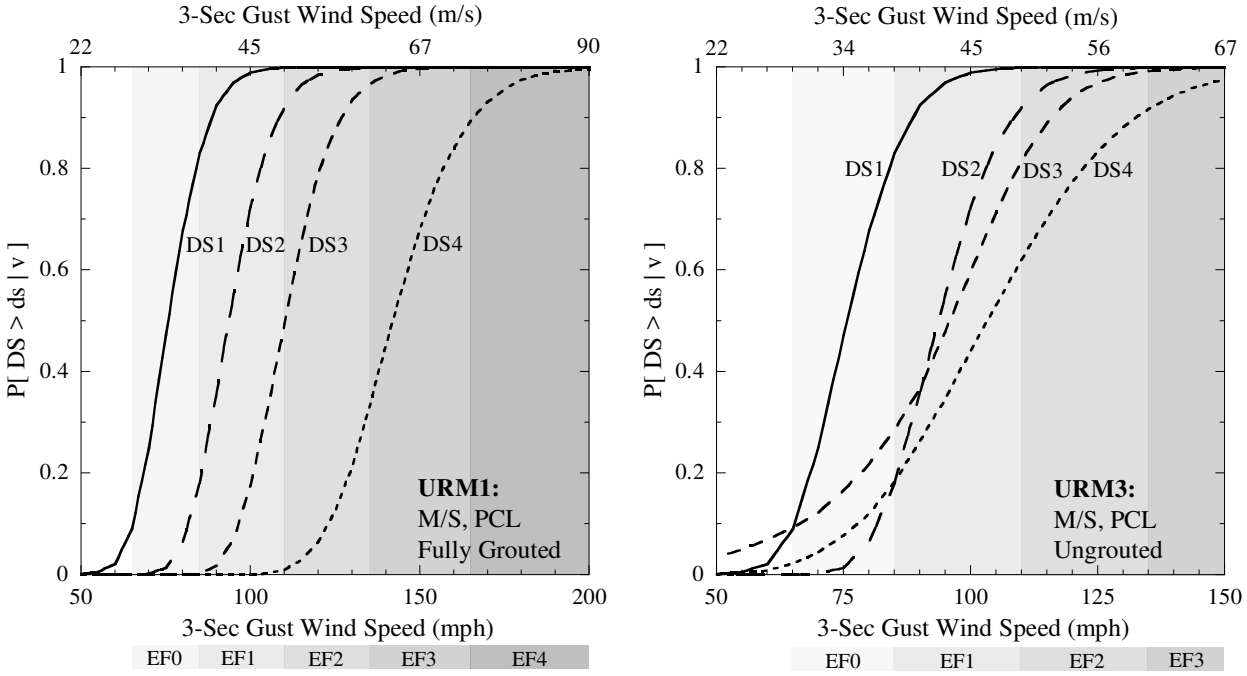

Figure 3-11. School Building Fragility Curves Based on Approach A

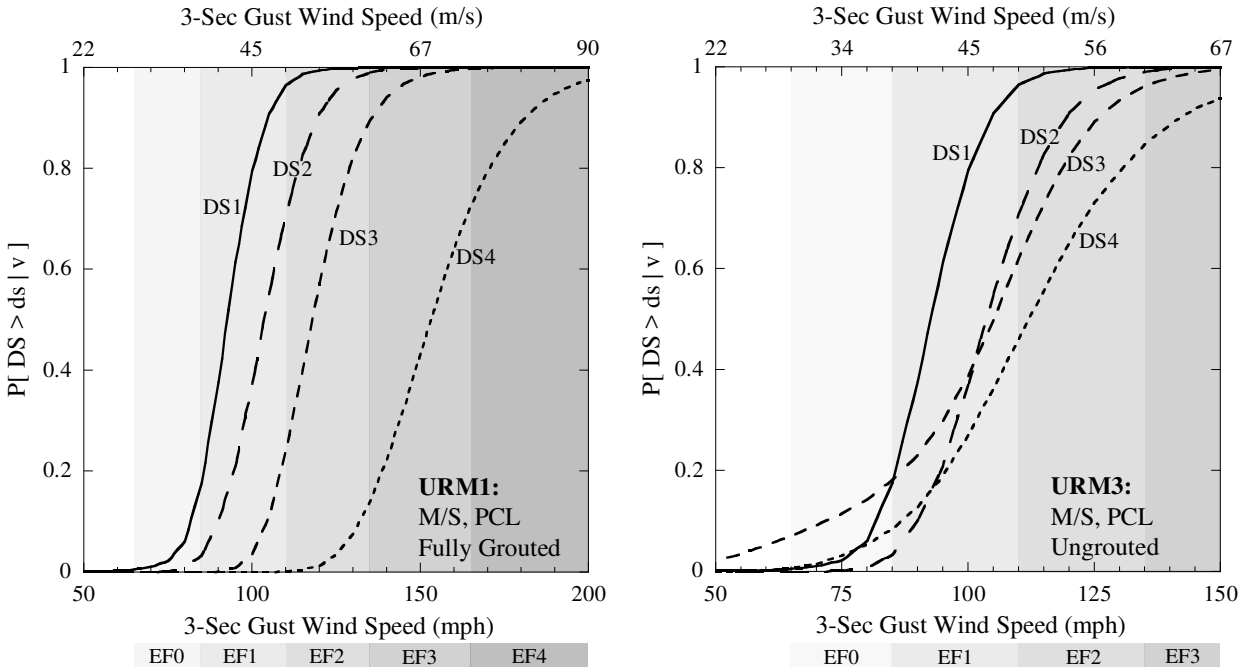

Figure 3-12. School Building Fragility Curves Based on Approach B

Fragility Parameters

The methodology described earlier was employed to generate tornado fragility curves for elementary schools, middle schools, and high schools. All the school buildings were assumed to be a one-story masonry building with flat roof and the same floor plan as shown in Figure 3-2 but with different footprint area as presented in Table 3-10. Four different construction types were considered to provide fragility parameters—namely reinforced masonry (with #3 bars at 6 inch o.c.), fully grouted unreinforced masonry, partially grouted unreinforced masonry, and ungrouted unreinforced masonry. Damage fragility parameters for school buildings are summarized in Table 3-11.

Table 3-10. The Properties of School Buildings

School Level	Building's Footprint Area (ft^2)	Number of Doors	Number of Windows	Additional Information
Elementary School	100,000	10	60	One Multi-purpose Large Room
Middle School	150,000	15	75	One Gym and One Auditorium
High School	250,000	20	100	Two Gym and One Auditorium

Table 3-11. Fragility parameters for the school buildings

Masonry Construction Type	School Level	Approach	Damage States							
			DS1		DS2		DS3		DS4	
			λ	ξ	λ	ξ	λ	ξ	λ	ξ
Reinforced Masonry with Bars #3 @ 6" and Fully Grouted	ES	A	4.29	0.12	4.56	0.11	4.70	0.11	5.14	0.13
		B	4.47	0.09	4.66	0.09	4.77	0.10	5.31	0.11
	MS	A	4.32	0.12	4.55	0.11	4.70	0.10	5.08	0.12
		B	4.51	0.09	4.66	0.11	4.77	0.10	5.19	0.12
	HS	A	4.33	0.12	4.54	0.11	4.70	0.11	5.07	0.12
		B	4.53	0.09	4.64	0.11	4.77	0.10	5.18	0.13
Unreinforced Masonry Fully Grouted	ES	A	4.29	0.12	4.56	0.11	4.70	0.11	5.07	0.12
		B	4.47	0.09	4.66	0.09	4.77	0.10	5.18	0.12
	MS	A	4.32	0.12	4.55	0.11	4.70	0.10	4.98	0.12
		B	4.51	0.09	4.66	0.11	4.77	0.10	5.06	0.12
	HS	A	4.33	0.12	4.54	0.11	4.70	0.11	4.96	0.12
		B	4.53	0.10	4.64	0.11	4.77	0.10	5.03	0.12
Unreinforced Masonry Partially Grouted	ES	A	4.29	0.12	4.56	0.11	4.69	0.11	4.93	0.16
		B	4.47	0.09	4.66	0.09	4.76	0.10	5.01	0.17
	MS	A	4.32	0.12	4.55	0.11	4.66	0.11	4.81	0.17
		B	4.51	0.09	4.66	0.11	4.75	0.11	4.89	0.16
	HS	A	4.33	0.12	4.54	0.11	4.64	0.12	4.76	0.16
		B	4.53	0.10	4.64	0.11	4.73	0.12	4.83	0.16
Unreinforced Masonry Ungrouted	ES	A	4.29	0.12	4.56	0.11	4.64	0.14	4.82	0.23
		B	4.47	0.09	4.66	0.09	4.73	0.13	4.91	0.22
	MS	A	4.32	0.12	4.55	0.11	4.59	0.17	4.69	0.21
		B	4.51	0.09	4.66	0.11	4.68	0.16	4.78	0.20
	HS	A	4.33	0.12	4.54	0.11	4.54	0.19	4.63	0.21
		B	4.53	0.10	4.64	0.11	4.63	0.18	4.72	0.19

λ = ln(median) (medians are in mph), and ζ = logarithmic standard deviation.

FRAGILITY CURVES FOR COMMUNITY COMPONENTS

The tornado fragility methodology developed in this dissertation has been used in several studies to investigate fragility curves for different types of buildings including: school buildings (Masoomi and van de Lindt, 2016), tilt-up big-box buildings (Koliou et al., 2017), wood-frame residential buildings (Masoomi et al., 2017a), light and heavy industrial buildings, fire stations, hospitals, office buildings, shopping centers, strip malls, community centers, government buildings, and mobile homes (Memari et al., 2017). Masoomi et al. (2017a) studied wind performance enhancement strategies for five wood-frame residential building archetypes in terms of fragility curves. They investigated nine construction product combinations for each building archetype as performance enhancement strategies. Memari et al. (2017) developed tornado fragility curves for 19 building types to provide a minimum portfolio of fragility functions representative of the buildings within a typical community in the United States.

In this dissertation, the residential buildings in pseudo-Norman were categorized into six types, including: 1-story gable-roof wood-frame buildings (two sizes), 2-story hip-roof wood-frame buildings, 2-story gable-roof wood-frame buildings (two sizes), and mobile homes. The fragility curves for wood-frame buildings and mobile homes were provided by Masoomi et al. (2017a) and Memari et al. (2017), respectively. Furthermore, ten building types were considered for workplace buildings in pseudo-Norman, including: industrial buildings (two sizes) (Memari et al., 2017), tilt-up precast concrete (i.e., big-box) buildings (two sizes) (Koliou et al., 2017), 1-story masonry buildings (four sizes) (Memari et al., 2017), and reinforced concrete buildings (a 2-story and a 4-story buildings) (Memari et al., 2017). Moreover, all school buildings in pseudo-Norman were assumed to have masonry construction. High schools were considered to be a 1-story reinforced masonry building with one auditorium and two gymnasiums, while middle schools and elementary

schools were modeled as unreinforced masonry buildings with fully grouted and ungrouted construction, respectively. Selection of the level of grouting and reinforcement was arbitrary and intended to represent different design code eras. One auditorium and one gymnasium were considered for the middle schools, while elementary schools were assumed to have only one long-span multi-purpose area.

Lopez et al. (2009) studied vulnerability of electrical facilities under wind hazard in Mexico and proposed wind fragility curves for a typical electrical substation and transmission tower. Although their study was related to straight-line winds, it was implemented here to represent the performance of the components of the EPN during a tornado. Therefore, the fragility parameters for a substation with a design wind speed of 56 m/s (125 mph) in Lopez et al. (2009) were used in this dissertation to represent the performance of both distribution and transmission substations for damage state 4 (DS4). In addition, DS1-DS3 for substations were assumed to have the same logarithmic standard deviation as DS4, but with median wind speed equal to 55%, 65%, and 80% of the median for DS4, respectively, since data for these are not yet available. Additionally, fragility parameters for a tall tower with a design wind speed of 45 m/s (100 mph) in Lopez et al. (2009) were extracted to be utilized in this dissertation as representative of transmission towers. Sub-transmission towers were assumed to have a fragility curve with the same logarithmic standard deviation but with 90 percent of the median wind speed for the fragility curve of the transmission towers. One damage state (i.e., DS4) was assumed for both transmission and sub-transmission towers in this dissertation in that if these towers experience any structural damage as the result of a tornado, they are replaced with a new tower. Furthermore, for the components of the WSN, the fragility parameters were assumed in this dissertation based on post-tornado observations because of a lack of information

on their performance in tornadoes. The fragility parameters for the community components in pseudo-Norman are tabulated in Table 3-12.

REPAIR TIME

The occurrence of any damage state for a community component was assumed to disturb the functionality of that component for a period of time. This non-functionality affects the functionality of other components that are supplied by the damaged component. In order to capture the effect of different damage states on functionality, each damage state for each community component was linked to a corresponding repair time. Therefore, the occurrence of a greater damage state for a component means that it takes more time to repair and, therefore, is non-functional for a longer time period.

Table 3-13 presents repair time statistics for the community components in pseudo-Norman for DS1 to DS4, which are based on a Weibull distribution. The repair time values for buildings, substations, water towers, and water treatment plants were extracted from FEMA (2003) but a Weibull distribution was fit to the corresponding normal distribution prescribed in FEMA (2003) due to the fact that time is a non-negative variable. Moreover, the values related to DS3 and DS4 for buildings were modified from FEMA (2003) based on post-disaster site investigations and recovery processes. In addition, the permitting time for buildings and repair time for transmission (or sub-transmission) towers were assumed here based on past tornado observations.

Table 3-12. Fragility parameters for the community components in pseudo-Norman

Network	Component	DS1		DS2		DS3		DS4	
		m	ξ	m	ξ	m	ξ	m	ξ
Residential Buildings	Small, 1-story	39.6 (88.7)	0.14	47.0 (105.1)	0.12	53.5 (119.7)	0.11	51.9 (116.2)	0.15
	Small, 2-story	36.6 (81.9)	0.13	42.9 (96.1)	0.12	49.9 (111.6)	0.11	54.6 (122.1)	0.14
	Medium, 1-story	37.0 (82.7)	0.13	43.4 (97.0)	0.12	50.4 (112.7)	0.11	61.6 (137.7)	0.12
	Medium, 2-story	41.7 (93.2)	0.13	47.9 (107.2)	0.12	54.6 (122.1)	0.11	61.6 (137.7)	0.14
	Large, 2-story	42.5 (95.1)	0.13	48.4 (108.3)	0.12	53.5 (119.7)	0.11	47.5 (106.2)	0.15
	Mobile Home	35.5 (79.5)	0.09	42.2 (94.4)	0.09	49.2 (110.0)	0.11	52.7 (117.8)	0.12
Workplace Buildings	Light Industrial	34.6 (77.5)	0.10	41.9 (93.7)	0.09	45.4 (101.5)	0.09	49.2 (110.0)	0.09
	Heavy Industrial	40.2 (90.0)	0.10	45.4 (101.5)	0.14	60.0 (134.3)	0.10	71.2 (159.2)	0.19
	Small Big-box	29.1 (65.0)	0.08	36.6 (81.9)	0.09	69.4 (155.3)	0.11	76.7 (171.6)	0.10
	Large Big-box	34.1 (76.3)	0.09	40.9 (91.4)	0.08	65.4 (146.2)	0.10	75.9 (169.9)	0.10
	Small Unreinforced Masonry	31.3 (70.1)	0.09	44.5 (99.5)	0.09	52.2 (116.8)	0.09	69.1 (154.5)	0.18
	Medium Unreinforced Masonry	36.4 (81.5)	0.13	40.7 (90.9)	0.11	52.2 (116.8)	0.10	66.4 (148.4)	0.21
	Large Reinforced Masonry	32.6 (73.0)	0.12	42.7 (95.6)	0.11	49.2 (109.9)	0.11	71.2 (159.2)	0.12
	Extra Large Reinforced Masonry	33.6 (75.2)	0.12	42.3 (94.6)	0.11	49.2 (109.9)	0.10	71.9 (160.8)	0.12
	2-story Reinforced Concrete	32.3 (72.2)	0.08	40.7 (90.9)	0.09	48.2 (107.8)	0.08	57.7 (129.0)	0.11
	4-story Reinforced Concrete	41.1 (91.8)	0.13	45.8 (102.5)	0.09	65.0 (145.5)	0.08	77.1 (172.5)	0.08
School Network	High School	41.5 (92.8)	0.09	46.3 (103.5)	0.11	52.7 (117.9)	0.10	79.4 (177.7)	0.13
	Middle School	40.6 (90.9)	0.09	47.2 (105.6)	0.11	52.7 (117.9)	0.10	70.4 (157.6)	0.12
	Elementary School	39.1 (87.4)	0.09	47.2 (105.6)	0.09	50.6 (113.3)	0.13	60.6 (135.6)	0.22
Electric Power Network	Transmission Substation and Distribution Substation	33.4 (74.8)	0.20	39.5 (88.4)	0.20	48.6 (108.8)	0.20	60.8 (136.0)	0.20
	Transmission Tower	-	-	-	-	-	-	60.8 (136.0)	0.12
	Sub-transmission Tower	-	-	-	-	-	-	55.9 (125.0)	0.12
Water Supply Network	Water Tower	34.4 (77.0)	0.15	40.7 (91.0)	0.15	50.1 (112.0)	0.15	62.6 (140.0)	0.15
	Water Treatment Plant	36.9 (82.5)	0.15	43.6 (97.5)	0.15	53.6 (120.0)	0.15	67.1 (150.0)	0.15

m: median, ξ: log-std. Medians are in m/s along with mph values in parentheses.

Table 3-13. Repair time statistics for community components in pseudo-Norman

Network	Component/Description	DS1		DS2		DS3		DS4	
		m	COV	m	COV	m	COV	m	COV
Residential Buildings	Repair Time	5	0.2	20	0.2	90	0.2	180	0.2
	Permitting Time	2	0.5	7	0.5	14	0.5	30	0.5
Workplace Buildings	Repair Time	5	0.2	20	0.2	90	0.5	180	0.5
	Permitting Time	2	0.5	5	0.5	10	0.5	30	0.5
School Buildings	Repair Time	5	0.2	20	0.2	180	0.2	730	0.2
	Permitting Time	2	0.5	10	0.5	30	0.5	30	0.5
Electric Power Network	Transmission Substation and Distribution Substation	1	0.5	3	0.5	7	0.5	30	0.5
	Transmission Tower	-	-	-	-	-	-	2	0.5
	Sub-transmission Tower	-	-	-	-	-	-	1	0.5
Water Supply Network	Water Tower	1.2	0.35	3.4	0.7	104	0.7	165	0.7
	Water Treatment Plant	0.9	0.35	1.9	0.6	36	0.7	98	0.6

m: mean (days).

CHAPTER 4: HAZARD MODELING AND SPATIAL DAMAGE SIMULATION

HAZARD MODELING—TORNADO PATH SIMULATION

The Enhanced Fujita (EF) scale rates the intensity of a tornado based on the degree of damage (DOD) observed following the event. The EF scale was introduced and implemented in 2007 in order to cope with an inconsistent rating of tornadoes when the Fujita (F) scale was used. The F scale had limitations such as a lack of damage indicators (DI) and neglecting construction quality and variability (McDonald and Mehta, 2006). Based on the EF scale, tornadoes are categorized into six categories ranging from EF0, minor or no damage, to EF5, which is the total destruction of buildings. Although a tornado is rated as one category, e.g., EF3, there are variations of its intensity along both the path width and length. Usually, the intensity of a tornado increases following its touchdown point as it moves through its path, and at some point the intensity starts decreasing until the tornado dissipates at its end point. Based on the observations of damage during past tornadoes, tornado intensity is frequently the highest at the center and gradually decreases along its width perpendicularly outward from the tornado centerline (Reinhold and Ellingwood, 1982). This is consistent with a Rankine vortex model and the tornado damage contours developed from the Tuscaloosa and Joplin tornado investigations. Therefore, each tornado given a particular EF rating includes all the lower EF intensities in addition to the main EF intensity at different spatial regions within its path (e.g., an EF4 tornado includes five sub-EF intensities ranging from EF0 to EF4). Considering these features, Standohar-Alfano and van de Lindt (2014) proposed the gradient method to simulate a tornado path. This method, as shown in Figure 4-1, models the highest intensity at the center and gradually decreases the intensity outward by idealizing a tornado path as a long rectangle which is occupied with several sub-rectangles corresponding to each sub-

EF intensity. However, a tornado path can have any shape (not necessarily a straight line) between its start (touchdown) and end (lift-off) points with different width at any point along its path. Because no two tornadoes will have the same wind field and subsequent damage path, an idealized version was found reasonable for implementation in this dissertation.

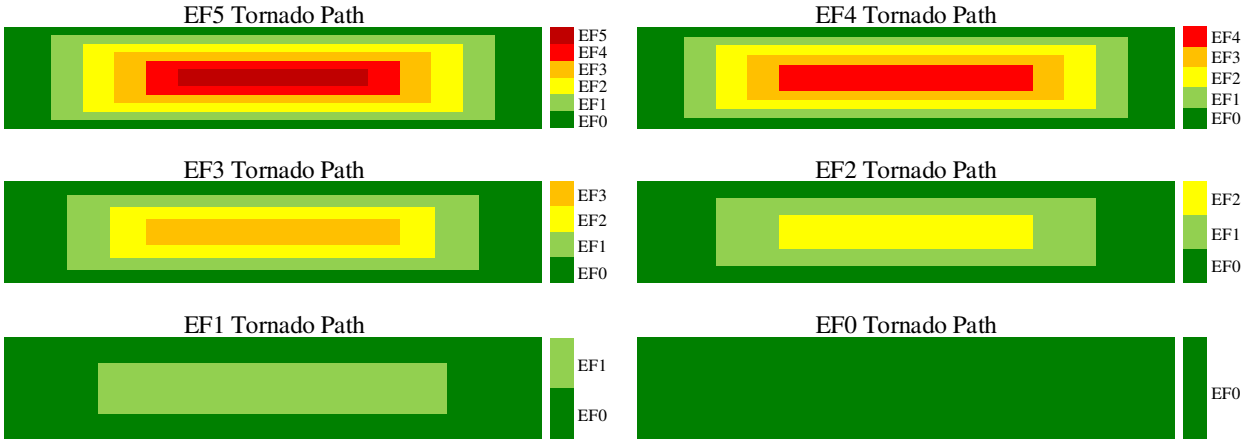

Figure 4-1. Tornado path simulation using the gradient method

Using the gradient method for simulating tornado paths in probabilistic studies requires statistics for tornado path length and width. Past tornado data is available from the Storm Prediction Center (SPC), and includes tornado properties such as the intensity of the tornado, and the path length and width as well as additional information. The length is defined as the closest distance (straight line) between the touchdown point and where the tornado lifts off. The width is measured at the widest point along a tornado path and is assumed to be constant along the entire path. Brooks (2004) studied the statistics of tornado path length and width and found that the Weibull distribution provides a good fit to the path lengths and widths of reported tornadoes in the SPC database from 1950 to 2001. The Weibull distribution parameters for tornado path width and length were updated here based on the reported tornadoes in SPC database until 2014. Although data on tornadoes have been collected from 1950 to present, the Fujita scale was first developed and implemented in 1973. Therefore, a dataset including only tornadoes from 1973 to 2014 was used here to estimate the

statistics for tornado path length and width. As shown in Figure 4-2, a Weibull distribution can be used to statistically represent tornado path length and width. Moreover, it is noted that considering a correlation between tornado path length and width was suggested in this dissertation based on the analysis of the SPC database. Statistics for tornado width and length as well as their correlation coefficient are presented in Table 4-1 for each EF scale.

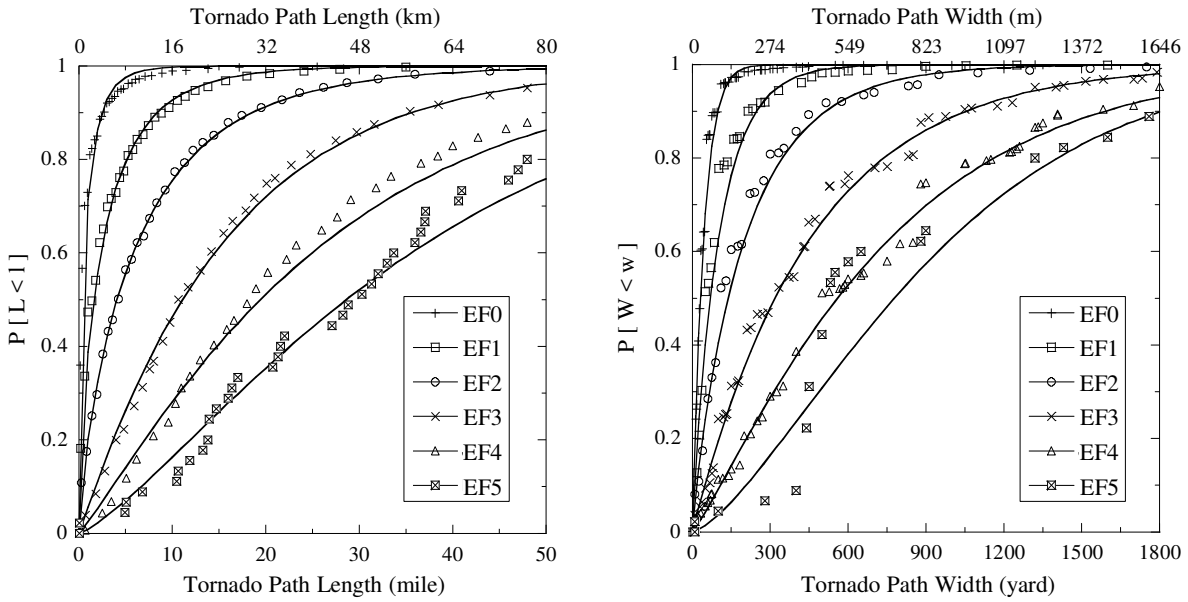

Figure 4-2. Empirical (dots) and fitted Weibull cumulative distribution for (a) tornado path length, and (b) tornado path width

Table 4-1. Distribution parameters for tornado path length and width

EF Scale	Marginal Weibull Parameters				Correlation Coefficient
	Length, km (mile)		Width, km (mile)		
	Scale Parameter (A)	Shape Parameter (B)	Scale Parameter (A)	Shape Parameter (B)	
EF0	1.155 (0.718)	0.675	0.041 (0.025)	1.043	0.225
EF1	4.299 (2.671)	0.727	0.093 (0.058)	0.943	0.250
EF2	10.484 (6.514)	0.796	0.188 (0.117)	0.912	0.253
EF3	25.533 (15.865)	1.031	0.420 (0.261)	1.004	0.180
EF4	43.448 (26.997)	1.117	0.703 (0.437)	1.150	0.307
EF5	61.274 (38.074)	1.291	0.921 (0.572)	1.423	0.367

Although the National Weather Service (NWS) surveys include the tornado rating, path length, maximum path width, touchdown and lift-off points; they do not typically report details regarding the variation of intensity along the path width and length. Therefore, there is not enough data to obtain comprehensive statistics for the gradient of tornado intensity along its path length and width. However, Standohar-Alfano and van de Lindt (2014) used the damage surveys after the tornadoes on April 27, 2011, Tuscaloosa, Alabama, and on May 22, 2011, Joplin, Missouri, to estimate the percentage of width for each intensity along path width. Moreover, the detailed survey after the April 3-4, 1974, super outbreak and other significant outbreaks of the time was used to estimate the percentage of each intensity along tornado length (Schaefer et al., 1986; Standohar-Alfano and van de Lindt, 2014). These deterministic values for variation of intensity along width and length of tornado paths are presented in Table 4-2, which are used for the width and length of sub-rectangles in Figure 4-1 as the percentage of the total width and length of tornado path.

Table 4-2. The percentage of width and length corresponding to each sub-EF scale (Data from Standohar-Alfano and van de Lindt, 2014)

EF Category	Width Percentage	Length Percentage
EF5 Tornado Path		
EF5	27.3	14.9
EF4	19.9	18.5
EF3	13.6	24.2
EF2	13.8	18.9
EF1	12.7	10.3
EF0	12.7	13.2
Total	100	100
EF4 Tornado Path		
EF4	27.3	21.2
EF3	18.7	21.0
EF2	19.0	27.8
EF1	17.5	15.8
EF0	17.5	14.2
Total	100	100
EF3 Tornado Path		
EF3	33.8	32.1
EF2	20.2	31.8
EF1	26.2	24.4
EF0	19.8	11.7
Total	100	100
EF2 Tornado Path		
EF2	47.5	36.7
EF1	31.4	35.2
EF0	21.1	28.1
Total	100	100
EF1 Tornado Path		
EF1	62.5	42.6
EF0	37.5	57.4
Total	100	100

Therefore, the parameters that are needed to simulate a tornado path based on the gradient method are the tornado path direction, length, width, and the coordinate of its center point. Depending on the type of study being conducted, each of these parameters can be considered either as a random variable or as deterministic. For the analyses in this dissertation, the tornado path direction was considered as a random variable with uniform distribution between 0 and π. Moreover, it was assumed that all the simulated tornado paths have a center point located randomly in the predefined boundary of pseudo-Norman (i.e., the area of 14.5 km by 12.9 km that was used to define the model of pseudo-Norman). Additionally, since the tornado path length and width are correlated

random variables with known marginal distributions, the Gaussian copula model (Haas, 1999; Limbourg et al., 2007) was utilized for generating the correlated random deviates for tornado path length and width based on the parameters provided in Table 4-1. In order to generate correlated random deviates X_1 and X_2 with arbitrary and possibly different marginal distributions (with the CDF of Ω_1 and Ω_2), and with correlation coefficient ρ; the following three-step transformation is used:

$$Z = [Z_1, Z_2] \sim N\left([0,0], \begin{bmatrix} 1 & \rho \\ \rho & 1 \end{bmatrix}\right) \qquad \textit{Equation 4-1}$$

$$U = [U_1, U_2] = [\Phi(Z_1), \Phi(Z_2)] \qquad \textit{Equation 4-2}$$

$$X = [X_1, X_2] = [\Omega_1^{-1}(U_1), \Omega_2^{-1}(U_2)] \qquad \textit{Equation 4-3}$$

where Z_1 and Z_2 are two correlated random deviates generated from a bivariate normal distribution, and Φ is the standard normal cumulative distribution function (CDF). Finally, a simulated EF4 tornado path that strikes pseudo-Norman is shown in Figure 4-3 as an example.

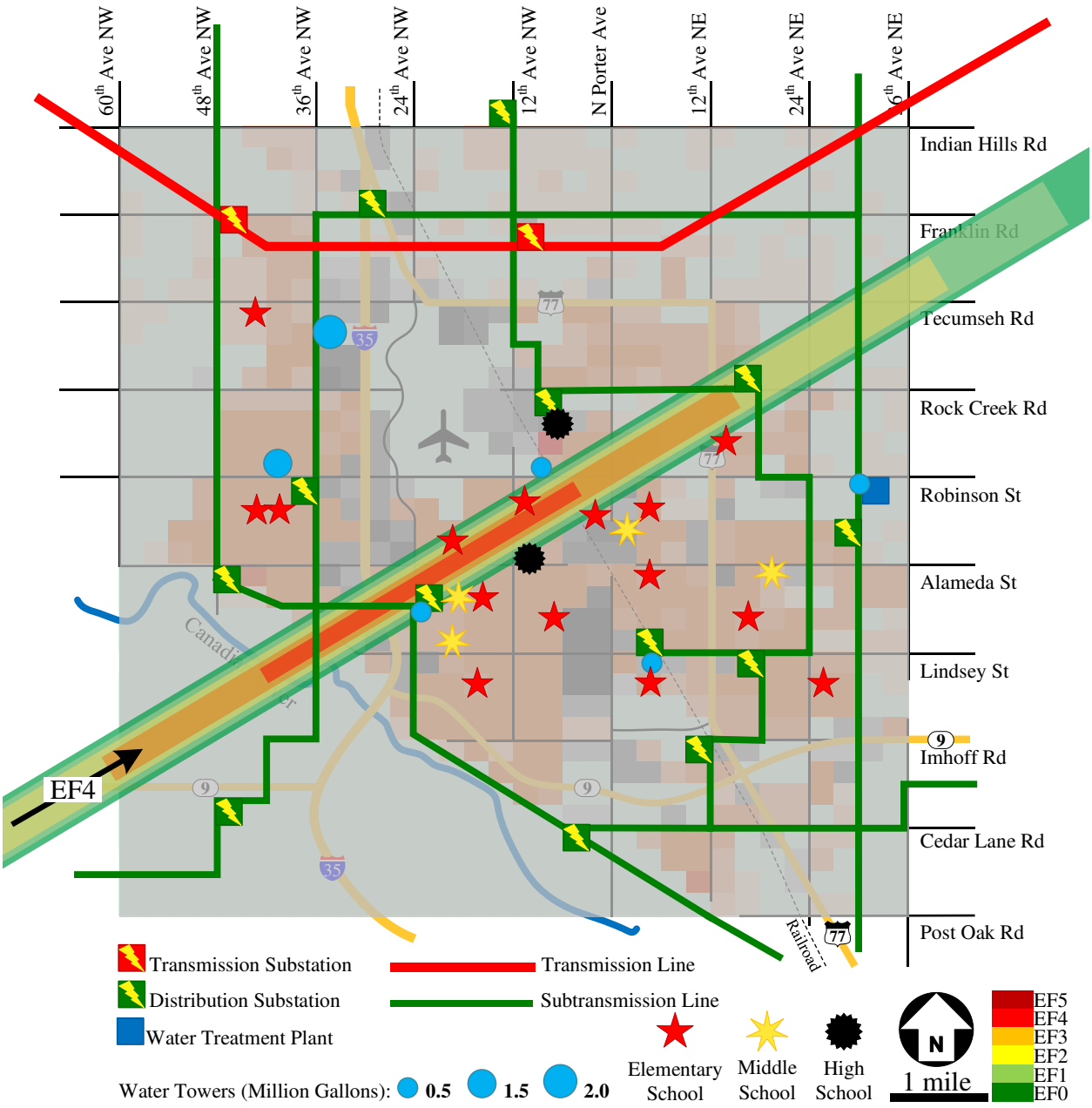

Figure 4-3. Schematic of an EF4 tornado path through pseudo-Norman

HAZARD-INDUCED SPATIAL DAMAGE SIMULATION

After simulating the tornado path, the community components that are located within the path (termed in-path components hereafter) are identified along with the associated EF intensity acting on them. According to the location of each in-path component in the tornado path, as shown in

Figure 4-4, a wind speed is assigned to the component, which is associated with the EF intensity acting on the component. Although a deterministic wind speed (i.e., the mean value of the wind speed range for each EF scale) was used in this dissertation to be representative of each EF intensity, a random wind speed can be utilized for each EF intensity by introducing a uniform distribution (or other relevant distributions) on the wind speed ranges presented in Table 4-3 for EF scales. Although a tornado path might cover a large number of components through a community, all the in-path components do not necessarily experience damage. The damage level for each community component was classified into five categories, namely, no damage, DS1, DS2, DS3, and DS4. Therefore, statistically, for each tornado path, there are numerous possible scenarios for the damage distribution over the area of the community covered by the tornado path.

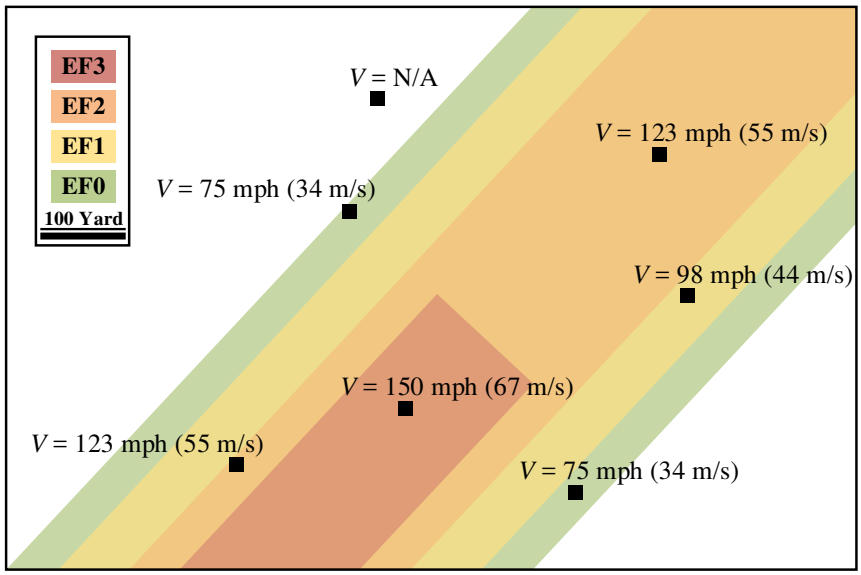

Figure 4-4. The in-path components and the corresponding tornado intensities acting on them

Table 4-3. The range of wind speed for each EF scale and the corresponding mean values

EF Scale	3-Sec Gust Wind Speed, m/s (mph)	
	Wind Speed Range (McDonald and Mehta, 2006)	Mean Value
EF0	29-38 (65-85)	34 (75)
EF1	39-49 (86-110)	44 (98)
EF2	50-60 (111-135)	55 (123)
EF3	61-74 (136-165)	67 (150)
EF4	75-89 (166-200)	82 (183)
EF5	>89 (>200)	101 (225)

In order to simulate a spatial damage scenario for the community components, random deviates generated based on the standard uniform distribution, *R*, were assigned to each in-path component and were compared to the probabilities for DS1 to DS4 of the component at the assigned wind speed to the component (the component's fragility curves). As shown in Figure 4-5, if *R* is less than P_{DS4}, the component is in DS4 level; if *R* is between P_{DS4} and P_{DS3}, it is in DS3; if *R* is between P_{DS3} and P_{DS2}, it is in DS2; if *R* is between P_{DS2} and P_{DS1}, it is in DS1; and the component is safe if *R* is greater than P_{DS1}.

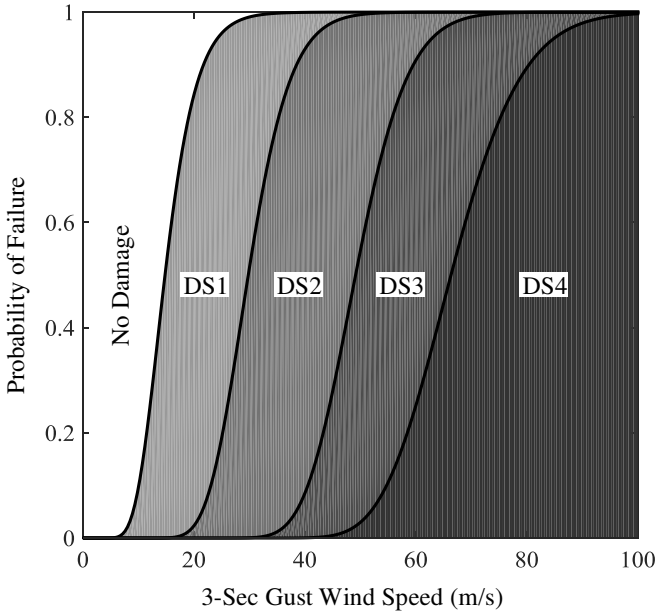

Figure 4-5. Regions corresponding to each damage state for defining damage level for each in-path component

CHAPTER 5: COMMUNITY RESTORATION ANALYSIS[1]

INTRODUCTION

A community as a complex system includes highly coupled networks. Any malfunction in a network or its components can result in a cascading failure, which, in turn, can cause a loss of functionality in all or part of the community. For example, the Northeast blackout of 2003 was a widespread power outage which affected about 50 million people in eight U.S. states and two Canadian provinces (Farmer and Allen, 2006) but originated as a point source. Therefore, in addition to the assessment of direct losses (i.e., injuries, fatalities, and property damages), indirect losses as a consequence of cascading failures (i.e., negative economic and social consequences) are key problems that need to be studied to enhance community resilience. Several studies have investigated cascading failures as a result of damage to infrastructure systems in the aftermath of disasters (e.g., Argyroudis et al., 2015; Dong and Frangopol, 2017; Javanbakht and Mohagheghi, 2014; Ouyang and Dueñas-Osorio, 2014; Scherb et al., 2015; Zhang et al., 2016). However, the extent of the time interval in which these failures remain within the community has a significant importance on the amount of indirect losses, which can be quantified by modeling the community restoration analysis.

Ouyang et al. (2012) studied the performance of an electric power network under random hazards and hurricane hazards. They investigated several resilience-improvement strategies by considering the effect of different numbers of recovery resource units on the restoration process. Ramachandran et al. (2015) investigated the community restoration time by accounting for the

[1] This section is based on the paper: Masoomi, H., & van de Lindt, J. W. (2018). Restoration and functionality assessment of a community subjected to tornado hazard. *Structure and Infrastructure Engineering*, 14(3), 275-291.

repair time and priorities for all components within transportation, electricity, communication, and water networks. However, they did not provide any information regarding the return to functionality during the restoration process. Çagnan and Davidson (2004) summarized the previous lifeline restoration models into two empirically based approaches, namely statistical curve fitting and deterministic resource constraint, as well as two theoretical approaches, namely Markov processes and network models. They also proposed the discrete event simulation (DES) method, a simulation-based model for post-disaster restoration process, which was built based on previous studies yet overcomes several limitations thereof. The method enables consideration of rules, constraints, and decisions from utility companies for restoration process such as recovery prioritization plans, mutual aid agreements, and number of available repair crews and materials. Moreover, uncertainties associated with the parameters such as inspection time, repair time, and amount of available resources are taken into account by defining these parameters as random variables with specified probability distributions. Çagnan and Davidson (2007) employed the DES approach to simulate the post-earthquake restoration process for the electric power system of the Los Angeles Department of Water and Power (LADWP) and simulated the restoration curve for the Northridge earthquake. Çagnan et al. (2006) utilized the DES approach and investigated several restoration improvement strategies to boost the seismic resilience of the LADWP electric power system. Moreover, Tabucchi et al. (2010) applied the DES method to the water supply system of the LADWP to simulate the restoration curve and spatial distribution of the restoration in the Northridge earthquake.

In this dissertation, the DES approach was extended and implemented to pseudo-Norman, a community built up of highly coupled networks that were modeled with the network based approach after Norman, Oklahoma. Therefore, spatial and temporal depiction of the restoration

process can be easily achieved such that one can generate/estimate restoration curve/time for each region of the community besides developing/estimating only one curve/time for the entire community or network. Using the network based approach along with the DES approach enables consideration of the effect of cascading failures in the analysis such that if a component has been repaired physically or has no damage, it remains non-functional until all its suppliers are recovered and functional. Moreover, it allows taking into account dependencies as well as priorities among networks and network components. It is noted that several studies have been done to optimize post-disaster restoration strategies (e.g., Bocchini and Frangopol 2010; González et al., 2016; Noda, 1993; Nozhati et al., 2018a and 2018b; Sarkale et al., 2018; Wang et al., 2004; Xu et al., 2007). However, optimization of restoration strategies is outside of the scope of this dissertation and only the restoration process was discussed here in detail.

INITIATION TIME

Following a tornado, some preliminary tasks including search and rescue, cleanup of the debris on roadways, rapid field inspections, and infrastructure damage assessment are necessary before community restoration begins. Therefore, an initiation time was defined in this dissertation as a random variable with a Weibull distribution. The statistics for initiation time are presented in Table 5-1. It is recognized that the initiation time varies significantly, and the values herein are based on the experience with post-disaster site investigations.

Table 5-1. Statistics for initiation time

EF Scale	EF0	EF1	EF2	EF3	EF4	EF5
mean (days)	0.2	0.4	0.8	1.5	2.0	3.0
COV	0.5	0.5	0.5	0.5	0.5	0.5

COMMUNITY RESTORATION METHODOLOGY

Monte Carlo simulation was conducted in this dissertation to investigate the restoration and resilience analyses for pseudo-Norman. The analyses were performed for each EF-scale tornado with 10,000 runs. The fundamental steps for the analyses are summarized in Figure 5-1. After simulating a tornado path and the resulting spatial damage, the intrinsic failure status is available for all community components. The intrinsic failure event, F_{int}, for a component, is defined as its failure based on its own physical damage experienced under a simulated tornado; which is considered, in this dissertation, to be either failed (i.e., 0 for the components with damage level of DS1, DS2, DS3, or DS4) or not-failed (i.e., 1 for the components without damage). Moreover, in order to capture the effect of different damage levels on the analyses, a repair and permitting time was assigned to each damaged component based on its damage level and the statistics provided in Table 3-13. The occurrence of a greater damage state for a component means it takes longer to be repaired and, therefore, will be non-functional for a longer period of time.

Using the intrinsic failure status of all the community components as well as their dependencies and cross-dependencies, the extrinsic failure status and, subsequently, functionality failure status are found for each community component. The extrinsic failure event, F_{ext}, for a component, is defined as its failure that results when interacting components outside of the component are considered either within its own network or other networks in the community. The functionality failure event, F_{fnc}, for a component, is the union of the intrinsic and extrinsic failure events for that component, which can be expressed as:

$$F_{fnc} = F_{int} \cup F_{ext} \qquad \textit{Equation 5-1}$$

Once the functionality failure status of all community components are known, a specified performance index at a network level or at the community level can be assessed. As will be discussed later, the restoration process is illustrated by updating the specified performance index over the time steps after the tornado hits the community until the full restoration of the community is achieved. In the restoration analysis in this dissertation, it was assumed that the recovery process of all networks are started simultaneously immediately after the initiation time. This assumption was logical in that each network has its own crews for inspection, assessment, and repair. Although recovery priority was not considered across networks, there might be some recovery priority within each network. Recall that since the networks are coupled, even if a component has been repaired physically or has no damage, it remains non-functional until all its suppliers are recovered and functional.

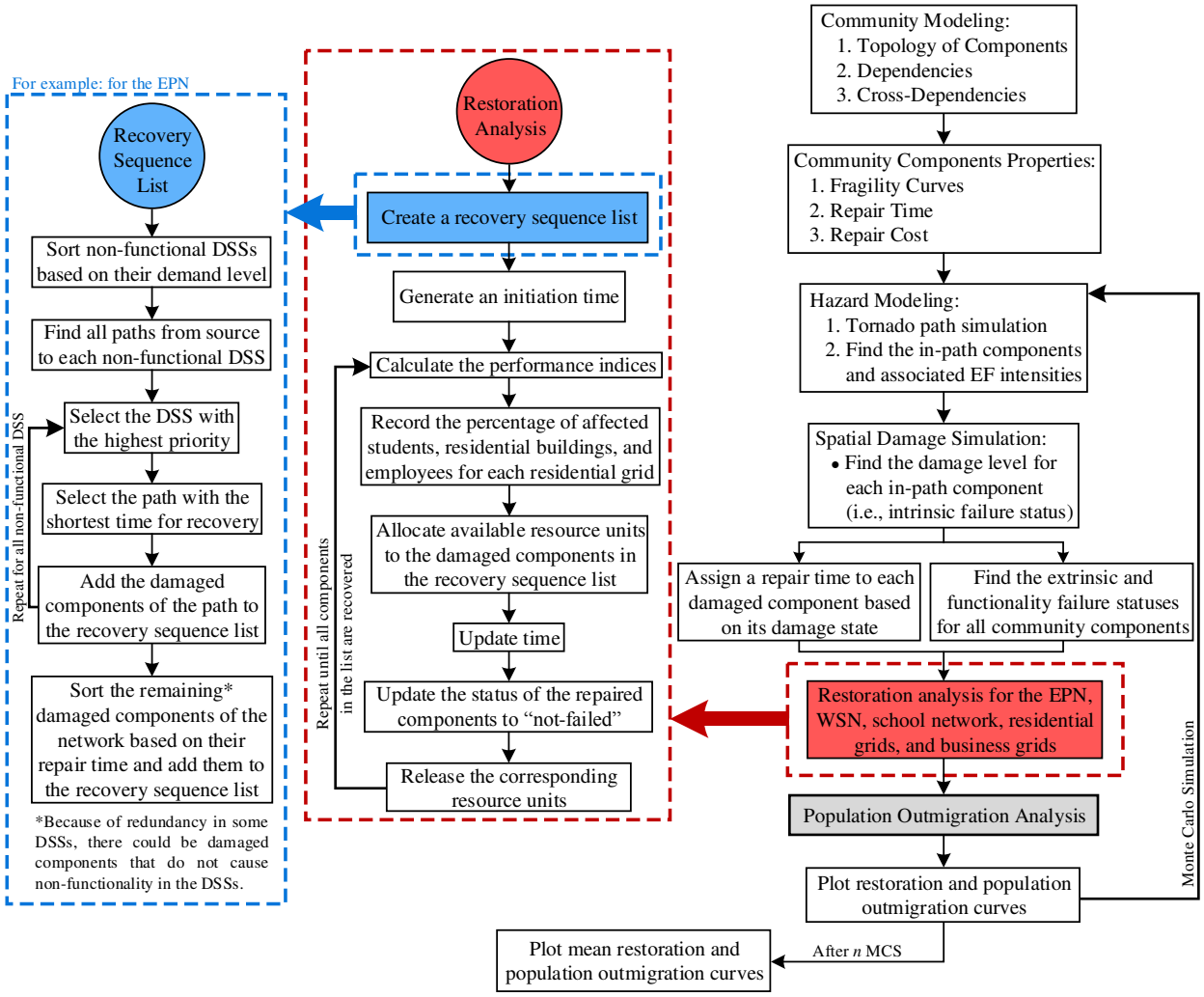

Figure 5-1. Flowchart for the restoration analysis

ELECTRIC POWER NETWORK

The electric power network (EPN) plays a substantial role in the vitality of a community in that the functionality of all other networks depend on the availability of electric power. Many critical facilities such as hospitals and police stations do have generators, but this particular sub-component of EPN was neglected in the analyses of this dissertation. The EPN in pseudo-Norman has underground distribution lines (as opposed to real Norman, Oklahoma) which were assumed to be undamaged from a tornado. Therefore, in this dissertation, the electric power distribution substations (DSS) were considered as the supplier nodes (in the EPN) for the demand nodes of

other networks. This means that the functionality failure status of a DSS dictates the extrinsic failure status of its demand nodes. The extrinsic failure status and functionality failure status of each DSS was investigated by considering the dependency among the EPN components. An adjacency matrix was used to find all the paths that transfer electricity to each DSS. The extrinsic failure status is 0 for a DSS if every path that feeds the DSS has at least one failed component, otherwise, the status is 1, which can be expressed mathematically as:

$$F_{fnc}^{DSS_i} = F_{int}^{DSS_i} \cup F_{ext}^{DSS_i} = F_{int}^{DSS_i} \cup \left[\bigcap_{j=1}^{n} F_{fnc}^{path_j} \right] \qquad \textit{Equation 5-2}$$

where $F_{fnc}^{DSS_i}$, $F_{int}^{DSS_i}$, and $F_{ext}^{DSS_i}$ are the functionality, intrinsic, and extrinsic failure events for the distribution substation *i*, respectively; and $F_{fnc}^{path_j}$ is the functionality failure event of the path *j* that provides electricity for the DSS_i.

In this dissertation, a recovery priority rule as well as a constraint for available recovery resource units were considered for the restoration process of the EPN. Recovery priority, in the EPN, was considered such that the distribution substation with the higher demand has to be recovered first. Since there are redundancies in providing electricity for some DSSs, the recovery time for all the paths to a DSS were calculated and the path with the shortest recovery time was selected to be recovered first. The path recovery took place from the source (i.e., transmission towers in this dissertation) to the distribution substation. In other words, in a path, the priority sequence was: transmission towers, transmission substations, sub-transmission towers, and distribution substation. The flowchart for creating the recovery sequence list for the EPN is shown in Figure 5-1. Furthermore, a number of available recovery resource units, *r*, as generic work teams including repair crews, equipment, and replacement components; was considered for assignment

to damaged components for the restoration process (Ouyang et al., 2012). Repairing of each damaged component was assumed to need only one recovery resource unit. During the restoration process, the available resource units are assigned sequentially to the damaged components in the recovery sequence list. When a component is repaired, the released resource unit will move to the next damaged component in the sequence list until the whole network is restored. The restoration process is summarized in Figure 5-1.

As mentioned before, the analyses in this dissertation were done for each EF-scale tornado by considering the uncertainties in tornado path direction, width, length, and location of the path center. Table 5-2 presents the mean functionality time (i.e., the time at which a component regains its functionality) computed for each distribution substation after an EF3/EF4/EF5 tornado hits pseudo-Norman by considering different numbers of recovery resource units. For example, after an EF5 tornado, DSS #13 will be operational after 36.6 days, on average, if only one recovery resource unit is available (i.e., $r = 1$). However, increasing r to five units significantly decreases the functionality time for this DSS to 10.6 days. Using additional resources may not considerably reduce the functionality time (8.4 days for $r = 10$ and 7.6 days for $r = 15$) because, for example, one of the damaged components may have a much higher repair time or the number of damaged components could be less than r.

Table 5-2. Mean functionality time (days) for each distribution substation for different numbers of recovery resource units (EF3-EF5)

DSS#	EF3				EF4				EF5			
	$r = 1$	$r = 5$	$r = 10$	$r = 15$	$r = 1$	$r = 5$	$r = 10$	$r = 15$	$r = 1$	$r = 5$	$r = 10$	$r = 15$
1	1.3	0.6	0.5	0.5	4.5	1.5	1.2	1.2	9.3	2.8	2.3	2.2
2	1.9	0.8	0.8	0.7	5.8	2.2	1.9	1.8	10.9	4.0	3.4	3.3
3	3.1	1.2	1.1	1.0	9.3	3.1	2.6	2.4	17.2	5.5	4.4	4.1
4	1.8	1.3	1.3	1.3	5.1	3.4	3.2	3.1	9.5	5.7	5.4	5.4
5	1.2	0.9	0.9	0.9	3.5	2.3	2.2	2.2	6.6	4.1	3.9	3.9
6	3.4	1.3	1.1	1.1	11.5	3.7	2.9	2.7	21.9	6.5	5.2	4.7
7	4.7	1.9	1.6	1.5	13.6	4.4	3.7	3.4	25.0	7.8	6.2	5.8
8	1.8	1.0	0.9	0.9	5.0	2.3	2.0	2.0	10.0	4.1	3.7	3.5
9	2.7	1.5	1.4	1.3	7.3	3.3	3.0	2.9	14.0	5.9	5.4	5.1
10	3.0	1.9	1.9	1.9	7.9	4.6	4.2	4.2	14.3	7.8	7.3	7.2
11	1.6	0.7	0.6	0.6	5.9	2.3	1.7	1.6	11.0	4.3	3.3	3.0
12	4.0	1.2	1.0	0.9	14.0	3.6	2.5	2.2	26.9	6.8	4.8	4.2
13	6.9	2.5	2.2	2.0	19.6	6.0	4.9	4.6	36.6	10.6	8.4	7.6
14	1.7	0.6	0.5	0.5	6.6	1.9	1.5	1.4	14.3	4.1	3.1	2.8
15	2.7	0.7	0.5	0.5	11.4	2.6	1.8	1.5	24.6	5.7	3.9	3.3
16	3.1	0.8	0.7	0.6	12.1	2.9	2.1	1.8	24.8	6.0	4.3	3.7
17	2.0	0.6	0.4	0.4	8.6	2.1	1.5	1.3	17.3	4.3	3.1	2.7
18	2.3	0.6	0.5	0.5	9.4	2.4	1.7	1.5	18.9	4.7	3.4	3.0

A performance index was defined for the EPN as the percentage of the community demand being supplied by the EPN. In order to illustrate the progress of restoration, the performance index was updated after each step when a damaged component was repaired. The mean restoration curve for the EPN (i.e., the mean value of the performance index following the event) is shown in Figure 5-2 (a) for each EF-scale tornado under the condition that only five recovery resource units are available. In order to shed light on the extent of uncertainty in the restoration curves, the 5^{th}, 25^{th}, 50^{th} (i.e., median), 75^{th}, and 95^{th}-percentile restoration curves are shown along with the mean curve for EF5 tornadoes in Figure 5-2 (b). When a tornado strikes pseudo-Norman, it may strike a populated area of the town or an undeveloped part of it, which is a source of uncertainty that stems from the unpredictability of the tornado path center, direction, length, and width. Moreover, there exist other significant uncertainties in the analyses such as uncertainties in the resulting damage to

the components as well as the uncertainties in the repair time for the damaged components. As shown in Figure 5-2 (b), after an EF5 tornado hits pseudo-Norman, the mean performance of the EPN is 49%, while the 5th, 25th, 50th, 75th, and 95th-percentile of the EPN performance are equal to 0, 15, 45, 76, and 100 percent, respectively. After two weeks of recovery, the mean EPN performance increases to 89%, while the 5th, 25th, 50th, 75th, and 95th-percentile of the EPN performance are equal to 39, 82, 100, 100, and 100 percent, respectively.

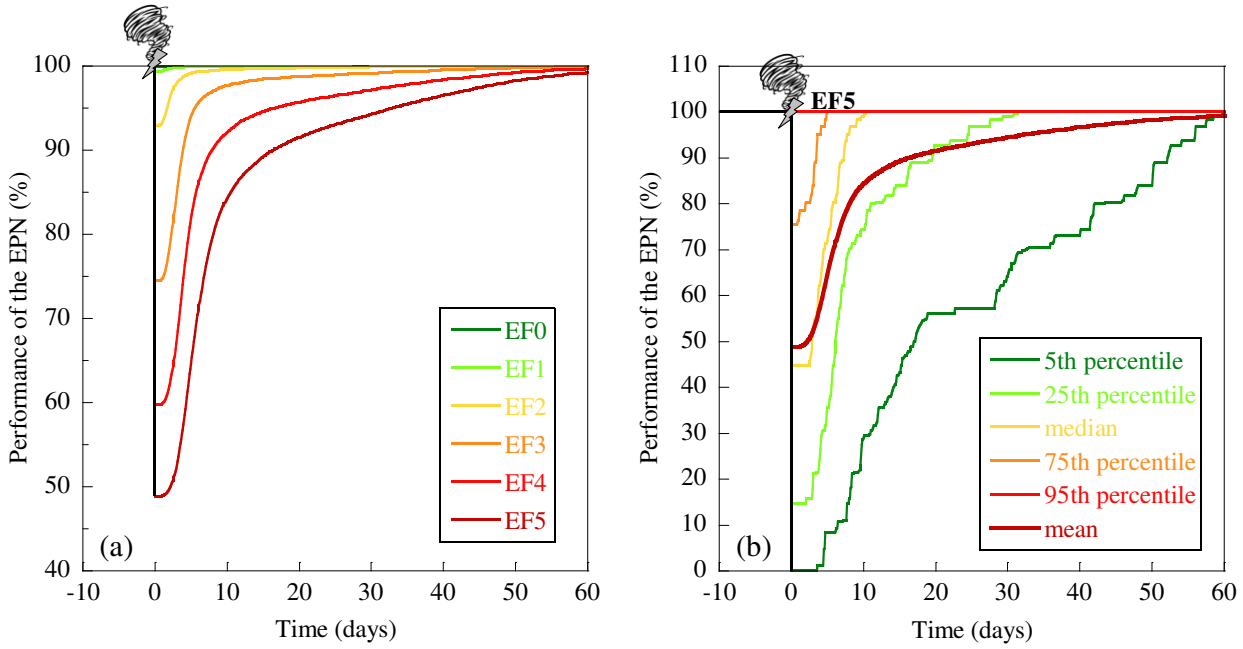

Figure 5-2. (a) Mean restoration curves for the EPN after each EF-scale tornado and (b) the uncertainty in the EF5 restoration curves

Moreover, in order to indicate the effects of using different numbers of recovery resource units, the restoration curves were plotted for EF4 and EF5 tornadoes (as examples) when one, five, ten, and fifteen recovery resource units are available, and are shown in Figure 5-3. After an EF5 tornado, 51% of pseudo-Norman, on average, would not have electric power. One week after the event, 60% of the community (on average) would have the electric power available if only one recovery resource unit was available, while it would be 76%, 81%, and 83% if five, ten, and fifteen

resource units are available, respectively. After one month, the mean performance of the EPN increases to 84% if only one resource unit is available, while it would be 95% for each of the five, ten, and fifteen available resource units. Five available recovery resource units (i.e., $r = 5$) were considered for the restoration of the EPN in the remained of analyses in this dissertation.

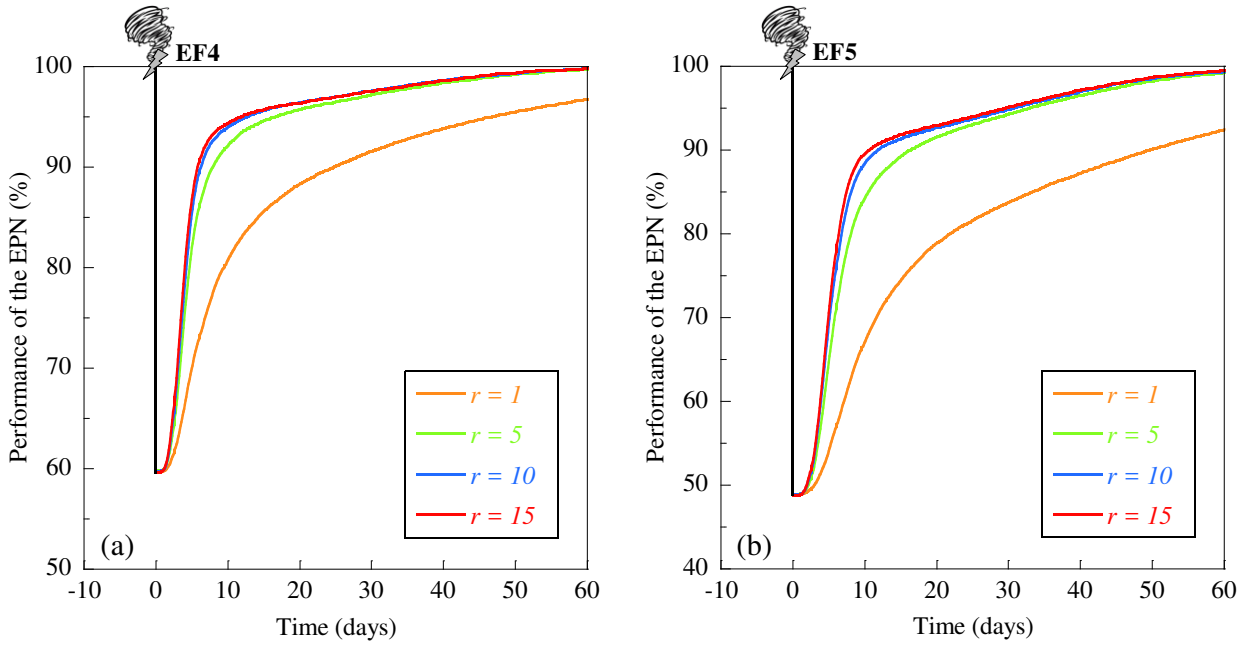

Figure 5-3. Mean restoration curves for the EPN for different numbers of available recovery resource units, r: (a) for EF4 tornado and (b) for EF5 tornado

With the purpose of examining the EPN-related business disruption in the wake of a tornado, the number of employees, who cannot work because of a lack of electric power at their workplaces, was calculated and updated in every step of the restoration. In addition, an EPN-related social disruption was defined as the number of residential buildings that are without electric power in the aftermath of a tornado. Figure 5-4 shows these surrogate measures of business disruption and social disruption for all EF-scale tornadoes. For example, the loss of electric power, after an EF5 tornado, affects 28,000 employees (out of 53,890) and 31,000 residential buildings (out of 41,254),

on average. Having five available recovery resource units, 3,160 employees and 2,290 residential buildings, on average, are still affected after one month by the loss of electric power.

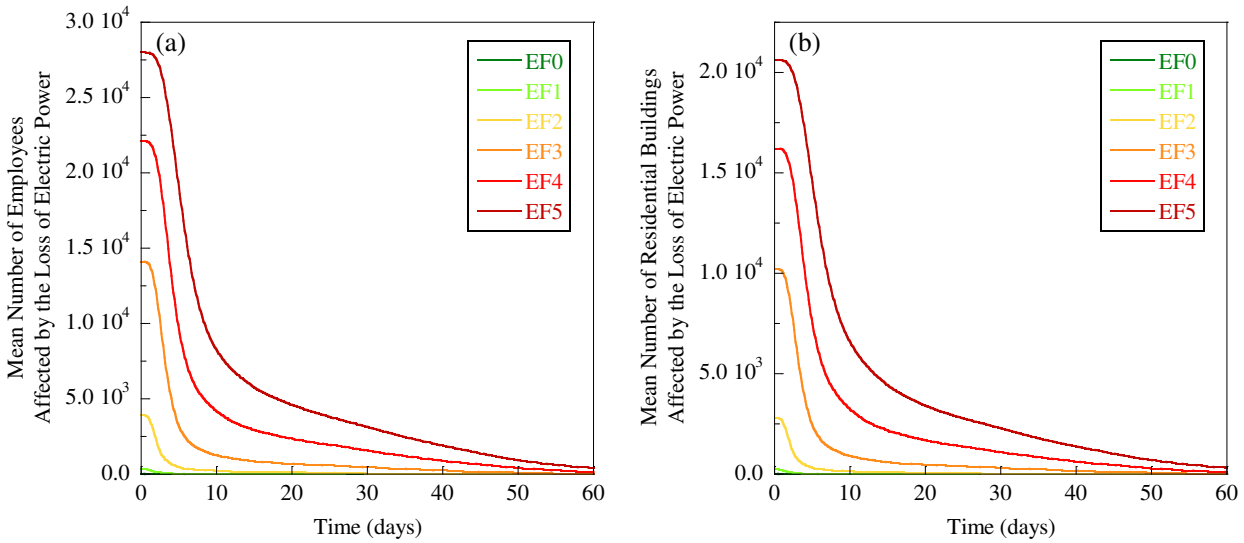

Figure 5-4. (a) Mean business disruption curves and (b) mean social disruption curves caused by the loss of electric power after each EF-scale tornado

WATER SUPPLY NETWORK

In the water supply network (WSN), the water towers (WT) are the supplier nodes for the demand nodes of other networks. Each WT has a pumping station that links the WT to a supplier node in the EPN (i.e., a DSS). Moreover, the WTs were assumed to lose their functionality if the water treatment plant (WTP) becomes non-functional. Therefore, based on the intrinsic failure status of the components in the WSN and the functionality failure status of DSSs, the functionality failure status for a WT is found by:

$$F_{fnc}^{WT_i} = F_{int}^{WT_i} \cup F_{ext}^{WT_i} = F_{int}^{WT_i} \cup \left(F_{fnc}^{WTP} \cup F_{fnc}^{DSS_j} \right) = F_{int}^{WT_i} \cup \left(F_{int}^{WTP} \cup F_{ext}^{WTP} \right) \cup F_{fnc}^{DSS_j} \qquad \textit{Equation 5-3}$$

where $F_{fnc}^{WT_i}$, $F_{int}^{WT_i}$, and $F_{ext}^{WT_i}$ are the functionality, intrinsic, and extrinsic failure events for the water tower *i*, respectively; and F_{fnc}^{WTP}, F_{int}^{WTP}, and F_{ext}^{WTP} are the functionality, intrinsic, and

extrinsic failure events for the water treatment plant, respectively. F_{ext}^{WTP} is equivalent to the functionality failure event for the DSS that feeds the WTP, and $F_{fnc}^{DSS_j}$ is the functionality failure event for the distribution substation that feeds WT_i.

In this dissertation, the only vulnerable components considered for the WSN were the six water towers and one water treatment plant. Therefore, it was assumed that there are enough available recovery resource units for the WSN to start repairing the damaged components at the same time. In other words, in order to restore the WSN, the same process that was used for the restoration of the EPN (i.e., Figure 5-1) was performed here except that there were no constraints for the available recovery resource units (i.e., infinite number of available recovery resource units) and, therefore, no recovery priority for the restoration of the WSN. In addition, it should be noted that there exist portable water treatment systems for WSNs but these were neglected in the analyses in this dissertation.

A performance index was defined here for the WSN as the percentage of the community demand being supplied by the network. In order to illustrate the progress of restoration, the performance index was updated when a damaged component was repaired or when a DSS that feeds the pumping station of a WT became functional. The mean restoration curve for the WSN is shown in Figure 5-5 (a) for each EF-scale tornado. For example, after an EF5 tornado, 64% of pseudo-Norman, on average, would not be supplied by the WSN. After 14, 30, and 60 days of recovery following the event, the mean performance of the WSN is returned to 82, 90, and 95 percent, respectively. Moreover, in order to elucidate the effect of the cross-dependencies among networks on the WSN mean restoration curve (i.e., the effect of the EPN performance loss on the performance of the WSN), the intrinsic and extrinsic performance loss were distinguished for the

mean restoration curve of the EF5 tornado and are shown in Figure 5-5 (b). The intrinsic performance loss is the loss of performance in the WSN that resulted from the intrinsic failure of the components within the WSN, while the extrinsic performance loss is that which resulted from the extrinsic failure of the components. As shown in Figure 5-5 (b), the majority of the performance loss in the WSN immediately after an EF5 tornado is due to the extrinsic failures (i.e., the loss of performance in the EPN). However, the intrinsic failures last longer such that the contribution of the intrinsic and extrinsic failures are approximately equal in the performance loss of the WSN during the full restoration (i.e., 48% vs 52%). This is because the components in the WSN require a significantly longer duration to be repaired compared to the components in the EPN (see Table 3-13).

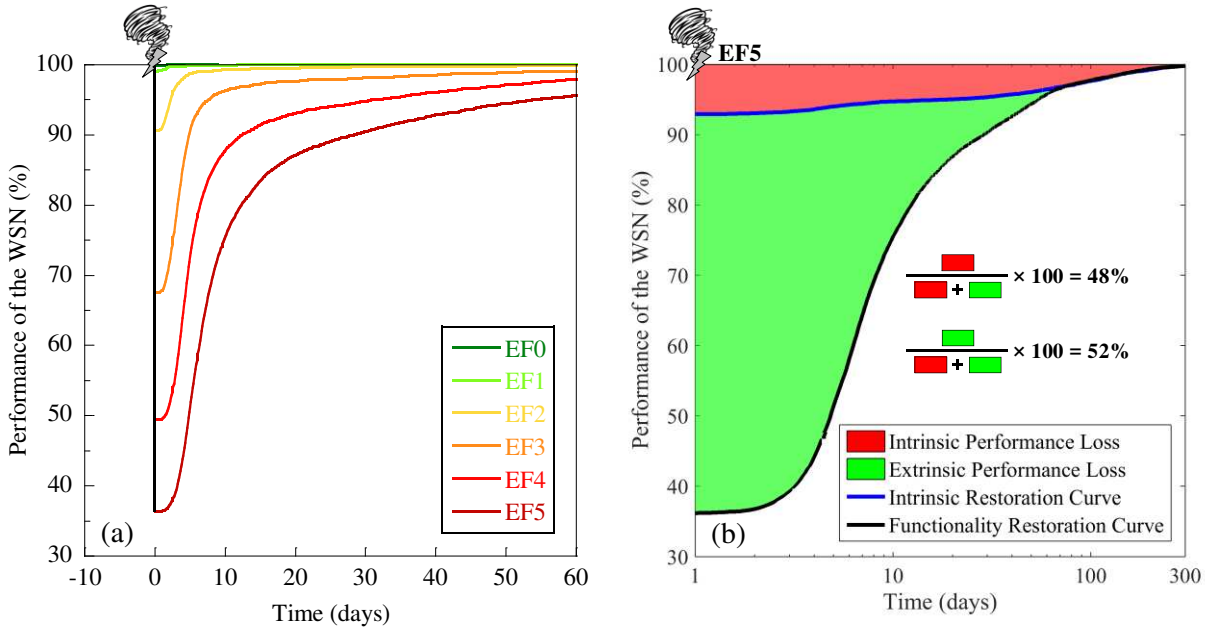

Figure 5-5. (a) Mean restoration curves for the WSN after each EF-scale tornado and (b) the effect of cross-dependencies on the WSN mean restoration curve after an EF5 tornado

WSN-related business and social disruptions were defined the same as the EPN-related disruptions but as a consequence of the performance loss of the WSN following a tornado. WSN-related business and social disruption curves are plotted in Figure 5-6. For example, after an EF5 tornado,

34,250 employees (out of 53,890) and 26,180 residential buildings (out of 41,254), on average, are affected by a lack of performance in the WSN. After two weeks of recovery, the network regains 82 percent of its performance, on average, which reduces the mean number of affected employees and residential buildings to 9,530 and 7,270, respectively.

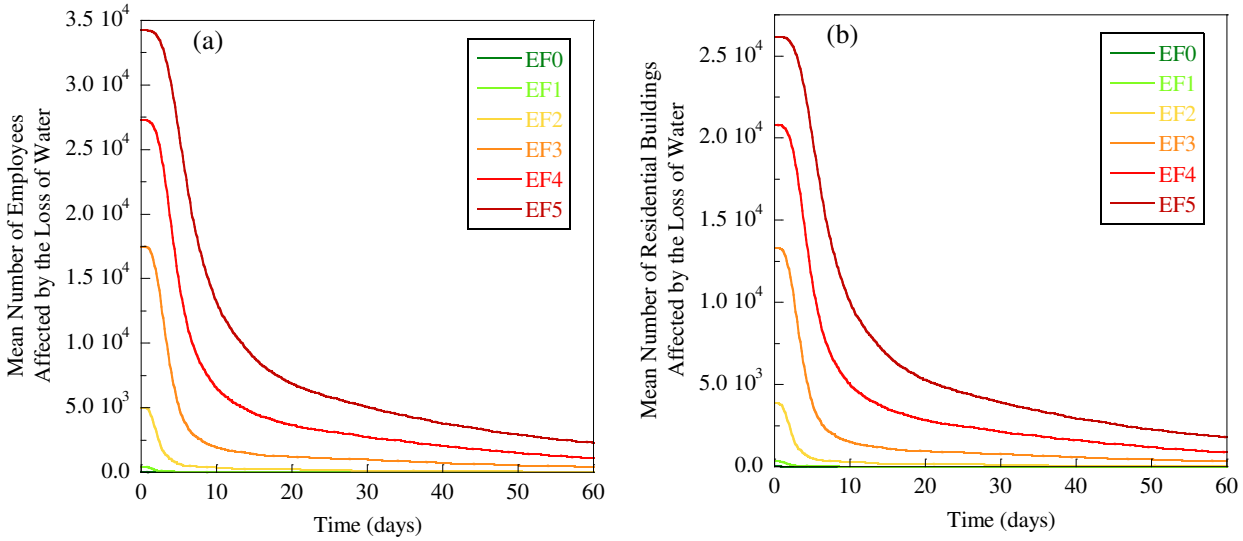

Figure 5-6. (a) Mean business disruption curves and (b) mean social disruption curves caused by the loss of water after each EF-scale tornado

SCHOOL NETWORK

The functionality of a school building (SB) was modeled to be a function of its own physical performance as well as the availability of both water and electric power. Electric power was provided for a component by one specific distribution substation (DSS). However, it was assumed that the water can be supplied to a component by one or more water towers, i.e., there might be some level of redundancy. The pressure in pipelines was not considered in the determination of availability of water for a component. It was assumed that the water demand for a component is not satisfied only under the condition that all water towers that are capable of supplying the component become non-functional. Therefore, the functionality failure status for a SB can be mathematically shown as:

$$F_{fnc}^{SB_i} = F_{int}^{SB_i} \cup F_{ext}^{SB_i} = F_{int}^{SB_i} \cup F_{fnc}^{DSS_j} \cup \left(\bigcap_{k=1}^{k=n} F_{fnc}^{WT_k} \right) \qquad \textit{Equation 5-4}$$

where $F_{fnc}^{SB_i}$, $F_{int}^{SB_i}$, and $F_{ext}^{SB_i}$ are the functionality, intrinsic, and extrinsic failure events for the school building i, respectively; the $F_{fnc}^{DSS_j}$ is the functionality failure event for the distribution substation that feeds the SB_i; and $F_{fnc}^{WT_k}$ is the functionality failure event for the n water towers that provide water for the SB_i.

A performance index was defined for the school network (SN) as the percentage of the students in pseudo-Norman that can be served by the SN. There was no constraint for the available recovery resource units (i.e., infinite number of available recovery resource units) in the restoration analysis of the SN because the possible number of damaged schools following a tornado was not high. In order to illustrate the progress of restoration, the performance index was updated when a damaged school was repaired or when water became available for a school or when a DSS that feeds a school became functional. The mean restoration curve for the SN is shown in Figure 5-7 (a) for each EF-scale tornado. For example, after an EF5 tornado, 69% of the students in pseudo-Norman, on average, would not be able to attend school. After 14, 30, and 60 days of recovery following the event, the mean performance of the SN is returned to 77, 85, and 92 percent, respectively. In order to illustrate the effect of the cross-dependencies among networks on the SN mean restoration curve (i.e., the effect of performance loss in the EPN and WSN on the performance of the SN), the intrinsic and extrinsic performance losses were distinguished for the mean restoration curve of the EF5 tornado and are shown in Figure 5-7 (b). Although the majority of the performance loss in the SN immediately after an EF5 tornado is due to the extrinsic failures (i.e., the loss of performance in the EPN and WSN), the intrinsic failures have a longer duration such that the contribution of

the intrinsic and extrinsic failures are 70% and 30%, respectively, in the performance loss of the SN during the full restoration.

Similar to the EPN and WSN, the SN-related social disruption was measured as the number of affected students, which are plotted in Figure 5-8 as a function of time following an event. Recall that an affected student is defined here as a student whose school is non-functional. Furthermore, it is noted that the percentage of the affected students in each residential grid, $P_S(t,RG_i)$, was calculated and recorded during the restoration process in order to be used in the population outmigration analysis presented in Chapter 6.

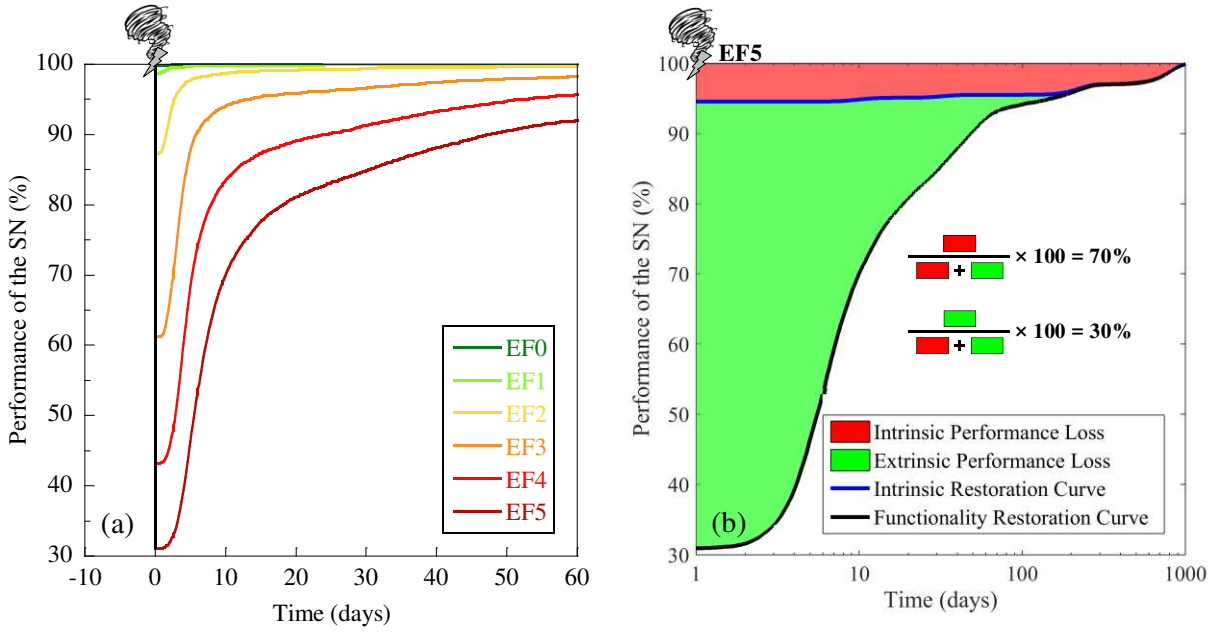

Figure 5-7. (a) Mean restoration curves for the SN after each EF-scale tornado and (b) the effect of cross-dependencies on the SN mean restoration curve after an EF5 tornado

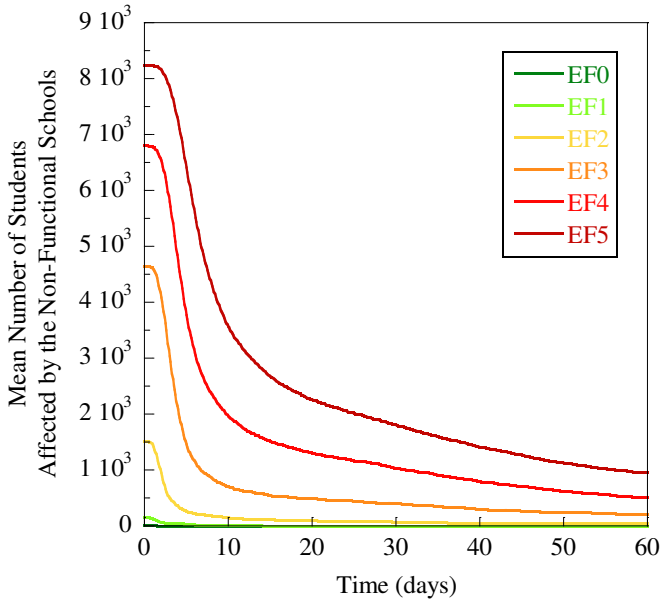

Figure 5-8. Mean social disruption curves for the SN after each EF-scale tornado

RESIDENTIAL SECTOR

The functionality of a residential building (RB) was defined in a similar way to that of a school building which was expressed mathematically in Equation 5-4. A community-level performance index was defined for the residential sector (RS) as the percentage of the residential buildings in pseudo-Norman that are functional. As mentioned before, pseudo-Norman has 41,254 residential buildings among which 37,785 buildings are occupied and the rest are unoccupied. Although a constraint was assumed for the available recovery resource units in the restoration of the RS, there was no recovery priority designated except that the unoccupied buildings are repaired after repairing all occupied buildings. In other words, the recovery resource units were assigned randomly to the damaged RBs (first occupied RBs and then unoccupied RBs). The performance index was assessed for both occupied and unoccupied RBs in the residential sector during the community restoration process and the mean restoration curves are shown in Figure 5-9 (a) for occupied RBs by using 250 available recovery resource units, *r*. For example, after an EF5 tornado,

on average, 70% of the occupied residential buildings in pseudo-Norman are non-functional. However, as shown in Figure 5-9 (b), only 5% of them are resulted from intrinsic failures (i.e., physical damage to RBs) and the rest 65% are non-functional due to the loss of utilities (i.e., the loss of water and electric power). After one month of recovery, 16% of the occupied RBs are still non-functional among which 5% (as it was at the beginning of recovery) are due to intrinsic failures and the rest are the result of extrinsic failures. Although the majority of the performance loss in the RS immediately after an EF5 tornado is due to the extrinsic failures (i.e., the loss of performance in the EPN and WSN), the intrinsic failures last longer (because of the longer repair time as shown in Table 3-13) such that the contribution of the intrinsic and extrinsic failures are 87% and 13%, respectively, in the performance loss of the RS during the full restoration.

The effects of using different values of r on the restoration process is shown in Figure 5-10 (a) for the restoration of the RS after an EF5 tornado. Since the early stage of the restoration process here is dominated by the extrinsic failures and the damaged RBs need a long repair time, using higher r values does not significantly affect the early stage of the restoration (e.g., first two months). Therefore, the intrinsic mean restoration curves are shown in Figure 5-10 (b) to illustrate additional details related to the effects of using different r values on the restoration curve. It is also worth mentioning that the majority of the damaged residential buildings following an EF5 tornado are in damage state 4. After an EF5 tornado, 5.4% of the RBs, on average, are damaged among which 0.5, 0.4, 0.4, 4.1% are in DS1 to DS4, respectively. For the restoration of RS in the remaining analyses presented in this dissertation 250 available recovery resource units were considered. Furthermore, the percentage of affected (i.e., non-functional) occupied residential buildings were calculated and recorded for each residential grid, $P_{OR}(t,RG_i)$, during the restoration process in order to be used in the population outmigration analysis presented in Chapter 6.

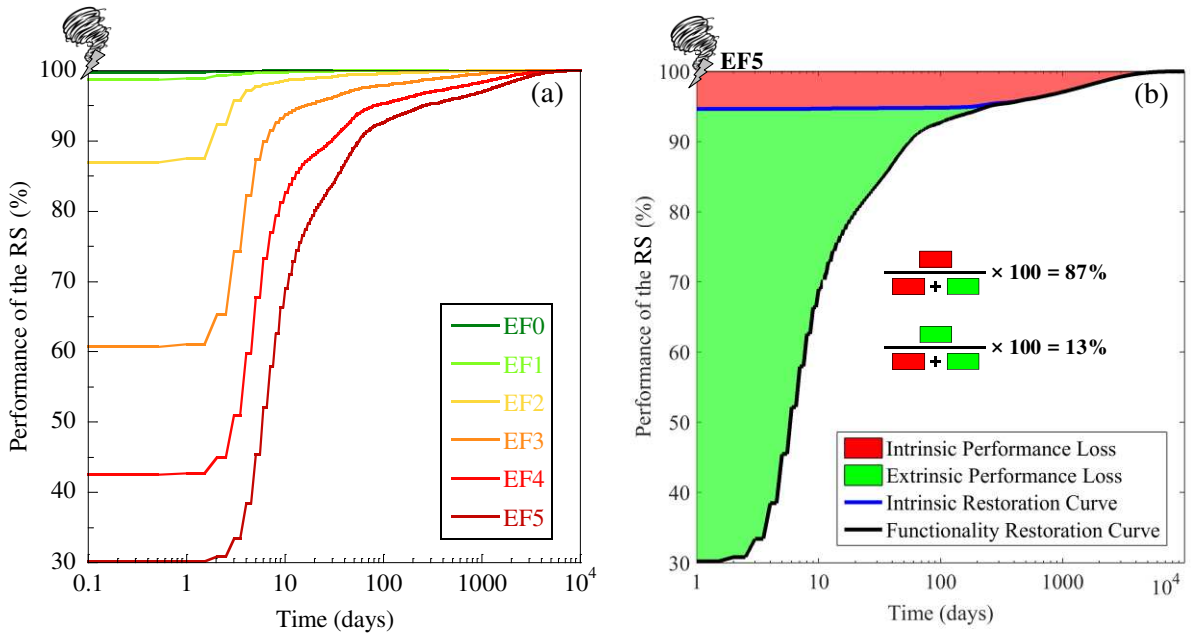

Figure 5-9. (a) Mean restoration curves for the residential sector after each EF-scale tornado and r = 250 and (b) the effect of cross-dependencies on the RS mean restoration curve after an EF5 tornado

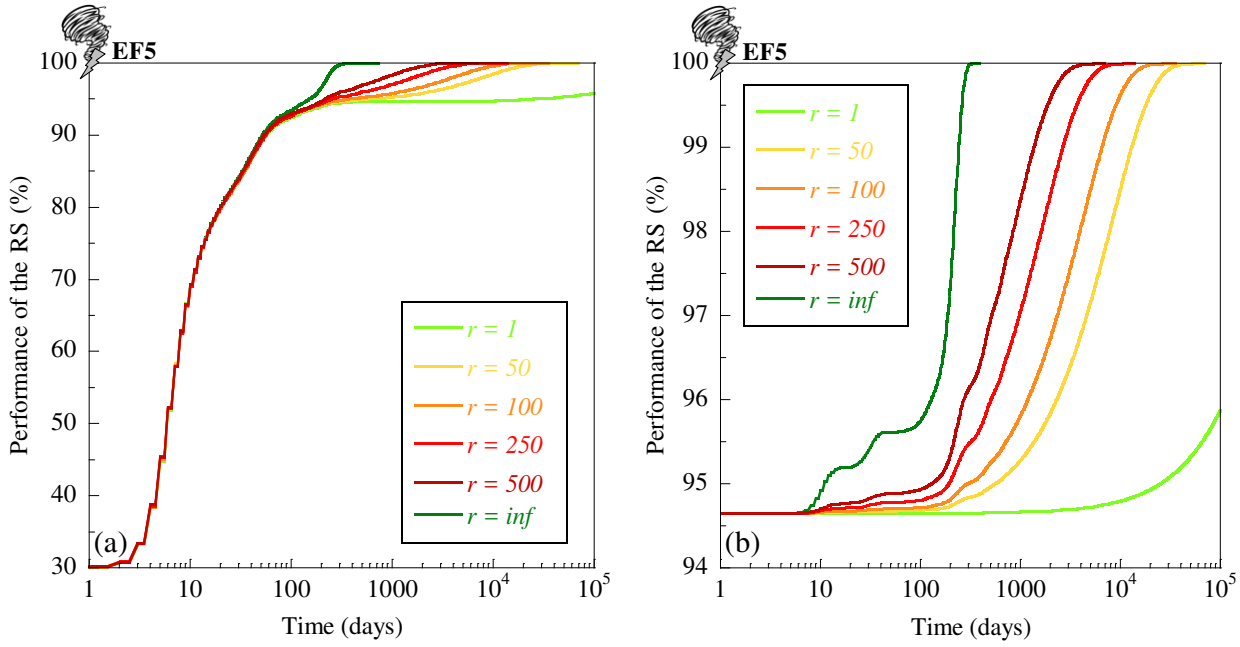

Figure 5-10. (a) Mean restoration curve and (b) mean intrinsic restoration curve for the residential sector after EF5 tornado by using different r

BUSINESS SECTOR

A workplace building (WB) was defined herein as any building type which can employ residents of pseudo-Norman, and which was assigned the same method for functionality as the school buildings expressed in Equation 5-4. A community-level performance index was defined for the business sector (BS) as the percentage of the employees who work in pseudo-Norman and are not affected by the loss of functionality of their workplaces. The performance index was evaluated during the community restoration process and the mean restoration curve is shown in Figure 5-11 (a) for the business sector. For example, after an EF5 tornado, on average, 68% of the employees who work in pseudo-Norman are affected (i.e., their workplace buildings are non-functional). However, as shown in Figure 5-11 (b), only 6% of the affected employees have non-functional workplaces due to intrinsic failures (i.e., physical damage to WBs) and the rest, 62%, are affected due to the loss of utilities in their workplaces (i.e., the loss of water and electric power). After one month of recovery, 16% of the employees in pseudo-Norman are still affected, among whom 5% are affected due to intrinsic failure of their workplaces and the rest as a result of extrinsic failures of their workplaces. Although the majority of the performance loss in the BS immediately after an EF5 tornado is due to the extrinsic failures (i.e., the loss of performance in the EPN and WSN), the intrinsic failures last longer such that its contribution is higher than extrinsic failure contribution in the performance loss of the BS during the full restoration, i.e., 63% vs 37%.

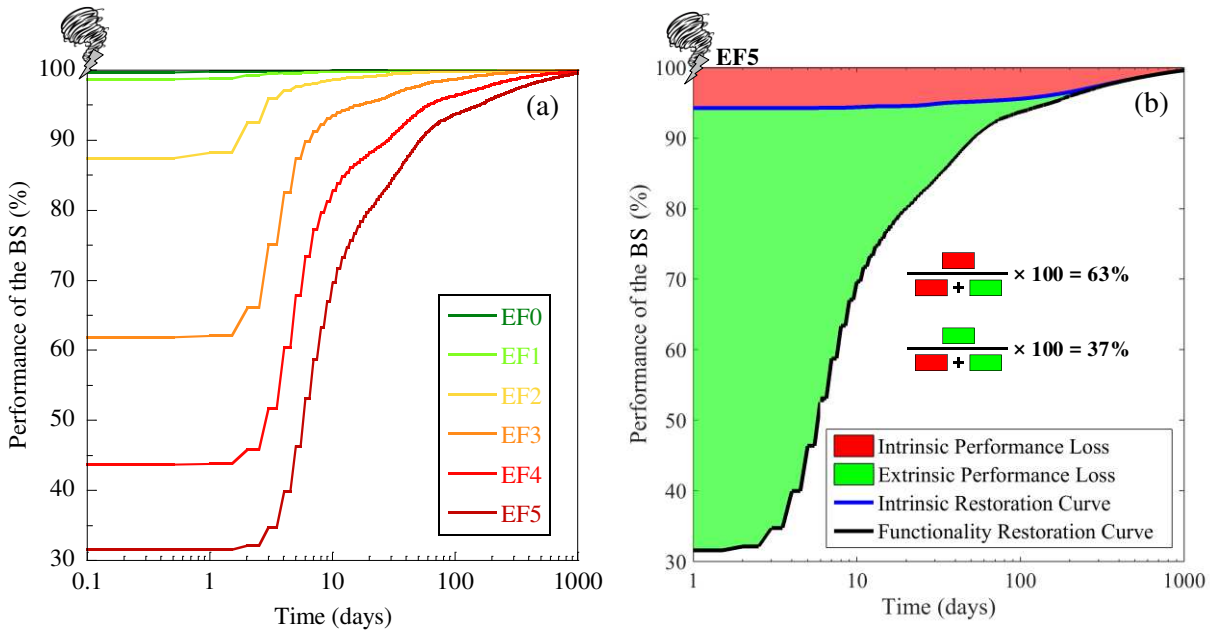

Figure 5-11. (a) Mean restoration curves for the business sector after each EF-scale tornado and r = 50 and (b) the effect of cross-dependencies on the BS mean restoration curve after an EF5 tornado

The effects of using different recovery resource units on the restoration process is shown in Figure 5-12 (a) for the restoration of the BS after an EF5 tornado. Since the early stage of the restoration process is dominated by the extrinsic failures and the majority of the damaged workplace buildings are in DS4 (i.e., the damaged WBs need a long repair time), using higher r values does not have a significant effect at the early stage of the restoration. Therefore, the intrinsic mean restoration curves are shown in Figure 5-12 (b) to illustrate additional details related to the effects of using different r values on the restoration curve. It is also worth mentioning that, after an EF5 tornado, 6.1% of the WBs, on average, are damaged; among which 0.9, 1.1, 1.3, 2.8% are in DS1 to DS4, respectively. For the restoration of the BS in the remaining analyses in this dissertation 50 available recovery resource units for the business sector were considered. Moreover, the percentage of affected employees who live in each residential grid, $P_E(t,RG_i)$, was calculated and recorded during the restoration process in order to be used in the population

outmigration analysis presented in Chapter 6. Recall that an affected employee is defined herein as an employee whose workplace is non-functional.

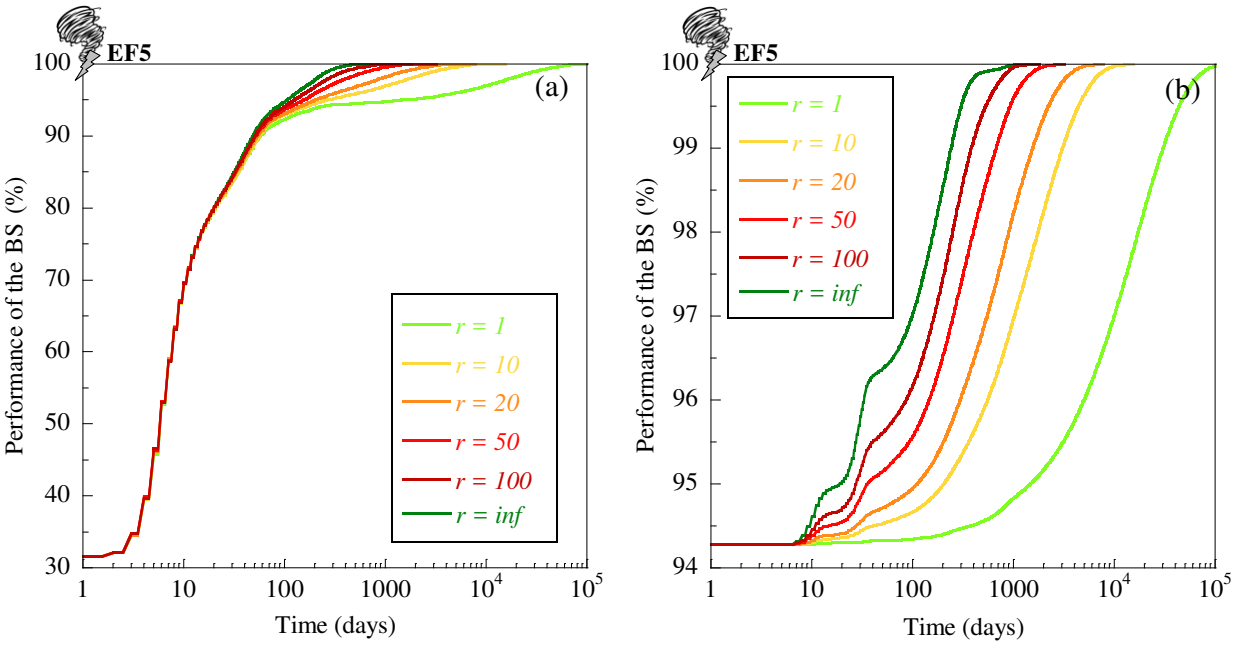

Figure 5-12. (a) Mean restoration curve and (b) mean intrinsic restoration curve for the business sector after EF5 tornado by using different r

Finally, it is noteworthy that the number of available recovery resource units (i.e., numbers of repair crews, equipment, and replacement components), used for the restoration of a network, would certainly be, to some extent, variable in an actual disaster. This number is a function of several parameters such as the expanse of the disaster, the timeframe after the event, temporary labor in-migration, and mutual aid agreements among utility companies (Chang et al., 2002). Therefore, although a constant number was considered for the available recovery resource units, *r*, in the analyses presented in the remainder of this dissertation, it would also be straightforward to apply a time-dependent *r* in the model or set it up as a random process if enough data were available.

CHAPTER 6: POPULATION OUTMIGRATION[1]

INTRODUCTION

A resilient community is one that has planned for potential hazards in order to be able to resist, absorb, and adjust to changing conditions as well as to return to a level of normalcy within a reasonable time following a disaster (Alexander, 2013; Bruneau et al., 2003; Platt et al., 2016). A number of metrics have been introduced to represent resilience (e.g., Attoh-Okine et al., 2009; Ayyub, 2014 and 2015; Bruneau et al., 2003; Bruneau and Reinhorn, 2007; Henry and Ramirez-Marquez, 2012; Omer et al., 2009; Ouyang et al., 2012; Reed et al., 2009). These metrics have been used in studies in order to quantify the resilience of, for example, healthcare facilities (e.g., Cimellaro et al., 2010), water networks (e.g., Chang and Shinozuka, 2004), electric power networks (e.g., Nan and Sansavini, 2017; Ouyang and Dueñas-Osorio, 2014; Reed et al., 2009), and transportation networks (e.g., Pant et al., 2014). In this dissertation, *population outmigration* was proposed as a socioeconomic resilience metric that takes into account the cross-dependencies among critical infrastructure systems within a community as well as the dependencies between the components of each system. Furthermore, a methodology was developed to quantify this metric at different levels, from the household level to the community level. It is noted that population dislocation (FEMA, 2003; Lin, 2009) differs from population outmigration.

Population dislocation has been defined as a post-disaster socioeconomic impact in which households are forced to move for some period of time due to damage to structures and infrastructure in the wake of natural disasters (Lindell and Prater, 2003; Mitchell et al., 2011; Xiao

[1] This section is based on the paper: Masoomi, H., van de Lindt, J.W., and Peek, L., (2017) "Quantifying Socioeconomic Impact of a Tornado by Estimating Population Outmigration as a Resilience Metric at the Community Level", accepted, *Journal of Structural Engineering*, DOI: 10.1061/(ASCE)ST.1943-541X.0002019

and Van Zandt, 2012). According to previous disaster studies (Baker, 1991; FEMA, 2003; Gladwin and Peacock, 1997; Lindell et al., 2006; Whitehead et al., 2000; Whitehead, 2005), population dislocation is a function of several factors including housing structural damage, housing type, disaster type, weather conditions, infrastructure disruption, and loss of employment. These factors are further influenced by socioeconomic characteristics of households and their surrounding neighborhoods. FEMA (2003), through their HAZUS model, proposed a methodology to measure population dislocation in order to estimate the number of people requiring short-term shelter. The methodology considers only structural damage and housing type such that all residents in completely damaged (i.e., damage state 4) single-family structures and completely damaged (i.e., damage state 4) multi-family structures, as well as 90 percent of residents in extensively damaged (i.e., damage state 3) multi-family structures will move after a natural disaster. Lin (2009) modified the population dislocation methodology in the HAZUS model in order to consider socioeconomic characteristics of households and their surrounding neighborhoods in addition to the housing type and its structural damage level for estimating population dislocation. The modified model was implemented in MAEviz (MAEC, 2006), a loss assessment software package developed by the Mid-America Earthquake (MAE) Center and the National Center for Supercomputing Applications (NCSA). Cavalieri et al. (2012) developed a more robust model that considers the interactions of residential buildings, electric power network, and the water supply network to investigate the inhabitability (i.e., functionality) of a residential building for estimating the displaced population after an earthquake. Their model also took into account the effects of weather conditions in assessing population dislocation.

In fact, the population dislocation models used in HAZUS (FEMA, 2003) and MAEviz (MAEC, 2006) as well as the model proposed by Cavalieri et al. (2012) consider only a couple of the factors

that affect households, while other factors play key roles in a household's tendency (or decision) to dislocate, such as infrastructure disruption, employment loss, and more importantly the time needed for the infrastructure and socioeconomic sectors to recover. It should be mentioned that these proposed models are reasonable as long as they are used to estimate the number of people requiring short-term shelter. Moreover, these models may not offer an accurate representation of resilience in that they only try to address robustness as a resilience property and do not consider the effect of the restoration process (which per se includes the other three properties of resilience—redundancy, resourcefulness, and rapidity) in population dislocation assessment.

Thus, the term population dislocation was conceptualized in previous studies as the households who are forced to leave their homes following a disaster for any period of time, either short-term or long-term. However, the metric proposed for use in this dissertation is the population who out-migrate, meaning they dislocate permanently or long enough to have a meaningful effect on indirect economic losses within a community. Based on previous studies, the return of households and businesses are mutually dependent (Xiao and Van Zandt, 2012). In fact, the return of households in the market area will increase the chances for businesses to return and vice versa. Furthermore, if the displaced households are not included in the US census, the population loss puts the community at risk of losing federal and state funding that are based on a certain threshold for the community's population (Xiao and Van Zandt, 2012).

In this dissertation, *population outmigration* is proposed as the permanent or long-term population loss of a community in the aftermath of a natural disaster as a result of households moving because of damage to buildings and infrastructure, school closure, loss of employment, or various combinations thereof. The factors that influence population dislocation also affect population outmigration. Therefore, the proposed model is formulated such that the disaster type, weather

conditions, and socioeconomic characteristics of households and their surrounding neighborhoods can be included in the model as a parameter describing the households' tendency toward outmigration. It is recognized that this is a significant simplification but does not misrepresent the potential inaccuracies that stem from a dearth of data on this complex topic. Furthermore, in this proposed methodology, population outmigration is updated during the restoration process until the full restoration of the community is achieved, which enables assessing population outmigration spatially and temporally at any level from household level to the community level.

POPULATION OUTMIGRATION METHODOLOGY

Population dislocation and, therefore, population outmigration (PO) are affected by housing structural damage, housing type, disaster type, weather conditions, infrastructure disruption, loss of employment, and myriad other socioeconomic characteristics of individuals and households (Baker, 1991; Gladwin and Peacock, 1997; Whitehead et al., 2000; Whitehead, 2005). In this dissertation, for each household in a residential grid, three parameters were considered to potentially stimulate a household to leave the city with a probability assigned to each and their combinations: (i) affected house (i.e., a non-functional house), (ii) affected employee (i.e., an employee member of the household whose workplace is non-functional), and (iii) affected student (i.e., a student member of the household whose school is non-functional). Recall that the functionality of a building (e.g., a school, a workplace, or a residential building) was modeled, in this dissertation, to be a function of the building physical performance as well as the availability of both water and electric power. Therefore, the three aforementioned parameters take into account buildings structural damage, disruption of infrastructure (i.e., electric power network, water supply network, and school network), and employment loss. Based on these three parameters, at a time

following the event, a household experiences one of eight states shown in Figure 6-1 and summarized in Table 6-1 (i.e., S1 to S8 which are mutually exclusive and collectively exhaustive).

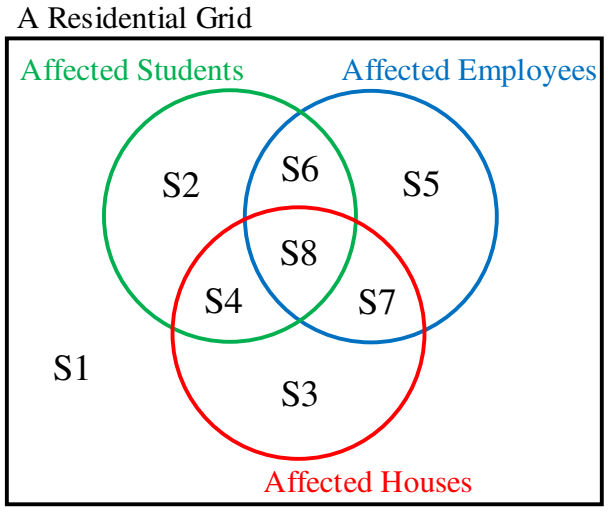

Figure 6-1. A Venn diagram which shows the possible states of a household after an event

Table 6-1. The states that a household experiences at a time following an event

State	Affected House	Affected Students	Affected Employees
S1			
S2		✓	
S3	✓		
S4	✓	✓	
S5			✓
S6		✓	✓
S7	✓		✓
S8	✓	✓	✓

Each state leads to a different probability of outmigration for the household; which is a function of time, the level of structural damage, housing type, disaster type, weather conditions, household income, race/ethnicity, tenancy status, and so on. For example, a household is assumed to have a greater tendency to out-migrate when state S8 occurs than state S3, and the longer the household remains in a state, the more likely they are to out-migrate. Households residing in multi-family

structures are more prone to dislocation (and therefore outmigration) than those living in single-family dwellings, and this vulnerability is even more significant for households living in mobile homes (Lin, 2009; Peacock and Girard, 1997). The disaster type can further influence the household's probability of outmigration in that, for example in the case of a flood, households may have to leave their house if it is in the flooded area regardless of the level of damage. Population outmigration can also be exacerbated by weather conditions since utility disruption affects the ability to heat or cool the house. In very cold or hot weather conditions, this may significantly decrease the tolerance (or safety) of households and therefore increase their probability of dislocation followed by outmigration. A household's socioeconomic status is one of the other factors that influences the household's probability of outmigration. Households with higher socioeconomic status have more potential for mobility following a natural disaster, meaning they have more resources to choose to relocate elsewhere, as well as to rebuild should they so choose (Drabek and Key, 1984; Weber and Peek, 2012). Moreover, tenancy status of households was found to have an inconsistent effect on household dislocation/outmigration (Peacock and Girard, 1997; Belcher and Bates, 1983). All the aforementioned factors should be considered in the household's probability of outmigration. However, in this dissertation, the probability of outmigration was assumed only as a function of time when a household is in each state (i.e., states S1 to S8) in order to illustrate the methodology to quantify population outmigration. This time-dependent probability, which is shown in Figure 6-2, indicates the conditional probability of outmigration for a household at time *t* following the disaster given that the household has not out-migrated until that time and is still in the same state as before. Even if a household is not affected by the three parameters (affected house, affected employee, and affected student), i.e., the state S1, a very low constant probability was considered for the household outmigration. It should be

noted that the focus in this dissertation was on the methodology development and the values in Figure 6-2 were assumed here and post-disaster surveys are recommended for full calibration.

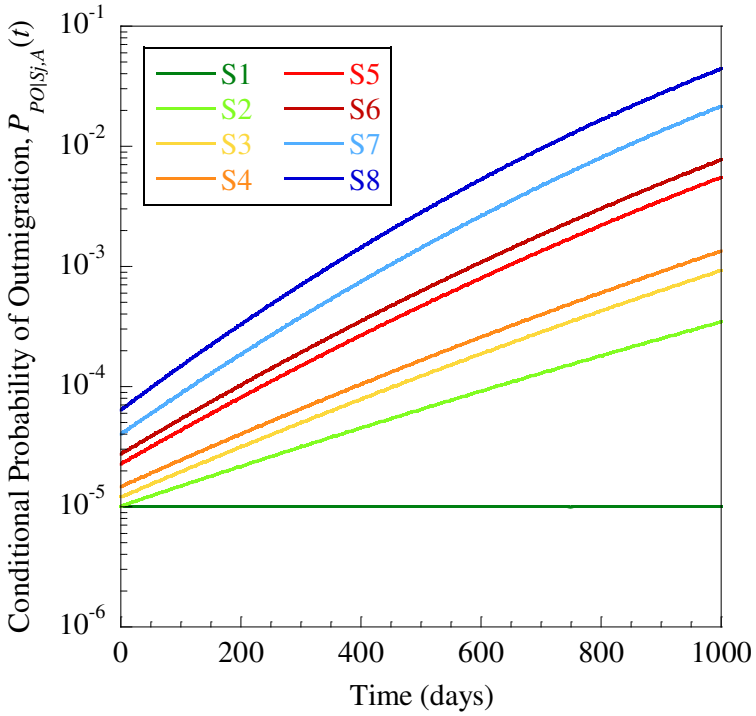

Figure 6-2. The household's conditional probability of outmigration as a function of time given state S_j occurred for the household and the household have not out-migrated until time t.

The fundamental steps toward population outmigration analysis were summarized in the flowchart in Figure 5-1. During the community restoration analysis, the percentage of affected students, $P_S(t,RG_i)$, the percentage of affected occupied residential buildings, $P_{OR}(t,RG_i)$, and the percentage of affected employees, $P_E(t,RG_i)$, were recorded for each residential grid (RG) as a function of time. The probability that household k (H_k) in residential grid i (RG_i) experiences one of the states in Figure 6-1 can be calculated at time t as:

$$P_{S1}(t,H_k,RG_i)=\left[1-P_{OR}(t,RG_i)\right]\left[1-P_S(t,RG_i)\right]^{n_S^{H_k}}\left[1-P_E(t,RG_i)\right]^{n_E^{H_k}} \qquad \textit{Equation 6-1}$$

$$P_{S2}(t,H_k,RG_i)=\left[1-P_{OR}(t,RG_i)\right]\left[1-\left[1-P_S(t,RG_i)\right]^{n_S^{H_k}}\right]\left[1-P_E(t,RG_i)\right]^{n_E^{H_k}} \quad \textit{Equation 6-2}$$

$$P_{S3}(t,H_k,RG_i)=P_{OR}(t,RG_i)\left[1-P_S(t,RG_i)\right]^{n_S^{H_k}}\left[1-P_E(t,RG_i)\right]^{n_E^{H_k}} \quad \textit{Equation 6-3}$$

$$P_{S4}(t,H_k,RG_i)=P_{OR}(t,RG_i)\left[1-\left[1-P_S(t,RG_i)\right]^{n_S^{H_k}}\right]\left[1-P_E(t,RG_i)\right]^{n_E^{H_k}} \quad \textit{Equation 6-4}$$

$$P_{S5}(t,H_k,RG_i)=\left[1-P_{OR}(t,RG_i)\right]\left[1-P_S(t,RG_i)\right]^{n_S^{H_k}}\left[1-\left[1-P_E(t,RG_i)\right]^{n_E^{H_k}}\right] \quad \textit{Equation 6-5}$$

$$P_{S6}(t,H_k,RG_i)=\left[1-P_{OR}(t,RG_i)\right]\left[1-\left[1-P_S(t,RG_i)\right]^{n_S^{H_k}}\right]\left[1-\left[1-P_E(t,RG_i)\right]^{n_E^{H_k}}\right] \quad \textit{Equation 6-6}$$

$$P_{S7}(t,H_k,RG_i)=P_{OR}(t,RG_i)\left[1-P_S(t,RG_i)\right]^{n_S^{H_k}}\left[1-\left[1-P_E(t,RG_i)\right]^{n_E^{H_k}}\right] \quad \textit{Equation 6-7}$$

$$P_{S8}(t,H_k,RG_i)=P_{OR}(t,RG_i)\left[1-\left[1-P_S(t,RG_i)\right]^{n_S^{H_k}}\right]\left[1-\left[1-P_E(t,RG_i)\right]^{n_E^{H_k}}\right] \quad \textit{Equation 6-8}$$

where $n_S^{H_k}$ is the number of student members of the household *k*, and $n_E^{H_k}$ is the number of employee members of the household *k*.

Therefore, by using the conditional probability of outmigration for each state shown in Figure 6-2, the conditional probability of outmigration for the household *k* at time *t* given that they have not out-migrated until time *t* (termed condition A herein) can be calculated as:

$$P_{PO|A}(t,H_k,RG_i)=\sum_j\left[P_{PO|S_j,A}(t)\times P_{S_j}(t,H_k,RG_i)\right] \quad \textit{Equation 6-9}$$

where $P_{Sj}(t,H_k,RG_i)$ is the probability that household k in residential grid i is in state S_j at time t, and $P_{PO|Sj,A}(t)$ is the household's conditional probability of outmigration at time t if state S_j occurred for the household and the household have not out-migrated until that time, which is shown in Figure 6-2.

In order to calculate the probability of outmigration for household k, $P_{PO|A}(t,H_k,RG_i)$ serves as the hazard function for the household outmigration in time-dependent reliability analysis. The hazard function indicates the likelihood of the event (i.e., outmigration here) between time t and $t + dt$ as $dt \rightarrow 0$ given that the event has not occurred before time t (Melchers, 1999). Therefore, the probability of outmigration for household k in $(0,t]$ can be expressed as:

$$P_{PO}(T \le t, H_k, RG_i) = 1 - \exp\left[-\int_0^t P_{PO|A}(\xi, H_k, RG_i) d\xi \right] \qquad \textit{Equation 6-10}$$

Once the probability of outmigration for household k is found, it can be aggregated for the households at each grid to estimate population outmigration (PO) at the grid level or be aggregated for all households in pseudo-Norman to estimate PO at the community level.

GRID-LEVEL POPULATION OUTMIGRATION

A spatiotemporal depiction of PO can be achieved by aggregating Equation 6-10 for the households living in a specified region (e.g., grids in this dissertation) as:

$$PO(T \le t, RG_i) = \sum_k \left[n^{H_k} \times P_{PO}(T \le t, H_k, RG_i) \right] \qquad \textit{Equation 6-11}$$

For example, population outmigration was assessed for pseudo-Norman after a simulated EF5 tornado hit the city and the mean PO for each grid is illustrated in Figure 6-3. Moreover, the mean

PO at time *t* following the disaster is shown in Figure 6-3 for three grids, as examples. The analysis was done for different tornado intensities and the grid-level mean PO is shown in Figure 6-4 for each EF-scale tornado.

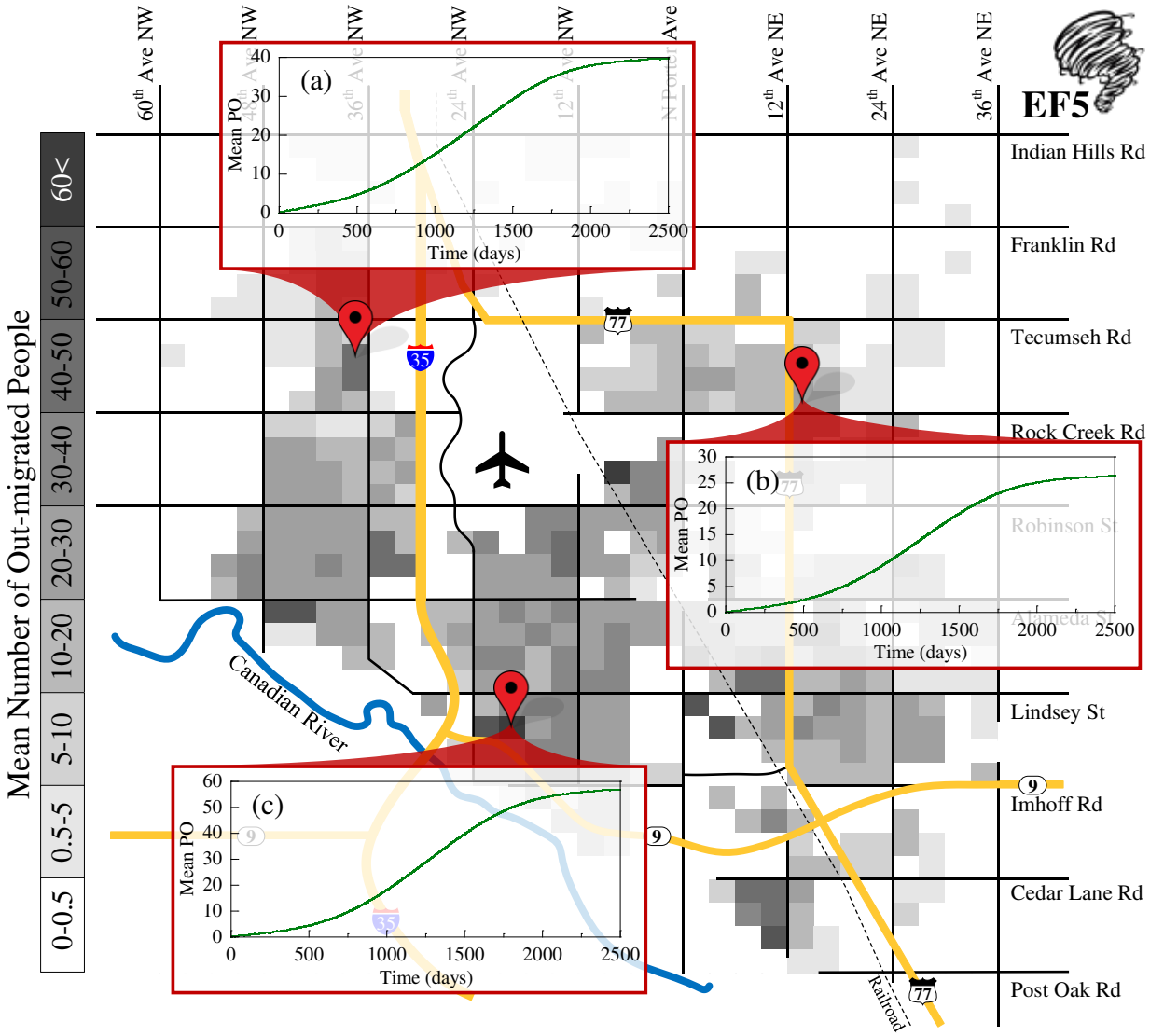

Figure 6-3. Spatiotemporal depiction of mean population outmigration in pseudo-Norman after an EF5 tornado

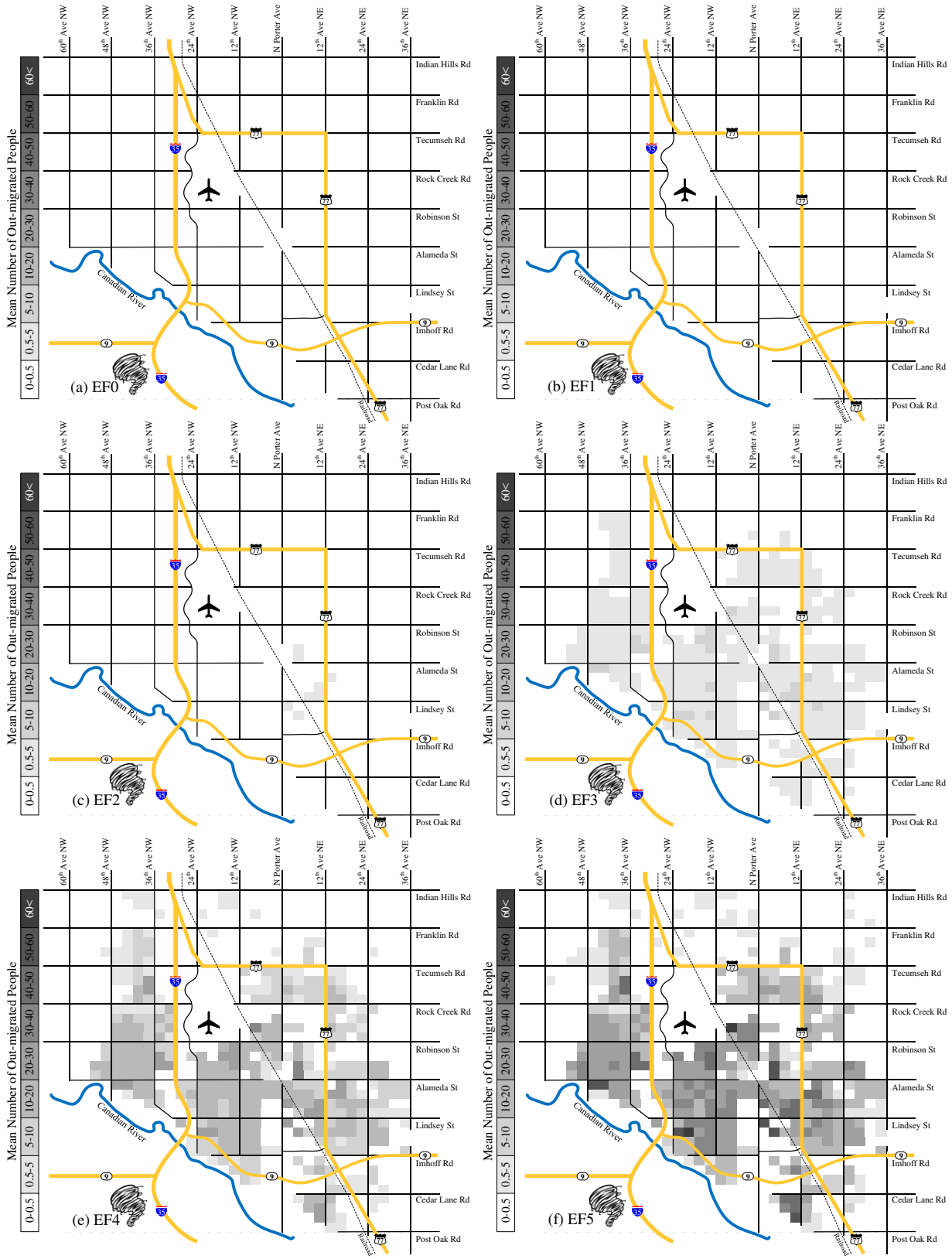

Figure 6-4. Mean number of out-migrated people in each grid in pseudo-Norman after an: (a) EF0, (b) EF1, (c) EF2, (d) EF3, (e) EF4, and (f) EF5 tornado

COMMUNITY-LEVEL POPULATION OUTMIGRATION

Although the spatial distribution of population outmigration provides information regarding areas in the city with a high potential of PO, an estimate for the community-level PO can be employed by community leaders and policymakers for making decisions regarding regional activities and developments. The percentage of population outmigration until time *t* after the event can be calculated for pseudo-Norman as:

$$PO(T \le t) = \frac{\sum_i \sum_k \left[n^{H_k} \times P_{PO}(T \le t, H_k, RG_i) \right]}{pseudo-Norman \;\; Population} \times 100 \qquad \textit{Equation 6-12}$$

where n^{H_k} is the number of people in household *k* and the *pseudo-Norman Population* is set equal to 110,844.

Population outmigration analysis was performed for pseudo-Norman subjected to tornadoes with different intensities and the mean percentage of population outmigration at the community-level is shown in Figure 6-5 (a) as a function of time after the event for each EF-scale tornado. In the case of an EF5 tornado (with the tornado path center located within the area of pseudo-Norman), 6.96% of the pseudo-Norman population (approximately 7,700 people) out-migrate, on average, as a result of physical-socio-economic disruptions in the community. In order to show the extent of uncertainty in the analysis, the 5th, 25th, 50th (i.e., median), 75th, and 95th-percentile of the results of the population outmigration after an EF5 tornado in pseudo-Norman are shown along with the mean of the results in Figure 6-5 (b). When a tornado strikes pseudo-Norman, it may strike a populated area of the town or an undeveloped part of it, which is a source of uncertainty that stems from the unpredictability of the tornado path center, direction, length, and width. Moreover, there exist other significant uncertainties in the analyses such as uncertainties in the resulting damage to

the components as well as the uncertainties in the repair time for the damaged components. As shown in Figure 6-5 (b), after an EF5 tornado hits pseudo-Norman, the mean population outmigration is 6.96%, while the 5th, 25th, 50th, 75th, and 95th-percentile of the PO are equal to 0.01, 0.08, 0.62, 9.06, and 30.96 percent, respectively.

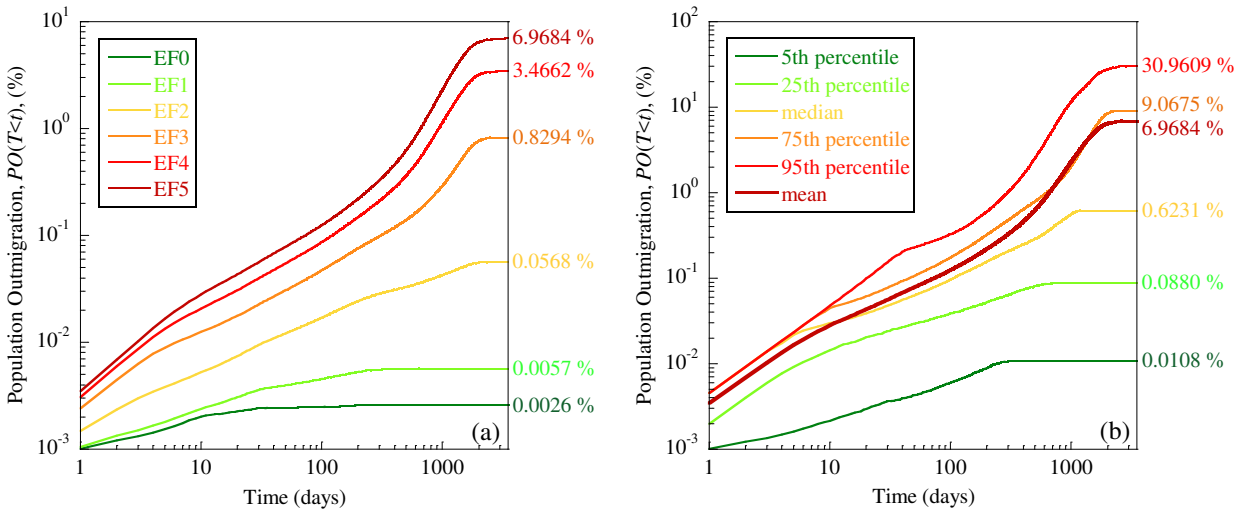

Figure 6-5. (a) Mean population outmigration in pseudo-Norman after each EF-scale tornado and (b) the uncertainty in the EF5 population outmigration

As mentioned before, population outmigration was formulated, in this dissertation, based on the functionality of the residential sector, business sector, and school network in pseudo-Norman; each of which depends not only on the physical performance of their own components but also on the functionality of the electric power network and the water supply network in the city. One might be interested in the contribution of each of these networks in the population outmigration calculation. In this regards, the contribution of physical damage to the buildings (i.e., residential buildings, workplace buildings, and school buildings) versus the contribution of utility loss (i.e., the loss of functionality in the EPN and WSN) in the population outmigration assessment were illustrated in Figure 6-6 (a) after an EF5 tornado in pseudo-Norman. As shown in this figure, the majority of the population outmigration was caused by the functionality loss due to physical damage to the

buildings. This is because the repair process for all the buildings in the residential sector, business sector, and school network takes a long time while the restoration of the EPN and WSN only takes several weeks (or a couple of months in severe cases). Furthermore, the contribution of the functionality of the residential sector, business sector, and school network (functionality includes either physical damage or loss of electric power or water) in causing population outmigration were distinguished in Figure 6-6 (b) after an EF5 tornado hit pseudo-Norman. As shown in this figure, the majority of contribution is for the residential sector while the school network has the lowest contribution. The reason is simply that of the number of buildings that are non-functional after an event. Restoring the EPN and WSN are faster than repairing the damaged buildings. When a tornado hits a city, usually, the largest number of damaged buildings is from the residential sector, then, the business sector and, lastly, the school network because of the distribution and number of these types of buildings within the city.

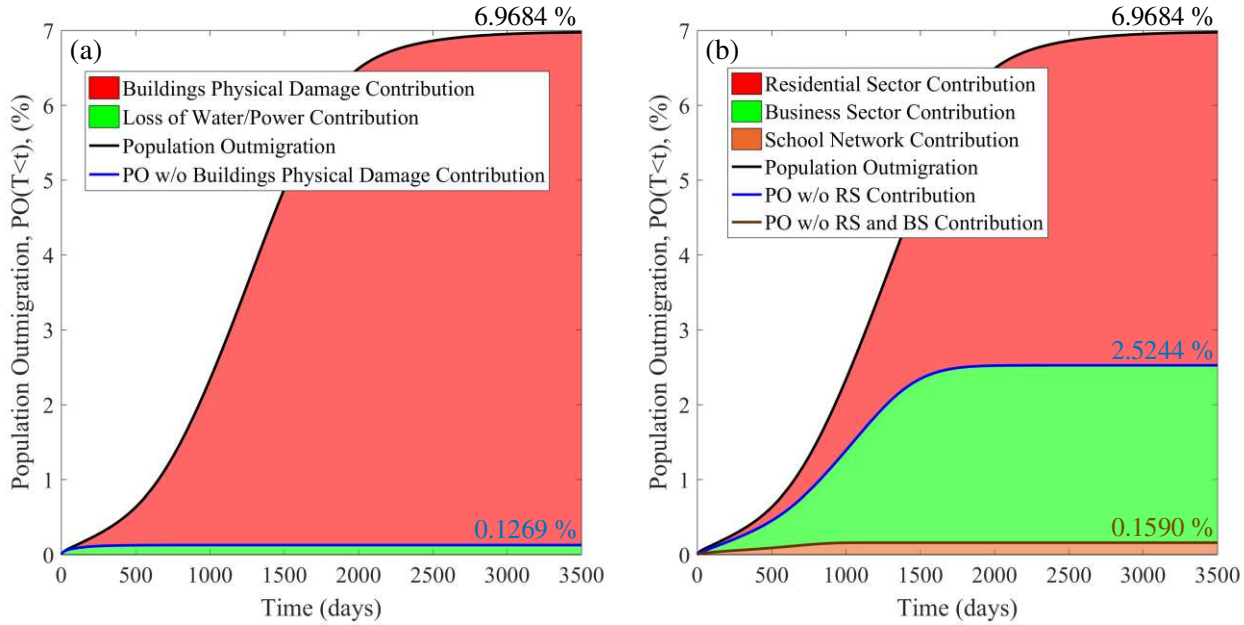

Figure 6-6. (a) Contribution of physical damage to buildings vs loss of utilities in resulting PO and (b) contribution of the functionality of business sector, residential sector, and school network in causing PO

The sensitivity analysis was performed to illustrate the influence of parameters used in the methodology on population outmigration assessment. The sensitivity of the population outmigration analysis on the number of available recovery resource units used for the restoration of the EPN, the business sector, and the residential sector is shown in Figure 6-7. Inspection of this figure shows that the PO is not sensitive to the r_{EPN} while it is highly sensitive to the r_{BS} and r_{RS}. Using 10 available recovery resource units for the restoration of the business sector results in 22% PO after an EF5 tornado (on average) while increasing the r_{BS} to 20 and 50 units decreases the PO to 13% and 7%, respectively. For the residential sector, using 50 available recovery resource units results in 10% PO after an EF5 tornado (on average) while increasing the r_{RS} to 250, 500, and 1500 decreases the PO to 7%, 4%, and 2.5%, respectively.

The sensitivity of the PO to the parameters of the fragility curves as well as the parameters of the repair/permitting time was examined separately for the parameters used in each network and the results are shown in Figure 6-8 and Figure 6-9. As illustrated in these figures, although the PO is insensitive to the logarithmic standard deviation of fragility curves and the COV of the repair/permitting time, it can be highly sensitive to the median of fragility curves and the mean of the repair/permitting time. Population outmigration was shown to be insensitive to the parameters that were used in the EPN, WSN, and school network; however, it is sensitive to these parameters for the business sector and residential sector. The reason is that of the contribution of these networks in resulting PO, as shown in Figure 6-6. Moreover, the parameters used for the business sector have the most influence on the calculation of PO since if a workplace building becomes non-functional its effects spread throughout the city in that employees may live in different parts of the city than they work.

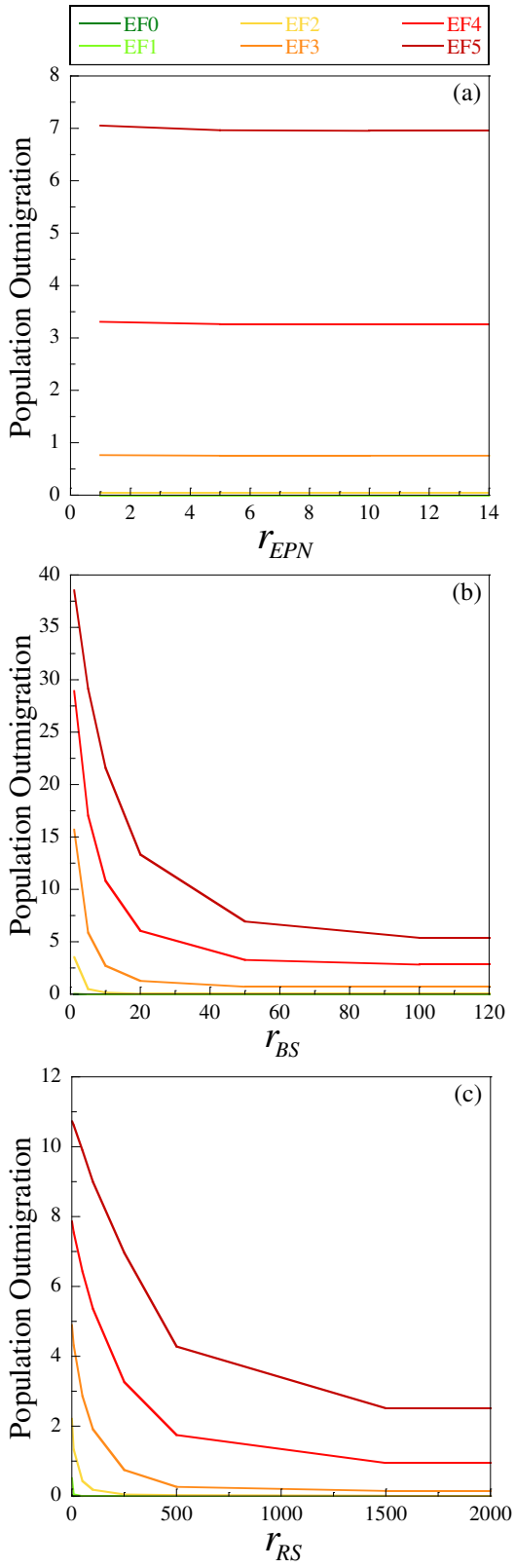

Figure 6-7. Sensitivity of population outmigration calculation to the number of available recovery resource units for the restoration of (a) electric power network, (b) business sector, and (c) residential sector

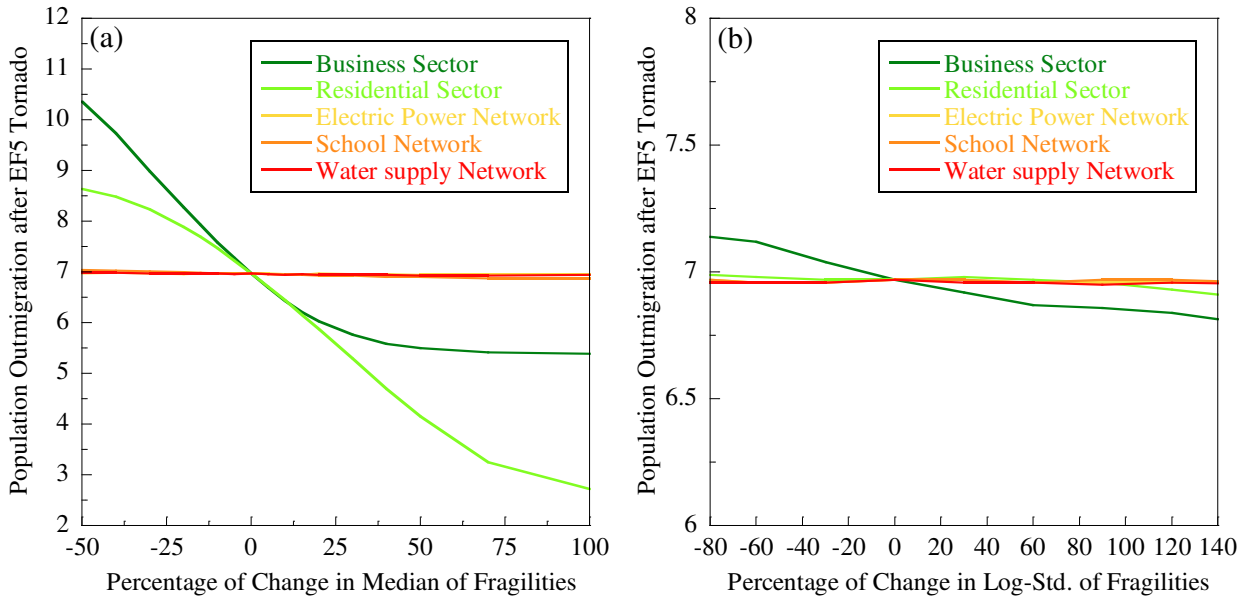

Figure 6-8. Sensitivity of population outmigration calculation to the parameters of fragility curves used for each network modeled in this dissertation

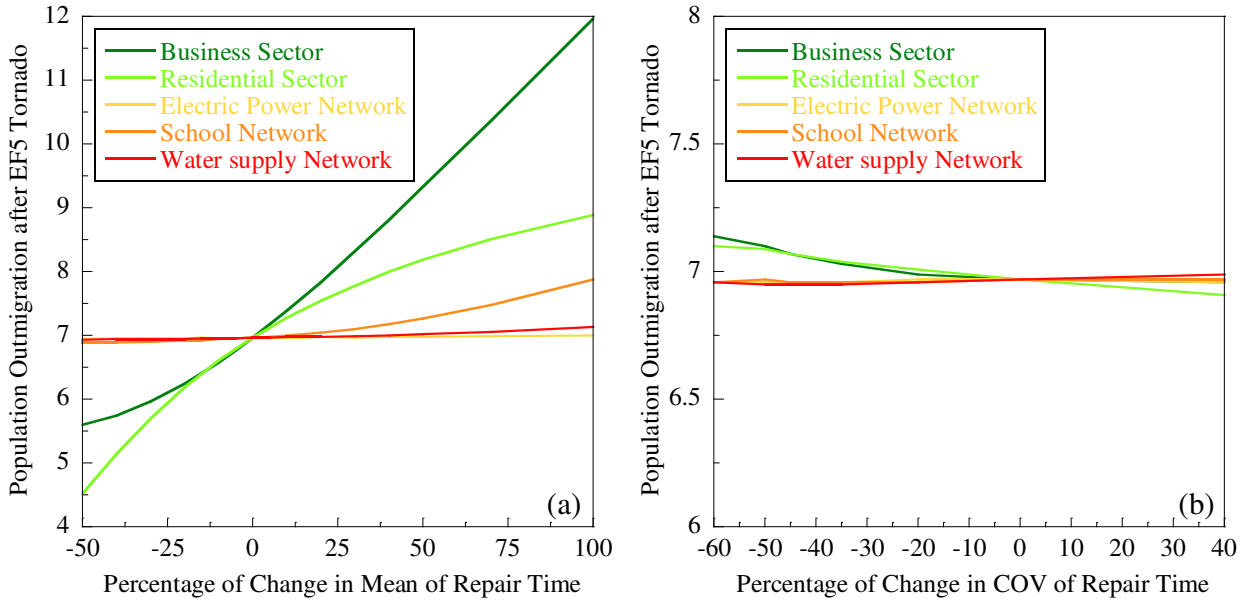

Figure 6-9. Sensitivity of population outmigration calculation to the parameters of repair/permitting time used for each network modeled in this dissertation

CHAPTER 7: TORNADO-INDUCED CASUALTIES[1]

INTRODUCTION

Tornadoes threaten life safety in many regions of the United States each year and have been the cause of the highest number of fatalities among natural hazards over the last 10 years (NOAA, 2017a). Since designing a building to resist intense tornadoes (i.e., EF3, EF4, and EF5 tornadoes) is not economically justifiable, van de Lindt et al. (2013) proposed a dual-objective design philosophy that reduces building damage for tornadoes in the EF0 to EF2 range, while focusing on life safety for tornadoes with higher intensity, i.e. EF3 to EF5. Moreover, from a community resilience perspective, risk mitigation policies and master planning of a new community not only have to satisfy community resilience metrics but must also meet life-safety requirements or targets at the community level. Therefore, the purpose of this chapter is to provide a predictive model for injuries and fatalities induced by a tornado at the community level. In this regard, a model will be developed for the contiguous United States based on the all relevant recorded historical tornadoes. Several tornado properties (e.g., tornado intensity and tornado path length) as well as the properties of the affected community (e.g., the number of housing units and people located in the tornado path) were used as explanatory variables in the regressive model to assess the expected number of tornado-induced injuries and fatalities. The model will then be applied to the pseudo-Norman community following the thread/theme throughout this dissertation as an illustrative example.

Shen and Hwang (2015) studied the expected risks of human injuries and fatalities for the continental United States by taking into account the effects of tornado disasters between 1950 and

[1] This section is based on the paper: Masoomi, H., and van de Lindt, J.W., (2018) "Fatality and Injury Prediction Model for Tornadoes", accepted, *ASCE Natural Hazards Review*, DOI: 10.1061/(ASCE)NH.1527-6996.0000295

2012. In this regard, they integrated the tornado database with the U.S. state boundary GIS database to find the spatial distribution of tornadoes and their corresponding effects at the state level. Ashley (2007) used the tornadoes between 1950 and 2004 to investigate the spatial and temporal analysis of tornado fatalities by assigning fatalities reported for each tornado to the nearest town or county seat. Fricker et al. (2017) improved the spatial distribution of tornado-induced casualties by allocating the total number of casualties reported for each tornado according to the underlying population within the tornado path and for the tornadoes between 1955 and 2016. Simmons and Sutter (2008) investigated the effect of tornado warnings on casualties by examining a dataset of tornadoes in the U.S. between 1986 and 2002. Their results show that although an increase in lead time up to 15 minutes reduces fatalities, longer lead times resulted in more fatalities compared with no warning. Simmons and Sutter (2014) updated this regression model by using 1990-2010 tornadoes in order to examine if the tornadoes in 2011 produced fatalities consistent with earlier tornadoes. Their fatality regression model did not correctly predict the number of fatalities in the individual 2011 tornadoes but noted that a high degree of precision was not expected because they were using the demographic data at the county level. In fact, they used the U.S. census data at the county level in order to find the average number of people in each storm path as well as other economic and demographic variables used in the model. This likely introduces an unbiased error because sometimes tornadoes strike a town in a populated county, and sometimes an undeveloped part of an urban county. Therefore, in this dissertation, an attempt was sought to reduce this error as much as possible by using a finer census level, i.e., block level.

PREDICTION MODEL FOR THE CONTIGUOUS UNITED STATES

The U.S. Tornado Database

Two different types of database were used here, namely the United States tornado database and U.S. Census database. The National Weather Service (NWS) Storm Prediction Center (SPC) has a database of tornadoes in the United States since 1950 (NOAA, 2017d). This database provides tornado properties such as the intensity of the tornado, the date and time when tornado occurred, number of induced injuries and fatalities, longitude and latitude for the touchdown and lift-off points, estimated property damage, and the path length and width as well as additional information. Figure 7-1 shows the annual tornado counts and the annual number of casualties reported in the United States between 1950 and 2015. As shown in Table 7-1, more than 60,000 tornadoes were reported in the United States in this period, which includes 46.47% EF0/F0, 33.64% EF1/F1, 14.85% EF2/F2, 4.01% EF3/F3, 0.94% EF4/F4, and 0.09% EF5/F5 tornadoes. These tornadoes caused approximately 94,000 injuries and 6,000 fatalities. Casualties corresponding to each EF/F scale are summarized in Table 7-1.

Due to improvement in communications and technological advances, there has been an increase in the number of tornado reports over the years, as shown in Figure 7-1 (a). The first national weather surveillance radar network was put in place in the late 1950s (Schaefer and Edwards, 1999). The number of EF0/F0 tornadoes increased remarkably since 1990. This increase is partly because of a policy change in 1982 to assign F0 to all tornadoes when the amount of damage was unknown or not observable as well because of more incorporation of local weather forecast offices in spotting storms after 1990 (McCarthy, 2003; Brooks, 2004). The annual fatalities and injuries between 1950 and 2015 are plotted in Figure 7-1 (c) and (d), respectively. Since the major casualties occur in intense tornadoes (i.e., EF3/F3 to EF5/F5 tornadoes), the annual number of

intense tornadoes were plotted in Figure 7-1 (b) for more detail. For example, although annual tornado counts are 126 tornadoes more in 2004 (the year with the largest number of reported tornadoes) than in 2011, the annual injuries and fatalities in 2011 are, respectively, 14 times and 16 times those of 2004. This is partly because the number of intense tornadoes in 2011 was 3 times those of 2004, and the number of casualties was much more substantial in the 2011 tornadoes because several tornadoes hit densely populated areas.

Rating tornadoes before 1973 was almost solely based on reading articles and looking at published photographs, which results in a high bias in rating of tornadoes for this period (Schaefer and Edwards, 1999). In 1971, the Fujita scale (F scale) was developed (Fujita, 1971) and implemented in 1973 to rank the intensity of tornadoes. Therefore, only the tornado dataset from 1973 to 2015 is included in the regression models in this dissertation. The number of tornadoes and casualties reported in this period is summarized in Table 7-1 for each EF/F scale. The F scale was used until 2007 when it was replaced by the Enhanced Fujita scale (EF scale). The corresponding F scales and EF scales were considered to be in the same category in this dissertation, e.g. F0 and EF0 were assumed to be the same category. It is not logical to reclassify the F scales into the EF scale as the scale is based on damage and not wind speeds (Standohar-Alfano and van de Lindt, 2014). It should be noted that both rating methods are subjective which results in some inevitable systematic biases. These biases are extremely difficult to detect and there is nothing that can be done about them (Brooks, 2004). The term “EF scale” will be used from this point forward.

The reported tornadoes in a database can have unrecorded properties such as the coordinates of touchdown and lift-off, intensity, or path width. Among tornadoes in the 1973-2015 dataset, 492 tornadoes were rated as unknown intensity, 473 tornadoes had unrecorded path width, and the latitude and/or longitude of start and/or end points were not reported for 26,033 tornadoes, which

resulted in 26,226 tornadoes with incomplete properties. These tornadoes were excluded from dataset, and finally as shown in Table 7-1, a filtered dataset including 20,001 tornadoes was used in the regression analyses.

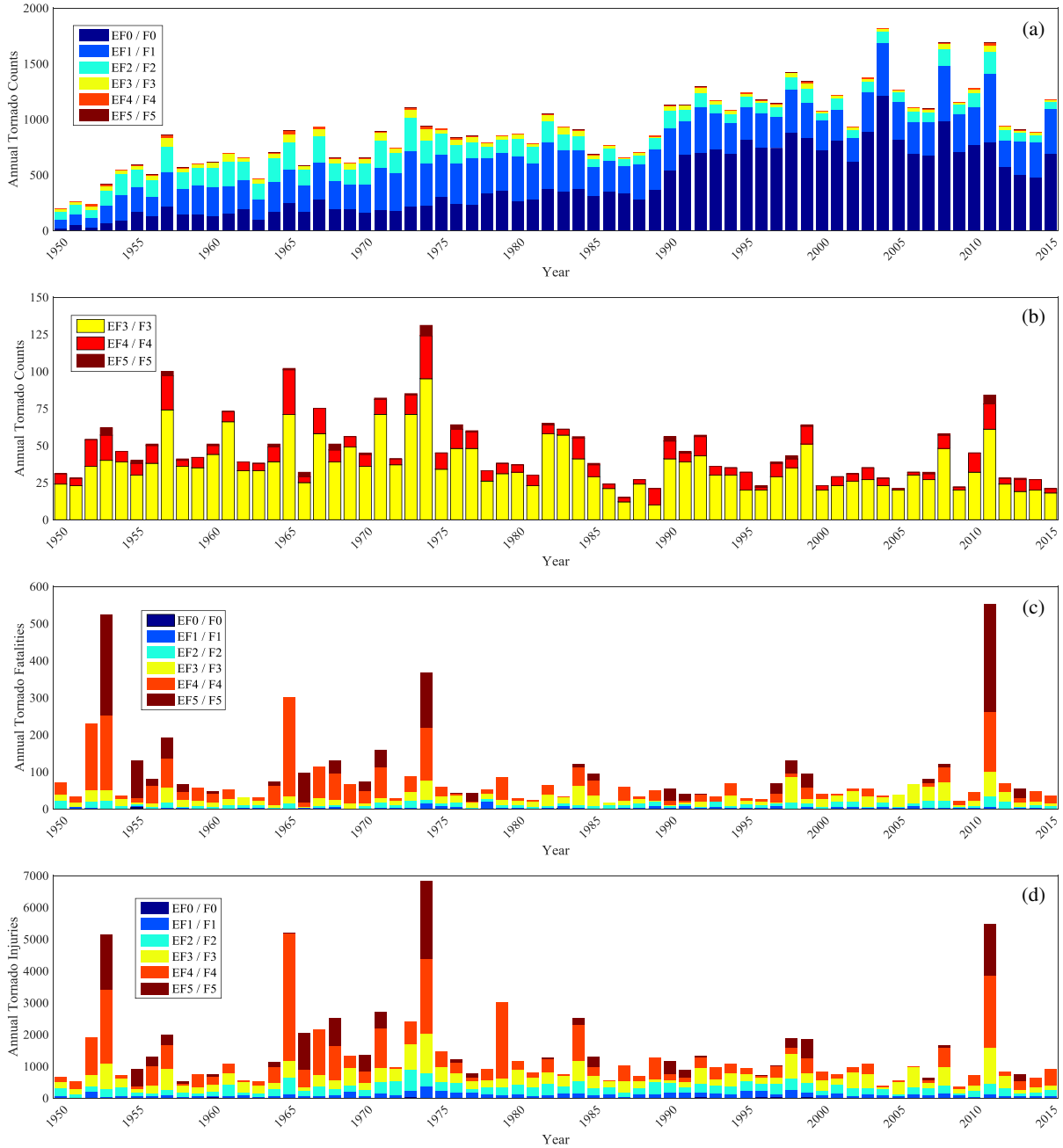

Figure 7-1. The annual tornado counts and the annual number of fatalities and injuries in the United States since 1950. (a) The annual tornado counts including all EF/F scale tornadoes, (b) the annual tornado counts including only EF3/F3 to EF5/F5 tornadoes (i.e. intense tornadoes), (c) the annual tornado fatalities, and (d) the annual tornado injuries

Table 7-1. The number of tornadoes and corresponding injuries and fatalities in each EF/F scale for different datasets

Tornado Intensity	1950-2015 Dataset			1973-2015 Dataset			1973-2015 Filtered Dataset		
	Tornado Counts	Injuries	Fatalities	Tornado Counts	Injuries	Fatalities	Tornado Counts	Injuries	Fatalities
All Intensities	60114	93856	5823	46227	57119	3202	20001	50933	3015
EF0/F0	27933	811	23	24530	669	13	7529	227	5
EF1/F1	20221	6954	227	14841	5158	182	7437	2895	108
EF2/F2	8924	15594	587	5051	10650	392	3424	8108	320
EF3/F3	2412	23012	1282	1436	15591	920	1256	14760	892
EF4/F4	565	34529	2357	335	18317	1015	321	18209	1010
EF5/F5	59	12956	1347	34	6734	680	34	6734	680

The U.S. Census Database

A tornado may strike a town in a populated area of a county or an undeveloped part of an urban county. These two scenarios result in two drastically different number of casualties for intense tornadoes. This puts emphasis on the importance of the number of housing units and people located in a tornado path on casualties. The number of damaged housing units and their level of damage are also two other imperative factors which might critically affect the number of casualties. The tornado database does not provide any information about these factors. However, the number of housing units and people in tornado path can be approximated by using the tornado track information (i.e., the longitude and latitude of touchdown and lift-off points as well as the tornado width) and the U.S. census data. The best approximation can be made by using the U.S. census database (American FactFinder, 2017) at the block level.

Finding an approximation for the number of damaged housing units and their level of damage for each tornado is challenging and cannot be done for a reasonable number of tornadoes to be used for a regression model. However, these parameters can be inferred and replaced by the estimated property damage reported in the tornado database. Tornado damage type was separated into two categories, property damage and crop damage, since 1996, and a dollar amount was assigned to

each (McCarthy, 2003). Before 1996, a value was assigned to a monetary range, which makes identifying this change in monetary amounts more challenging. The damage assessment is a subjective process and the estimated property damage is based on available figures supplied by insurance companies. If this is not available, the dollar estimate is aquired from emergency management, utility companies, or newspaper articles (McCarthy, 2003).

In order to estimate the number of housing units and people located in each tornado path, the U.S. census data for the years 1970, 1980, 1990, 2000, and 2010 and the American Community Survey (ACS) 5-year estimate for the year 2015 were utilized. Then, the intercensal estimate was calculated for each tornado by simple linear interpolation based on the year of occurrence. The U.S. census data for the years 1970 and 1980 were found at the county level along with the cartographic boundary shapefiles from the National Historical Geographic Information System (NHGIS) (Minnesota Population Center, 2016). The NHGIS provides population, housing, agricultural, and economic data along with GIS boundary files for the United States since 1790. The U.S. census data for the year 1990 was found at the block group level from Centers for Disease Control and Prevention (CDC, 2017). American FactFinder (2017) was used to obtain the U.S. census data for the year 2000 and the ACS 5-year estimate for the year 2015, both at the census tract level. And, the U.S. census data for the year 2010 was obtained at the block level along with the cartographic boundary shapefiles from the Topologically Integrated Geographic Encoding and Referencing (TIGER, 2017) geographic database developed by the U.S. Census Bureau. The cartographic boundary shapefiles for 1990 at the block group level and for 2000 and 2015 at the census tract level were downloaded from the United States Census Bureau website (2017).

Different census levels are shown in Figure 7-2 for the State of Alabama as an example. Alabama had 67 counties, 1181 census tracts, 3438 block groups, and 252,266 census blocks in 2010. In

order to see the details better, Tuscaloosa County, marked in Figure 7-2 (a), is shown in Figure 7-3 at four different census levels along with the path of the EF4 tornado occurred in 2011 in the city of Tuscaloosa, Alabama.

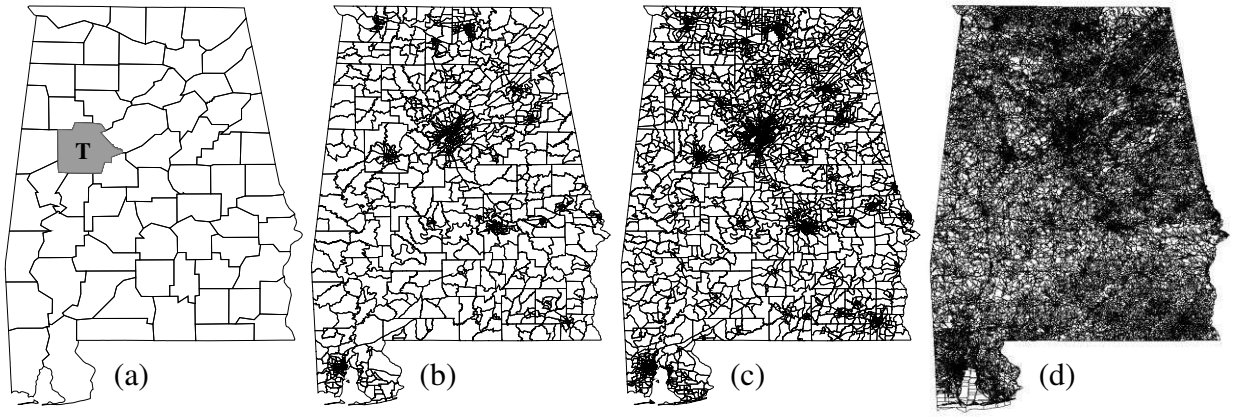

Figure 7-2. Different Census Levels for the State of Alabama: (a) Counties, (b) Census Tracts, (c) Block Groups, and (d) Census Blocks. The county marked in part (a) is Tuscaloosa County

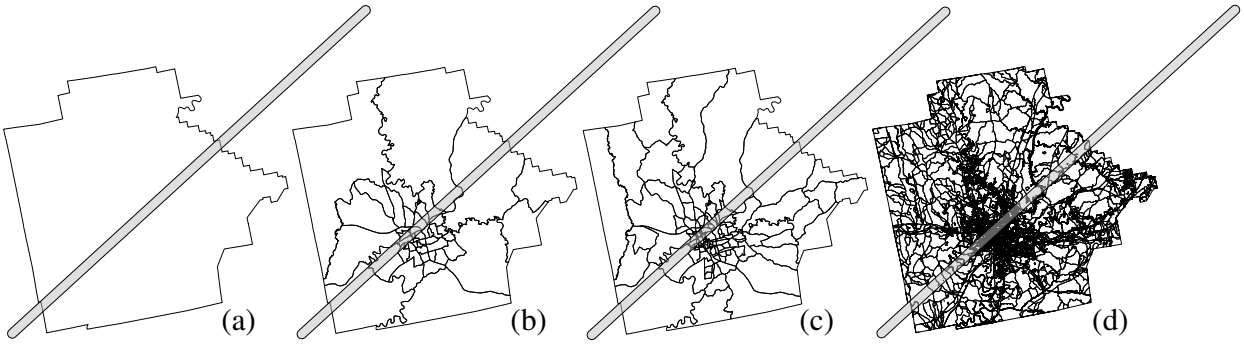

Figure 7-3. Different Census Levels for the Tuscaloosa County: (a) Counties, (b) Census Tracts, (c) Block Groups, and (d) Census Blocks. The EF4 tornado occurred on April 27, 2011 in the city of Tuscaloosa Alabama is also shown

Since a tornado track has a relatively narrow width, using the finest census level, i.e. block level, provides the best estimate for the number of housing units and people located in each tornado path, which will be explained further later. However, as mentioned before, only the census data for 2010 was available at the block level. Therefore, the census data for the other aforementioned years

were adjusted here to represent block-level data.[1] For example, for the 2000 census data which is at the census tract level, instead of considering uniformly distributed population and housing unit counts over a census tract area, the distribution was weighted based on the corresponding population and housing unit counts for the 2010 blocks located in that census tract area. In other words, the 2010 census data at the block level was used for all other years, but the population and housing unit counts were adjusted to satisfy the amount of corresponding parameters in the considered year (e.g., 2000) at the available census level (e.g., census tract level). The blocks size are fine enough to give a reasonable estimation for the population and housing unit counts distributed uniformly over a block area.

Housing Unit Counts and Population

This section explains the procedure to estimate the affected community properties for each tornado in the dataset (i.e., the number of housing units and people located in a tornado path). ArcMap GIS software was used to develop the tornado paths and intersect them with the census data shapefiles. The steps to estimate the number of housing units and people located in the tornado path is presented in Figure 7-4 with an example at the county level for the EF4 tornado that occurred on April 27, 2011, in Tuscaloosa, Alabama.

Based on the longitude and latitude for the touchdown and lift-off points for each tornado a line is drawn which was then buffered based on the corresponding tornado width to obtain the tornado path. The tornado path is intersected with the boundary shapefiles to find the portion of the census-level entities located in the tornado path. As an example, the Tuscaloosa EF4 tornado hit the three

[1] Although this adjustment may result in misestimation for tornadoes in counties that have had a large population increase, it did not have a significant effect on the regression results.

counties of Jefferson, Tuscaloosa, and Greene as shown in Figure 7-4. The population and housing unit counts can then be calculated as:

$$P = \sum_{i=1}^{n} \left(\frac{A_i^T}{A_i^C} \right) P_i^C \qquad \textit{Equation 7-1}$$

$$H = \sum_{i=1}^{n} \left(\frac{A_i^T}{A_i^C} \right) H_i^C \qquad \textit{Equation 7-2}$$

where, P and H are the estimated population and housing unit counts located in the tornado path at the corresponding census level, respectively. n is the number of census-level entities located in the tornado path (e.g., n is three in Figure 7-4) and A_i^T is the potion of the area of the census-level entities in the tornado path. A_i^C, P_i^C, and H_i^C are the area, population, and housing unit counts for the census-level entities, respectively.

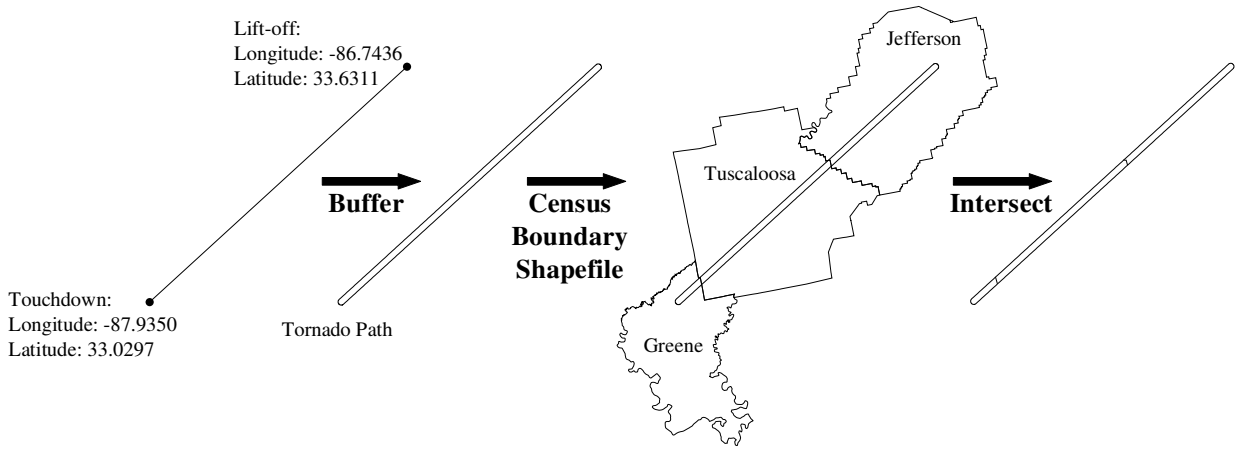

Figure 7-4. The steps for estimating population and housing unit counts located in a tornado path. The estimation at county level for the EF4 tornado on April 27, 2011 in Tuscaloosa, Alabama is presented here as an example

In order to check the consistency of the identified counties hit by the mapped tornadoes with the corresponding counties reported in the SPC database, the overlap percentage of the identified

counties with the counties reported in the SPC database were evaluated for each tornado. As shown in Table 7-2, the mapped tornado paths herein are reliable regarding the identified Census blocks being in the correct counties reported in the SPC database.

Table 7-2. The percentage of tornado paths that contains Census blocks that have x% overlap with the SPC reported counties

EF Scale	Overlap Percentage			
	= 100	≥ 75	≥ 50	= 0
EF0	98%	98%	99%	1%
EF1	97%	97%	99%	1%
EF2	96%	96%	99%	1%
EF3	96%	96%	99%	1%
EF4	91%	95%	100%	0
EF5	94%	97%	100%	0

Figure 7-5 shows the intersected tornado path with four different census-level boundaries. Incidentally, for this particular example, the estimations at the four levels are close (i.e., less than 10% error). However, if the estimated parameters for the part of the tornado path at each county are considered for comparison, as tabulated in Table 7-3, the error can be as high as 77.2% when the census data at the county level is used. Although the estimated parameters at the block group level and census tract level have up to 20% error in this example, this error is expected to be higher for the tornado paths with lower width (The Tuscaloosa EF4 tornado on April 27, 2011, had a maximum path width of 2380 meters while an EF4 tornado has a mean width of approximately 700 meters).

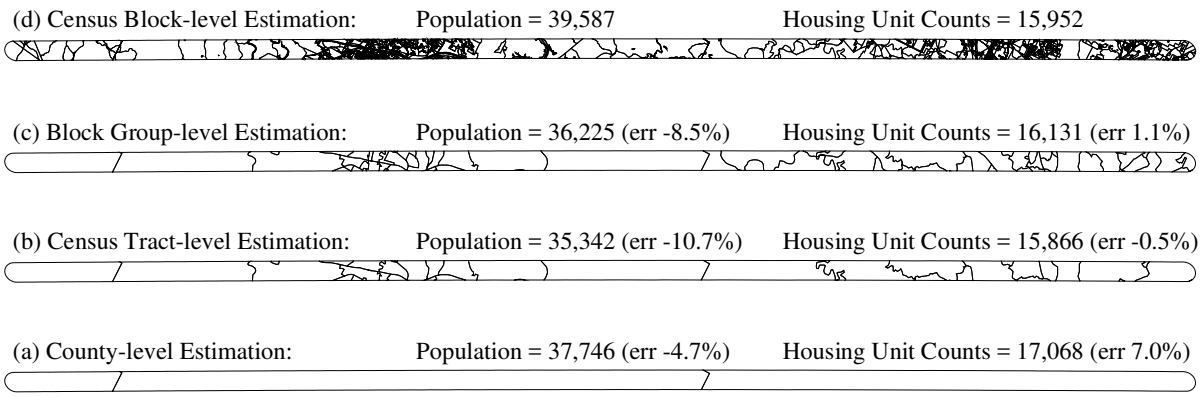

Figure 7-5. Estimated population and housing unit counts located in the EF4 tornado path that occurred on April 27, 2011 in Tuscaloosa, Alabama for different census levels: (a) County level, (b) Census Tract level, (c) Block Group level, and (d) Census Block level. The error is shown in parenthesis with respect to the block-level estimation

Table 7-3. Estimated parameters at different census level for the total tornado path as well as the part of the tornado path in each county

Parameters	Tornado Part	Blocks Est.	Block Groups Est.	Error (%)	Census Tracts Est.	Error (%)	Counties Est.	Error (%)
P	Total	39587	36225	-8.5	35342	-10.7	37746	-4.7
	Greene	110	97	-11.8	87	-20.9	154	40.0
	Jefferson	16928	15949	-5.8	16110	-4.8	28969	71.1
	Tuscaloosa	22549	20179	-10.5	19145	-15.1	8623	-61.8
H	Total	15952	16131.0	1.1	15866	-0.5	17068	7.0
	Greene	56	54.0	-3.6	50	-10.7	85	51.8
	Jefferson	7464	7281.0	-2.5	7105	-4.8	13223	77.2
	Tuscaloosa	8432	8796.0	4.3	8711	3.3	3760	-55.4

In order to compare the effect of using county-level versus block-level data for estimating population and housing unit counts within each tornado path, the median of estimated parameters as well as the average and maximum absolute difference of county-level and block-level estimation were evaluated for each EF scale and presented in Table 7-4. The errors are higher for the lower EF scales.

Table 7-4. Comparison of estimated parameters using county-level and block-level data

EF Scale	Parameters							
	Population				Housing Unit Counts			
	Block-level Median	County-level Median	MAD*	Maximum AD**	Block-level Median	County-level Median	MAD*	Maximum AD**
EF0	1	2	27	33977	0	1	10	5496
EF1	7	11	89	19459	3	5	38	9319
EF2	29	36	216	75444	12	16	88	30568
EF3	103	129.5	421	14998	43	54	176	6925
EF4	403.5	369	1328	60122	175.5	152.5	542	16838
EF5	2967	1816	2492	18584	1011	637	1027	8189

*MAD: Mean Absolute Difference; **AD: Absolute Difference.

The procedure explained above was applied for all 20,001 tornadoes in the 1973-2015 filtered tornado dataset and the considered parameters were estimated by using census data at the modified block level for the years 1970, 1980, 1990, 2000, 2010, and 2015. Finally, the intercensal estimate was generated for each tornado by simple linear interpolation based on the year of occurrence. One caveat to this process is that the tornado path is assumed to be a straight line between touchdown and lift-off points with a constant width as reported in the tornado database. The assumption of a straight line path may underestimate or overestimate the affected community properties (i.e., the number of housing units and population located in the tornado path). For example, Figure 7-6 shows the EF5 tornado in Joplin on May 22, 2011, as a simplified angular path which is close to the observed path (Figure 7-6 (a)) and as an assumed straight path (Figure 7-6 (b)). The estimated properties are drastically different in these two cases because the angular path goes through a dense residential portion in Joplin, Missouri. The estimated housing unit counts and population are equal to 6,830 and 14,870 for the angular tornado path, respectively, while they were estimated equal to 1,821 and 4,480 when the straight tornado path was used. Although the straight path assumption drastically underestimates the affected community properties in this example, there are other cases in which the modeled straight path goes through a populous area (i.e., an overestimation) while

the observed tornado had a curved path which skipped the populous area. Therefore, since the straight path assumption cannot be relaxed because of the lack of information in the tornado database, it was accepted in the analyses as an unavoidable error and noted.

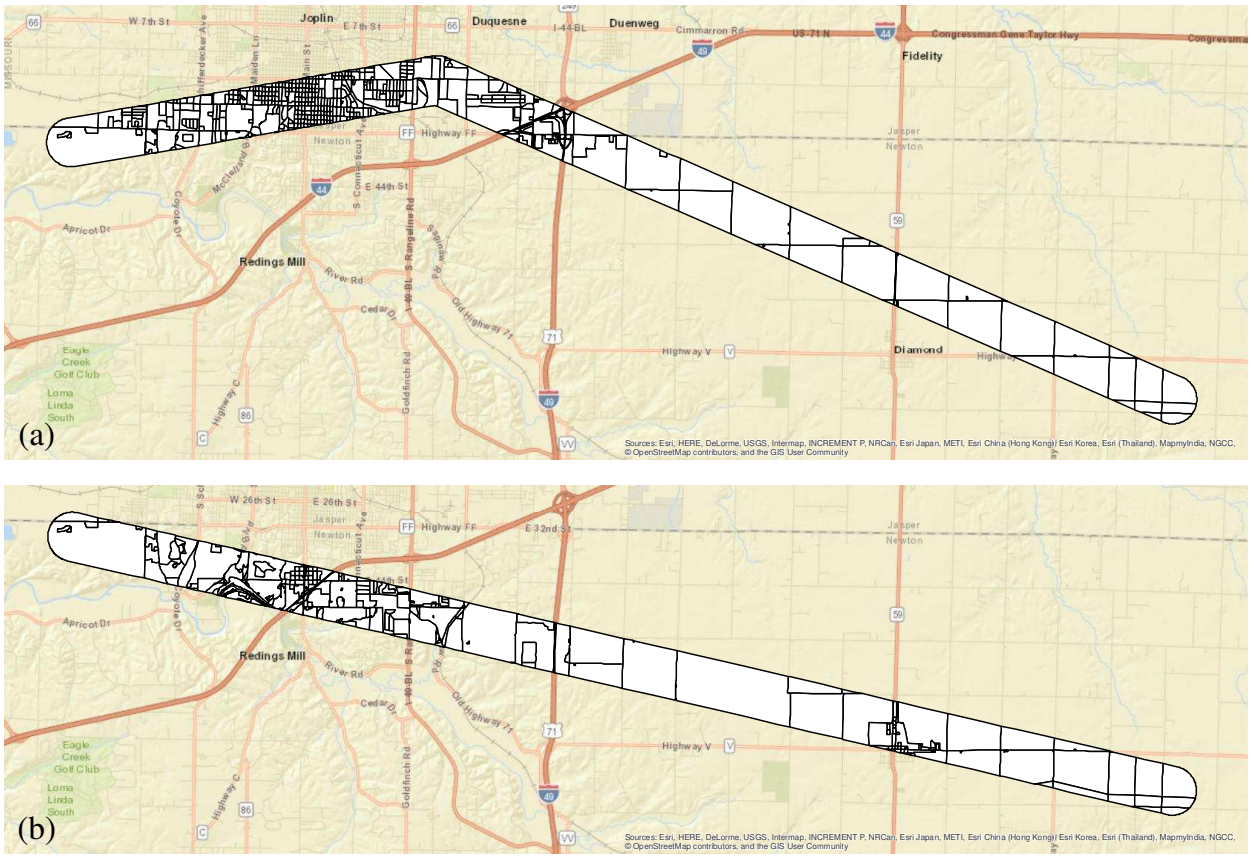

Figure 7-6. Simplified path model for the EF5 tornado in Joplin on May 22, 2011: (a) an angular tornado path based on the observed tornado path, and (b) a straight tornado path

Regression Model

One of the common approaches for developing models in order to predict variables of interest based on past data is a statistical regression model. In this regard, generalized linear models (GLM) (Nelder and Wedderburn, 1972; Cameron and Trivedi, 1998) were used, which are the common regression models for count data. In this dissertation, both a Poisson GLM and negative binomial GLM were investigated and will be discussed further later. The reason for using a negative

binomial GLM is its flexibility to model the overdispersed count data, i.e. when the variance is greater than the mean for the counts. However, the variance and mean are equal in a Poisson GLM with the probability density function (PDF) conditional on a vector of explanatory variables, **X**, as:

$$f(y \mid \mathbf{X}) = \frac{e^{-\lambda}\lambda^{y}}{y!} \qquad \textit{Equation 7-3}$$

$$E[y \mid \mathbf{X}] = \text{var}[y \mid \mathbf{X}] = \lambda = \exp\left(\beta_0 + \sum_i \beta_i x_i\right) \qquad \textit{Equation 7-4}$$

where y are the counts of injuries/fatalities, x_i are the explanatory variables, β_i are the regression parameters, and λ is the link parameter which is the conditional mean and variance for the Poisson distribution.

In a negative binomial GLM, the count data follow a negative binomial probability mass function (PMF) conditional on **X** and α as shown in Equation 7-5:

$$f(y \mid \mathbf{X}, \alpha) = \frac{\Gamma(y + \alpha^{-1})}{\Gamma(y+1)\Gamma(\alpha^{-1})}\left(\frac{\alpha^{-1}}{\alpha^{-1} + \lambda}\right)^{\alpha^{-1}}\left(\frac{\lambda}{\alpha^{-1} + \lambda}\right)^{y} \qquad \textit{Equation 7-5}$$

$$E[y \mid \mathbf{X}, \alpha] = \lambda = \exp\left(\beta_0 + \sum_i \beta_i x_i\right) \qquad \textit{Equation 7-6}$$

$$\text{var}[y \mid \mathbf{X}, \alpha] = \lambda + \alpha\lambda^2 \qquad \textit{Equation 7-7}$$

where α is the overdispersion parameter and is greater than zero. As α goes to zero, the negative binomial distribution approaches the Poisson distribution. Therefore, α can be used as a

dimensionless criterion to compare fitted models for a data set such that if α is not significantly different from zero, the Poisson GLM and, otherwise, the negative binomial GLM is the correct choice for regression model. Moreover, the Akaike information criteria (AIC) was used as an alternative criterion for comparing the fitted models such that the model with a smaller AIC is preferred. The AIC for a fitted model is defined as (Akaike, 1974):

AIC = –2 log(Likelihood) + 2 (Number of Independent Parameters) *Equation 7-8*

In order to measure the goodness of fit for the negative binomial GLM models, pseudo-R^2 statistic based on α, R^2_α, was calculated for each model as shown in Equation 7-9 (Liu et al., 2005; Han et al., 2009):

$$R_\alpha^2 = 1 - \frac{\alpha}{\alpha_0} \qquad \textit{Equation 7-9}$$

where α and α_0 are the overdispersion parameters for the fitted model and the intercept-only model, respectively.

Model 1: Basic Model

Injuries and fatalities are the dependent variables and the tornado path width, tornado path length, tornado intensity, and population and housing unit counts located in the tornado path are the explanatory variables for the basic model. However, using both population and housing unit counts variables in a regression model resulted in an inconsistency such that the regression parameter for population was negative. This means that increasing the population in a tornado path results in lower injuries and fatalities which is not logical. One of the reasons for this outcome is that the population and housing unit counts variables were found to be linearly correlated. Therefore, the variable housing unit counts was omitted and only the population located in the tornado path was

used as an explanatory variable in the regression models. Moreover, tornado path width was excluded from the explanatory variables vector in that it was found to be an insignificant predictor based on its two-tailed p-value in the models. The reported tornado path width in the database was measured at the widest point along a tornado path and has a high level of uncertainty, which makes it unreliable if included as an explanatory variable. Since different tornado intensities have drastically different mean injury and fatality counts, tornado intensities were categorized into moderate tornadoes (i.e., EF0 and EF1), strong tornadoes (i.e., EF2 and EF3), and violent tornadoes (i.e., EF4 and EF5) and three regression models were developed for both injuries and fatalities. The explanatory variables in each model are LENGTH (the tornado path length in kilometers), POP (the population located in the tornado path), EF1 for moderate tornado model (a dummy variable that equals one if the tornado is EF1 and zero for an EF0 tornado), EF3 for strong tornado model (a dummy variable that equals one if the tornado is EF3 and zero for an EF2 tornado), and EF5 for violent tornado model (a dummy variable that equals one if the tornado is EF5 and zero for an EF4 tornado).

Although Simmons and Sutter (2008) suggested using a Poisson GLM for fatalities and a negative binomial GLM for injuries, comparing the overdispersion parameters as well as AIC for the models here shows that a negative binomial GLM outperforms a Poisson GLM for both injuries and fatalities. For example, as shown in Table 7-5 for violent tornadoes, the overdispersion parameter is equal to 2.444 and 2.212 for injuries and fatalities, respectively, which indicates that based on Equation 7-7, the variance is significantly greater than the mean and thus a negative binomial GLM should be used for the regression model. Moreover, AICs are significantly lower for negative binomial GLM than those for Poisson GLM (3010 vs 39744 for injuries and 1449 vs 3043 for fatalities). Therefore, a negative binomial GLM is suggested for both injuries and fatalities.

Table 7-6 shows the regression parameters, α, AIC, and pseudo-R^2 for negative binomial GLM for injuries and fatalities of moderate and strong tornadoes. Since there is a significant level of uncertainty in the models for injuries and fatalities, it is recommended that the maximum estimated number of injuries and fatalities from the models be constrained (capped) by the maximum of the corresponding variables in the tornado dataset which are presented in Table 7-5 and Table 7-6.

Table 7-5. Basic model: Regression parameters, overdispersion parameter, AIC, and pseudo-R^2 tests for Poisson and negative binomial GLMs for injuries and fatalities of violent tornadoes

Parameter	Poisson GLM				Negative binomial GLM			
	Injuries		Fatalities		Injuries		Fatalities	
	Estimate	Std. Error	Estimate	Std. Error	Estimate	Std. Error	Estimate	Std. Error
LENGTH	5.335e-03 [a]	1.144e-04	6.416e-03 [a]	4.262e-04	5.773e-03 [b]	2.037e-03	9.005e-03 [a]	2.017e-03
POP	5.005e-05 [a]	3.790e-07	3.783e-05 [a]	2.061e-06	1.317e-04 [a]	1.432e-05	6.806e-05 [a]	1.382e-05
EF5	1.146 [a]	1.492e-02	1.747 [a]	5.216e-02	1.302 [a]	2.987e-01	1.843 [a]	2.890e-01
Intercept	3.520 [a]	1.082e-02	6.369e-01 [a]	4.316e-02	3.134 [a]	1.299e-01	3.503e-01 [b]	1.350e-01
α	-	-	-	-	2.444	3.070 e-02	2.212	4.940 e-02
AIC	39744	-	3043	-	3010	-	1449	-
R^2_α	-	-	-	-	0.23	-	0.38	-

The maximum number of injuries and fatalities are 1740 and 64 for EF4 tornadoes, and 1150 and 158 for EF5 tornadoes, respectively. (Significance codes: 0 < 'a' ≤ 0.001 < 'b' ≤ 0.01 < 'c' ≤ 0.05 <'d' ≤ 0.1 < 'e' ≤ 1).

Table 7-6. Basic model: Regression parameters, overdispersion parameter, AIC, and pseudo-R^2 tests for negative binomial GLM for injuries and fatalities of moderate and strong tornadoes

Parameter	Moderate Tornadoes				Strong Tornadoes			
	Injuries		Fatalities		Injuries		Fatalities	
	Estimate	Std. Error	Estimate	Std. Error	Estimate	Std. Error	Estimate	Std. Error
LENGTH	4.189e-02 [a]	4.650e-03	3.361e-02 [a]	9.840e-03	1.447e-02 [a]	1.687e-03	1.986e-02 [a]	2.056e-03
POP	1.252e-03 [a]	5.903e-05	4.742e-04 [a]	9.573e-05	3.527e-04 [a]	1.272e-05	1.095e-04 [a]	1.344e-05
EF1/EF3	2.082 [a]	1.088e-01	2.476 [a]	4.782e-01	1.218 [a]	7.814e-02	1.768 [a]	1.075e-01
Intercept	-4.009 [a]	9.438e-02	-7.509 [a]	4.590e-01	3.214e-01 [a]	4.939e-02	-2.942 [a]	8.575e-02
α	17.603	2.950 e-03	41.237	6.920 e-03	4.855	6.210 e-03	5.081	1.580 e-02
AIC	8582	-	867.4	-	17344	-	4173.2	-
R^2_α	0.47	-	0.57	-	0.25	-	0.55	-

The maximum number of injuries and fatalities are 238 and 25 for EF3 tornadoes, 119 and 6 for EF2 tornadoes, 50 and 2 for EF1 tornadoes, and 13 and 1 for EF0 tornadoes, respectively. (Significance codes: 0 < 'a' ≤ 0.001 < 'b' ≤ 0.01 < 'c' ≤ 0.05 <'d' ≤ 0.1 < 'e' ≤ 1).

In order to compare the models developed here with a recently developed existing model by Simmons and Sutter (2014), the projected fatalities for the selected violent tornadoes of 2011 were

estimated as shown in Table 7-7. In this regard, the models in Table 7-5 and Table 7-6 were regenerated by using the tornado dataset from 1973 to 2010 to be able to project the fatalities for the 2011's tornadoes.

Table 7-7. Comparison of projected fatalities for selected 2011 tornadoes based on the model in Simmons and Sutter (2014) and the model in this study

State	Date	EF	Fatal.	Simmons and Sutter (2014)			This Study (Model 1)			Additional Information for This Study (Model 1)		
				Est.	AE*	RE**	Est.	AE	RE	Standard Deviation	95%-CI lower bound	95%-CI upper bound
MS	4/27	5	3	13	10	333 %	10	7	233 %	15.8	0	56
AL	4/27	4	6	4	2	33 %	4	2	33 %	5.7	0	20
AL	4/27	5	72	174	102	142 %	185	113	157 %	283.4	0	999
MS	4/27	5	23	13	10	43 %	12	11	48 %	18.8	0	66
AL	4/27	4	13	2	11	85 %	11	2	15 %	17.4	0	61
AL	4/27	4	14	14	0	0 %	4	10	71 %	5.9	0	21
AL	4/27	4	64	10	54	84 %	63	1	2 %	96.8	0	341
AL	4/27	4	1	4	3	300 %	2	1	100 %	3.7	0	13
MS	4/27	4	7	4	3	43 %	8	1	14 %	12.2	0	43
AL	4/27	5	25	28	3	12 %	14	11	44 %	21.7	0	76
AL	4/27	4	22	5	17	77 %	9	13	59 %	13.5	0	47
GA-TN	4/27	4	20	9	11	55 %	5	15	75 %	8.3	0	29
AL	4/27	4	7	5	2	29 %	3	4	57 %	4.4	0	15
TN	4/27	4	4	10	6	150 %	3	1	25 %	4.3	0	15
MO	5/22	5	158	48	110	70 %	12	146	92 %	19.1	0	67
OK	5/24	5	9	36	27	300 %	23	14	156 %	35.5	0	125
OK	5/24	4	1	3	2	200 %	3	2	200 %	4.2	0	15
AR	5/24	4	4	5	1	25 %	3	1	25 %	4.6	0	16
Mean Error:				-	20.8	110 %	-	19.7	78 %	-	-	-

*AE: Absolute Error; **RE: Relative Error

As shown in Table 7-7, although the mean absolute error in estimating fatalities for these tornadoes was approximately the same (i.e., approximately 20 fatalities) for the model in this dissertation and the model by Simmons and Sutter (2014), the mean relative error was 78% and 110%, respectively. Moreover, the models in this dissertation are based on only three explanatory variables while Simmons and Sutter (2014) and most typical models use more than 40 explanatory variables. This is an advantage of the model developed here since methods such as AIC penalizes

models that use larger numbers of explanatory variables when comparing fitted models. All the fatality counts for the tornadoes in Table 7-7 are within the 95% confidence interval (CI), except for the Joplin, Missouri tornado with 158 fatalities. Fatalities were underpredicted for the Joplin tornado, which is no surprise since this tornado was the deadliest tornado in the U.S. since 1950. The probability of 158 fatalities or more for this tornado is less than one percent based on the model developed here and, unfortunately, difficult for any model to predict. If the population within the Joplin tornado path estimated by the angular tornado path (i.e. 14,870 instead of 4,480 that was estimated using the straight tornado path) was used to project the number of fatalities, 25 fatalities were predicted for the Joplin tornado (with the upper bound 95% confidence interval of 137), which has the absolute error of 133 fatalities.

Model 2: Basic Model plus Time and Date

Previous studies have shown that timing affects tornado casualties (Simmons and Sutter, 2008; 2014). During peak tornado months, residents may pay closer attention to high risk tornadoes and particularly the warnings, which in turn results in tornadoes being less likely to result in casualties. Regarding the time of day, residents are less likely to be prepared and shelter for tornadoes after midnight. In addition, during evening and night, residents are more likely to be in wood buildings (since these make up 85% of the housing stock in the U.S.), than in less vulnerable buildings. Therefore, combining these two factors, tornadoes at night are expected to have a greater potential to cause casualties. Based on Simmons and Sutter (2008), a dummy variable SEASON was considered to control for month of the year that tornado occurs and three dummy variables DAY, EVENING, and NIGHT were used to control for time of the day that tornado occur. SEASON was assumed equal to one for tornadoes during March, April, May, or June and equal to zero for tornadoes in any other month. The dummy variable DAY is one if the tornado happens between

0600 and 1759 local time, EVENING is one if the tornado occurs between 1800 and 2359 local time, and NIGHT equals one for tornadoes between 0000 and 0559 local time. The variable NIGHT was excluded from the models, therefore, the regression parameters for DAY and EVENING indicates the relative effects of tornadoes at these times to the NIGHT. Table 7-8 compares the effect of using county-level and block-level data in regression analyses for Model 2 for injuries and fatalities of violent tornadoes.

Table 7-8. Model 2 for injuries and fatalities of violent tornadoes, county-level and block-level estimations

Parameter	Violent Tornadoes (County Level)				Violent Tornadoes (Block Level)			
	Injuries		Fatalities		Injuries		Fatalities	
	Estimate	Std. Error	Estimate	Std. Error	Estimate	Std. Error	Estimate	Std. Error
LENGTH	6.542e-03 [b]	2.099e-03	8.108e-03 [a]	2.075e-03	6.496e-03 [b]	2.043e-03	9.126e-03 [a]	2.041e-03
SEASON	-3.071e-01 [e]	2.208e-01	1.650e-01 [e]	2.284e-01	-4.514e-01 [c]	2.216e-01	5.441e-02 [e]	2.321e-01
DAY	-8.803e-02 [e]	4.646e-01	-6.684e-02 [e]	4.842e-01	-2.979e-01 [e]	4.568e-01	-1.351e-01 [e]	4.809e-01
EVENING	-2.564e-01 [e]	4.773e-01	9.265e-02 [e]	4.963e-01	-3.187e-01 [e]	4.699e-01	-7.295e-02 [e]	4.940e-01
POP	1.057e-04 [a]	1.915e-05	5.387e-05 [b]	1.863e-05	1.316e-04 [a]	1.428e-05	6.828e-05 [a]	1.390e-05
EF5	1.229 [a]	2.913e-01	1.814 [a]	2.822e-01	1.413 [a]	2.995e-01	1.854 [a]	2.927e-01
Intercept	3.758 [a]	4.520e-01	4.230e-01 [e]	4.714e-01	3.719 [a]	4.434e-01	4.088e-01 [e]	4.664e-01
α	2.506	2.830e-02	2.272	4.510e-02	2.403	3.140e-02	2.210	4.950e-02
AIC	3353.1	-	1617.4	-	3009.7	-	1455	-
R^2_α	0.16	-	0.32	-	0.24	-	0.38	-

The maximum number of injuries and fatalities are 1740 and 64 for EF4 tornadoes, and 1150 and 158 for EF5 tornadoes, respectively. (Significance codes: $0 <$ 'a' $\leq 0.001 <$ 'b' $\leq 0.01 <$ 'c' $\leq 0.05 <$'d' $\leq 0.1 <$ 'e' ≤ 1).

The models developed with block-level data have a lower AIC and a higher goodness of fit. As shown in this table, timing variables (i.e. SEASON, DAY, and EVENING) are not significant predictors for violent tornadoes based on their two-tailed p-value. The injury and fatality models for moderate and strong tornadoes are presented in Table 7-9. Time of the day and month of the year variables have substantial effects in predicting injuries and fatalities for strong tornado. Based on the likelihood ratio test, Model 2 outperforms Model 1 for moderate and strong tornadoes, but not for violent tornadoes. Therefore, one would have the choice of using Model 1 for violent tornadoes and Model 2 for moderate and strong tornadoes.

Table 7-9. Model 2 for injuries and fatalities of moderate and strong tornadoes

Parameter	Moderate Tornadoes				Strong Tornadoes			
	Injuries		Fatalities		Injuries		Fatalities	
	Estimate	Std. Error	Estimate	Std. Error	Estimate	Std. Error	Estimate	Std. Error
LENGTH	4.206e-02 [a]	4.640e-03	3.515e-02 [a]	9.479e-03	1.448e-02 [a]	1.682e-03	2.041e-02 [a]	2.000e-03
SEASON	-2.297e-01 [c]	9.726e-02	-7.228e-01 [b]	2.700e-01	-1.642e-01 [c]	7.219e-02	-3.801e-01 [a]	1.096e-01
DAY	-3.680e-01 [c]	1.660e-01	-4.302e-01 [e]	4.065e-01	-4.107e-01 [a]	1.175e-01	-1.087 [a]	1.631e-01
EVENING	-4.307e-01 [c]	1.750e-01	-7.394e-01 [e]	4.500e-01	-4.278e-01 [a]	1.224e-01	-6.839e-01 [a]	1.676e-01
POP	1.243e-03 [a]	5.880e-05	4.100e-04 [a]	8.910e-05	3.527e-04 [a]	1.267e-05	1.097e-04 [a]	1.277e-05
EF1/EF3	2.075 [a]	1.093e-01	2.438 [a]	4.768e-01	1.235 [a]	7.812e-02	1.823 [a]	1.078e-01
Intercept	-3.512 [a]	1.845e-01	-6.629 [a]	5.888e-01	7.891e-01 [a]	1.182e-01	-1.966 [a]	1.596e-01
α	17.458	2.970e-03	34.614	8.320e-03	4.811	6.280e-03	4.552	1.810e-02
AIC	8576.3	-	862.9	-	17328	-	4114.8	-
R^2_α	0.48	-	0.64	-	0.26	-	0.59	-

The maximum number of injuries and fatalities are 238 and 25 for EF3 tornadoes, 119 and 6 for EF2 tornadoes, 50 and 2 for EF1 tornadoes, and 13 and 1 for EF0 tornadoes, respectively. (Significance codes: $0 < \text{'a'} \leq 0.001 < \text{'b'} \leq 0.01 < \text{'c'} \leq 0.05 < \text{'d'} \leq 0.1 < \text{'e'} \leq 1$).

Model 3: Basic Model plus Property Damage

Having a model that links a life safety metric (e.g., tornado-induced casualties) to the number of damaged housing units and their level of damage is significantly useful in community resilience studies. The number of damaged housing units and their level of damage are two imperative factors which might critically affect the number of casualties. However, the tornado database does not provide any information about these factors. Moreover, finding an approximation for the number of damaged housing units and their level of damage for each tornado is challenging and cannot be done for a reasonable number of tornadoes to be used for a regression model. However, these parameters can be inferred and replaced by the estimated property damage reported in the tornado database. Therefore, Model 3 was developed here for applications in community resilience studies. In this regard, only the tornadoes after 1996 in the dataset were used in the regression analyses since estimates of property damage are available only for post-1996 SPC entries. The explanatory variable DAMAGE was considered in Model 3 as the tornado property damage in millions of dollars. Table 7-10 presents Model 3 for injuries and fatalities of moderate, strong, and violent

tornadoes, while Table 7-11 presents an alternative model that also considers the timing effects in predicting tornado casualties. Based on the likelihood ratio test, Model 3 with timing effects outperforms the corresponding model without timing effects only for strong tornadoes. Therefore, simpler models presented in Table 7-10 can be used for moderate and violent tornadoes when property damage has to be considered as a predictor (e.g., in community resilience studies).

Table 7-10. Model 3 without timing effects for injuries and fatalities of moderate, strong, and violent tornadoes

Parameter	Moderate Tornadoes		Strong Tornadoes		Violent Tornadoes	
	Injuries	Fatalities	Injuries	Fatalities	Injuries	Fatalities
LENGTH	3.204e-02 [a]	4.936e-02 [a]	1.790e-02 [a]	2.310e-02 [a]	6.543e-03 [c]	1.211e-02 [a]
DAMAGE	1.615e-01 [a]	1.198e-03 [e]	3.043e-02 [a]	1.715e-02 [a]	7.326e-04 [e]	7.375e-04 [d]
POP	1.228e-03 [a]	4.043e-04 [a]	1.104e-04 [a]	-4.050e-05 [e]	1.315e-04 [a]	2.664e-05 [e]
EF1/EF3/EF5	1.920 [a]	2.385 [a]	9.756e-01 [a]	1.633 [a]	5.060e-01 [e]	1.602 [a]
Intercept	-4.100 [a]	-7.710 [a]	1.265e-01 [d]	-2.822 [a]	2.828 [a]	2.900e-01 [e]
α	22.356	16.835	4.526	5.118	2.334	1.572
AIC	5447.6	591.88	8341.1	2211.2	1215.7	638.99
R^2_α	0.49	0.72	0.33	0.60	0.32	0.55

The maximum number of injuries are 13, 50, 119, 238, 1740, and 1150 for EF0-EF5 tornadoes, respectively. The maximum number of fatalities are 1, 2, 6, 25, 64, and 158 for EF0-EF5 tornadoes, respectively. (Significance codes: 0 < 'a' ≤ 0.001 < 'b' ≤ 0.01 < 'c' ≤ 0.05 <'d' ≤ 0.1 < 'e' ≤ 1).

Table 7-11. Model 3 with timing effects for injuries and fatalities of moderate, strong, and violent tornadoes

Parameter	Moderate Tornadoes		Strong Tornadoes		Violent Tornadoes	
	Injuries	Fatalities	Injuries	Fatalities	Injuries	Fatalities
LENGTH	3.228e-02 [a]	4.982e-02 [a]	1.857e-02 [a]	2.451e-02 [a]	8.003e-03 [c]	1.312e-02 [a]
DAMAGE	1.545e-01 [a]	1.063e-03 [e]	3.008e-02 [a]	1.467e-02 [a]	7.728e-04 [d]	7.627e-04 [c]
SEASON	-1.552e-01 [e]	-2.274e-01 [e]	-2.187e-01 [c]	-4.276e-01 [b]	-3.369e-01 [e]	2.440e-01 [e]
DAY	-2.287e-01 [e]	-2.660e-01 [e]	-4.926e-01 [b]	-9.019e-01 [a]	-5.398e-01 [e]	-7.653e-01 [e]
EVENING	-3.994e-01 [d]	-3.466e-01 [e]	-4.325e-01 [b]	-5.100e-01 [c]	-3.654e-01 [e]	-3.859e-01 [e]
POP	1.222e-03 [a]	3.826e-04 [a]	1.050e-04 [a]	-2.241e-05 [e]	1.325e-04 [a]	2.403e-05 [e]
EF1/EF3/EF5	1.922 [a]	2.371 [a]	9.822e-01 [a]	1.659 [a]	6.183e-01 [e]	1.673 [a]
Intercept	-3.742 [a]	-7.299 [a]	6.474e-01 [a]	-2.004 [a]	3.425 [a]	6.409e-01 [e]
α	22.202	16.129	4.455	4.651	2.286	1.506
AIC	5447.9	596.87	8329.7	2189.4	1218.8	641.43
R^2_α	0.49	0.73	0.34	0.64	0.33	0.57

The maximum number of injuries are 13, 50, 119, 238, 1740, and 1150 for EF0-EF5 tornadoes, respectively. The maximum number of fatalities are 1, 2, 6, 25, 64, and 158 for EF0-EF5 tornadoes, respectively. (Significance codes: 0 < 'a' ≤ 0.001 < 'b' ≤ 0.01 < 'c' ≤ 0.05 <'d' ≤ 0.1 < 'e' ≤ 1).

APPLICATION IN PSEUDO-NORMAN

Model 1 (i.e., the Basic Model) was applied to pseudo-Norman to estimate casualties for a simulated tornado in pseudo-Norman. The mean, 5th-, 25th-, 50th-, 75th-, and 95th-percentile of the expected number of casualties are shown in Figure 7-7 for tornadoes with different intensities in pseudo-Norman. As shown in Figure 7-7, the mean values for the expected number of injuries are 0.08, 0.16, 2.03, 11.41, 35.49, and 150.89, respectively, after an EF0 to EF5 tornado in pseudo-Norman and the corresponding mean values for fatalities are 0, 0, 0, 0.56, 2.48, and 18.52, respectively. This information will be utilized later in the community-resilience-based design (CRBD) methodology outlined in Chapter 8.

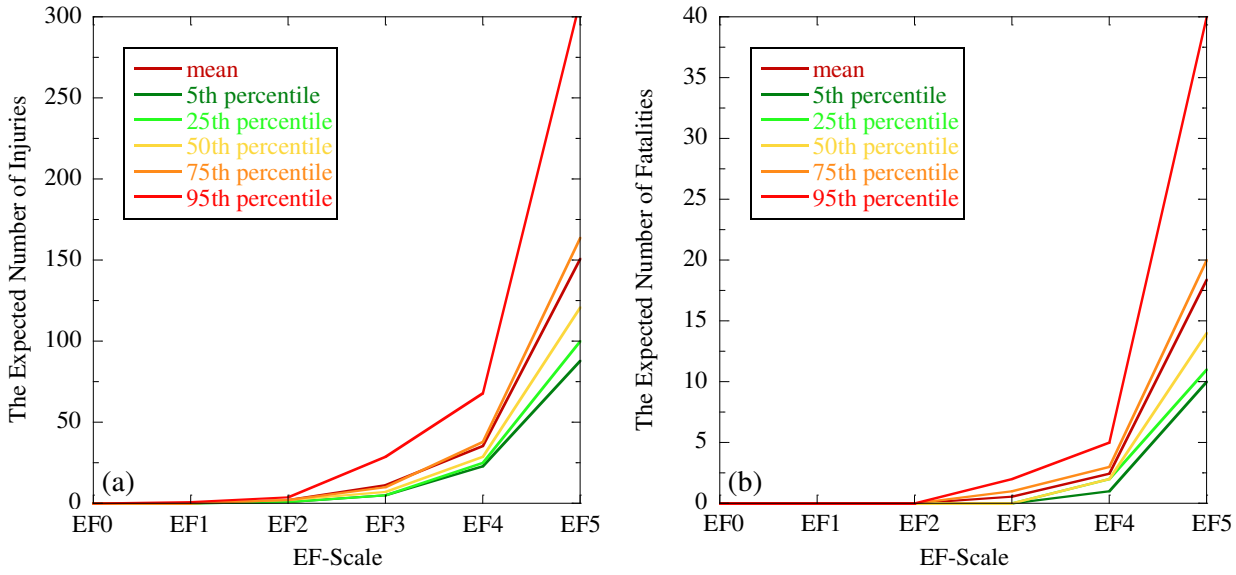

Figure 7-7. The expected number of (a) injuries and (b) fatalities in pseudo-Norman after each EF-scale tornado

CHAPTER 8: COMMUNITY-RESILIENCE-BASED DESIGN (CRBD)

INTRODUCTION

The concept of resilient communities grows progressively and has gained the attention of policymakers, community leaders, and stakeholders. This concept sheds light on the fact that some level of failure is inevitable but can be mitigated and planned for to enable the community to resist, absorb, and adjust to changing conditions as well as to return to a level of normalcy within a reasonable time following a disaster in order to minimize socioeconomic consequences. In this regard, a resilience assessment methodology needs a model that is expanded from component level (i.e., considering an isolated component in the built environment) to the network level or effectively to the community level. This model also involves (i) the interactions (i.e., dependencies) across components and networks for considering the cascading failures, (ii) the spatiotemporal properties of components for realizing high risk areas within the community as well as for managing timely actions after disruptions, and (iii) policies such as prioritization rules of restoration and resource (e.g., material, labor, and budget) allocation for realizing the constraints or for optimizing the policies. In fact, using such a model enables considering all four properties of resilience (i.e., robustness, redundancy, resourcefulness, and rapidity) in a proposed resilience assessment methodology.

Lin et al. (2016) and Wang et al. (2018) presented a disaggregation framework through an optimization problem, which seeks performance objectives (or the best alternative construction or retrofit type) for individual buildings that satisfy a predefined community-level goal based on the percentage of the buildings within a community that become unsafe to occupy after a particular hazard. They considered the physical performance of buildings in a block of residential buildings

in their analysis. The damage to buildings served as a proxy for continued occupancy of the building, which was the community metric that was used as a proxy for community resilience. Their approach focuses on robustness (as one of the resilience properties highlighted in this dissertation), but does not address the other three properties of resilience, i.e., rapidity, resourcefulness, and redundancy.

Reinhorn and Cimellaro (2014) and Cimellaro et al. (2015) proposed the concepts and a general formulation for resilience-based design (RBD). The functionality of an individual structure is not governed only by its own physical performance, but also by the performance/functionality of other entities within the community. For example, a hospital in a community is non-functional without electric power and/or water even if the structure itself is physically intact. Therefore, RBD considers the interaction of all structures (i.e., components) and networks within a community to model the functionality restoration for individual components and assess the desired community-level resilience metrics. Moreover, RBD provides decision makers with a wealth of information beyond those offered by current practices, which is critically beneficial to the selection of a cost-effective design or risk-mitigation strategy that, simultaneously, satisfies the desired community-level resilience objectives.

Mieler et al. (2015) introduced a conceptual framework that disaggregates community-level resilience goals to specific performance targets for the networks and components within the community. They illustrated the methodology by disaggregating the community-level resilience goal of less than 1% probability of significant outmigration after an earthquake with a 500-year return period to a performance target for new residential building construction. The results required new residential buildings have less than a 5% probability of being unsafe to occupy following the event in order to satisfy the specified community-resilience objective. As was noted in their paper,

the example was only a simplified and generalized illustration of the concepts of the framework without any detail.

Salem et al. (2017) proposed a simplified framework for resilience-based design at the building level under blast loads and illustrated their proposed methodology with an application to an 11-story administrative building. They introduced a functionality loss index and a resilience indicator to quantify their resilience-based design framework. Although their framework considers direct functionality losses to the building as a result of physical damage as well as the building's downtime following the event, it neglects the interactions of the building with the community (e.g., the effects of disruption of the transportation system on the restoration of the building) and, therefore, the socioeconomic consequences of the event. Therefore, although their framework satisfies the building-level resilience objectives of stakeholders, it is not necessarily sufficient to meet community-level resilience objectives.

Zhang et al. (2018) presented a methodology for resilience-based design of networks under disruptive events. Their proposed design process is an optimization problem with the objective of minimizing the cost while meeting system resilience constraints. The capability of system restoration in a timely manner after the occurrence of a disruptive event is a fundamental characteristic of resilience-based design, which was effectively addressed in their methodology.

COMMUNITY-RESILIENCE-BASED DESIGN (CRBD)

In this dissertation, a methodology is presented for community-resilience-based design (CRBD) of the components of the built environment within a community. The methodology disaggregates several prescribed community-level objectives (including resilience objectives) into a set of required performance targets for the components of the built environment (either the entire

community, a network, or part of a network). Moreover, the methodology can be implemented to design an optimized recovery policy or to design the architecture of a network within a community (e.g., adding redundancies to enhance the community resilience).

The methodology for the community-level analyses, presented thus far in this dissertation, are summarized in Figure 8-1. As shown in this figure, a community-level resilience metric, i.e., population outmigration, as well as a community-level life-safety metric, i.e., tornado-induced casualties, were formulated and quantified in this dissertation. These two metrics are linked together based on the number of damaged housing units and their level of damage. The number of damaged housing units and their level of damage are two imperative factors which can critically affect the number of casualties. Therefore, improving the performance of residential buildings decreases the level of damage and/or the number of damaged housing units, which, in turn, decreases population outmigration and number of tornado-induced casualties. In fact, improving the performance of residential buildings improves robustness and rapidity, two of the four resilience properties, and decreases property damage, one of the parameters used in Model 3 in Chapter 7 to predict the tornado-induced casualties.

Based on the community-level analyses methodology and the two community-level metrics presented in Figure 8-1, a community-resilience-based design (CRBD) methodology was proposed in this dissertation which is shown in Figure 8-2. This CRBD methodology can be performed by using a multi-objective optimization algorithm, which disaggregates community-level objectives into a required performance targets for the specified components of the built environment. In order to perform the optimization approach, one or more competing community-level objectives such as community-level sustainability metrics and repair/retrofit cost (the red boxes in Figure 8-2) need to be employed along with the proposed metrics in this dissertation (the green boxes in Figure 8-2).

The decision variable(s) in the optimization approach can be selected based on the resilience actions shown in Figure 8-2 with the blue boxes. These blue boxes are connected with the blue parts in Figure 8-1. For example, in order to improve robustness the fragility curves can be enhanced, which, in turn, improves rapidity by decreasing the level of damage and, therefore, lowering repair time. Redundancy can be improved by modifying the dependencies and cross-dependencies in the community modeling or by adding back-up components for critical facilities such as hospitals or police stations. Moreover, resourcefulness and rapidity can be enhanced through the restoration process by defining better policies for resource allocation or restoration prioritization rules.

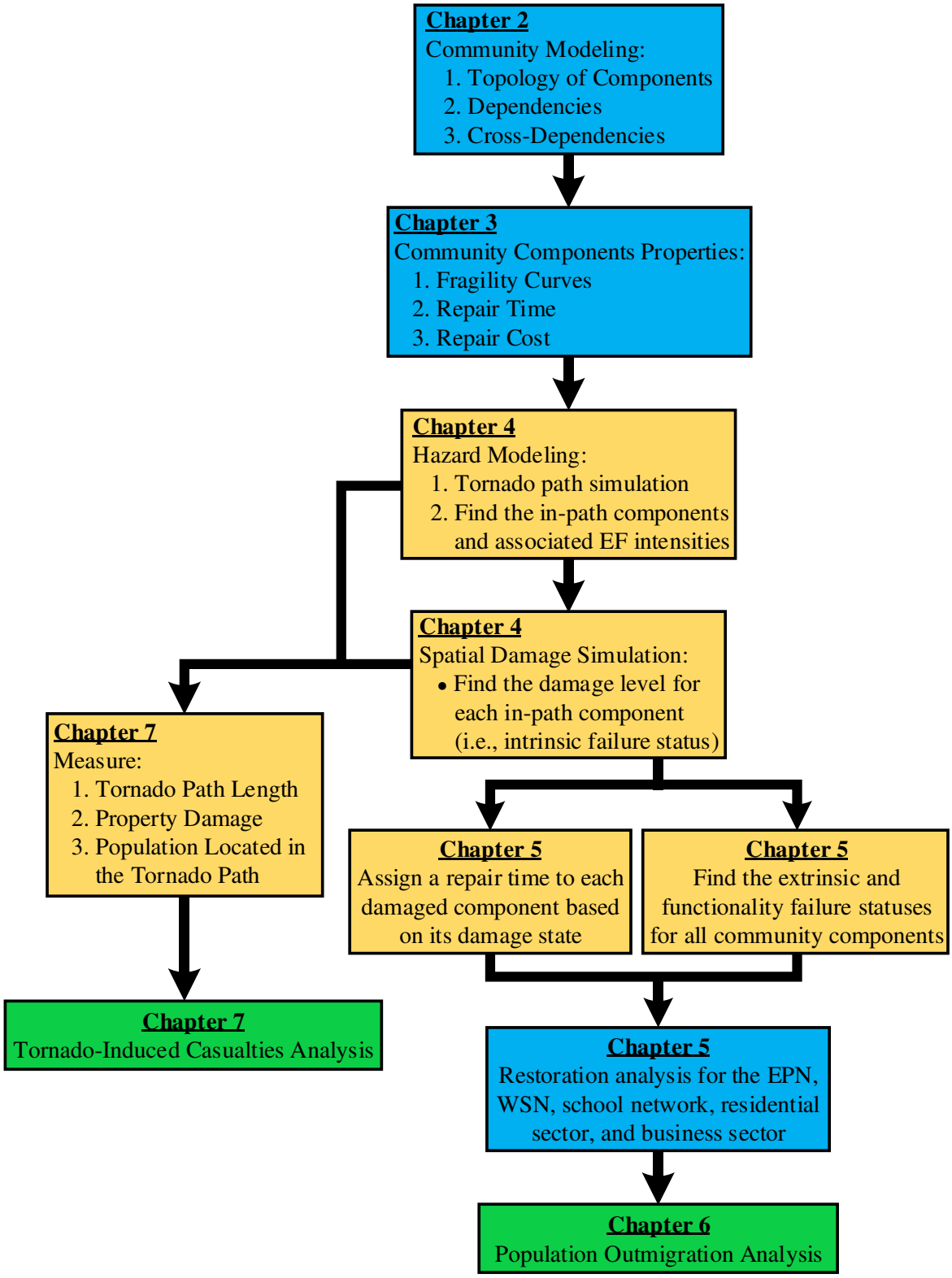

Figure 8-1. Overview of the community-level analyses proposed in this dissertation for the community-resilience-based design methodology

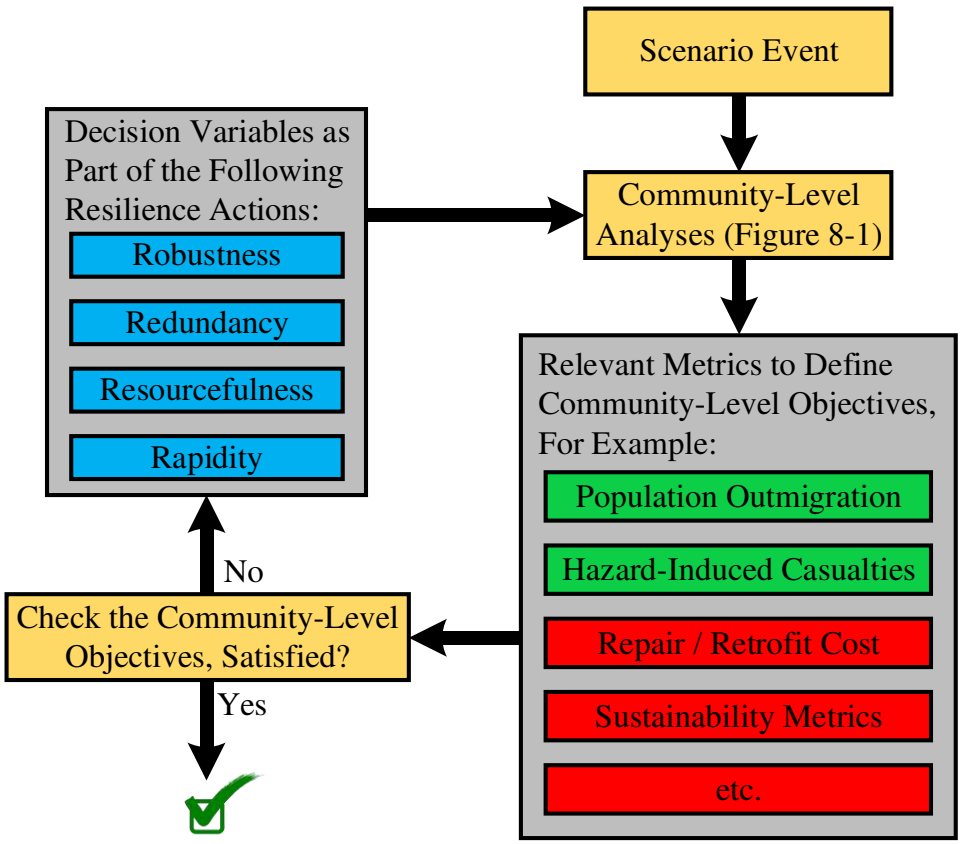

Figure 8-2. Community-resilience-based design (CRBD) methodology

In order to shed light on the proposed CRBD methodology, an extensive full analysis of pseudo-Norman was conducted to seek a predefined goal for each population outmigration and number of tornado-induced injuries and fatalities after an EF3 tornado in pseudo-Norman. In this example, for simplicity, the percent change in the median of the fragility curves that were used for the residential buildings in pseudo-Norman was considered as a decision variable while a myriad combination of decision variables can be assumed (based on the required policies) when an optimization analysis is conducted. As shown in Figure 8-3, after an EF3 tornado in pseudo-Norman, the mean population outmigration, the mean number of injuries, and the mean number of fatalities are equal to 919, 68.3, and 4.6, respectively. The values for these community-level metrics can be decreased to 266, 35.7, and 2.1, respectively, by 25% increase in the decision

variable. They can be further reduced into 167, 12.9, and 0.8, respectively, if 50% increase is chosen for the decision variable. The estimated values of these metrics can be checked with the predefined community-level objectives to find if they are satisfactory. It is worth mentioning that the decision variables can be considered for each grid (or any specific area) separately in order to have a more flexible problem and, subsequently, solutions. Moreover, recall that considering only one sector/network to be upgraded for achieving community-level objectives may not result in a desired solution in that different sectors/networks within a community may have some level of contribution in the selected community-level metrics. For example, as discussed in Chapter 6 and shown in Figure 6-6, all the residential sector, business sector, school network, electric power network, and water supply network contributes in the assessment of population outmigration but with different levels.

For predicting tornado-induced injuries and fatalities using Model 3 in Chapter 7, the property damage that results from the simulated tornado needs to be estimated. In this regard, the median house value for each grid in pseudo-Norman was derived from the U.S. census data and a cost ratio was assumed for each damage level as the ratio of the repair cost to the median house value.

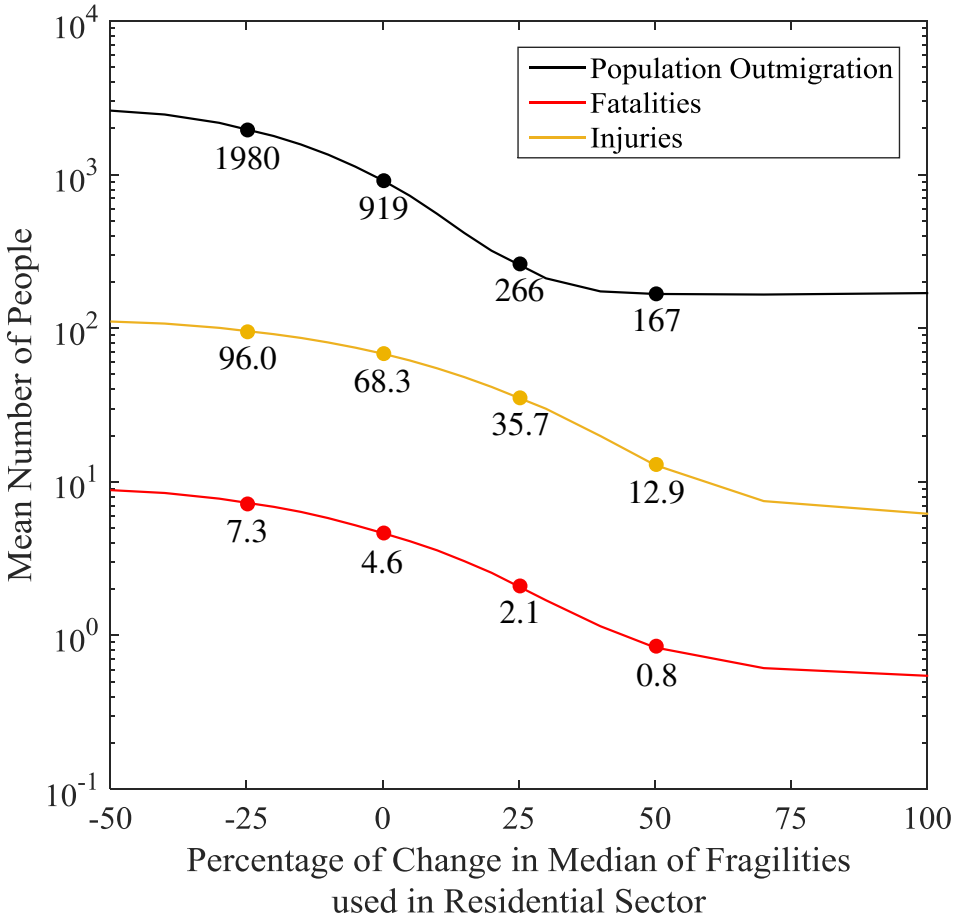

Figure 8-3. Mean population outmigration, mean number of fatalities, and mean number of injuries after an EF3 tornado corresponding to different performance change for the buildings in the residential sector of pseudo-Norman

CHAPTER 9: SUMMARY, CONTRIBUTIONS, AND RECOMMENDATIONS

SUMMARY AND CONCLUSIONS

In this dissertation, a methodology was proposed and explained in detail for community-resilience-based design (CRBD) of the components of the built environment within a community. The purpose of the CRBD methodology is to disaggregate several prescribed community-level objectives (including resilience objectives such as population outmigration) into a set of required performance targets for specified (or all) components of the built environment. The proposed methodology can be further implemented to find an optimized recovery policy or to master-plan a new community or network.

As a basis for the proposed CRBD methodology, a community-level physical-socioeconomic analysis was discussed in detail in the chapters of this dissertation. The topology of an illustrative community was discussed in Chapter 2 through several layers which are the networks/sectors that make up the community. The dependencies and cross-dependencies across components and networks were also discussed in this chapter. Moreover, tornado hazard was studied here not only to illustrate the proposed methodology (including restoration analysis, i.e., Chapter 5, population outmigration analysis, i.e., Chapter 6, and CRBD analysis, i.e., Chapter 8) but also to introduce a methodology to develop tornadic fragility curves for the individual structures within the community (Chapter 3), an approach to simulate tornado paths for the community-level analysis (Chapter 4), and several models to predict tornado-induced injuries and fatalities (Chapter 7).

After modeling the community in Chapter 2, the properties of community components were discussed and assigned in Chapter 3. In this regard, a tornado fragility methodology was presented and the fragility curves were developed for several building archetypes as representative of the

buildings in pseudo-Norman. Moreover, a repair time and permitting time was selected and assigned to each community components for different damage levels. Furthermore, in Chapter 4, an approach was discussed to simulate a tornado path statistically as well as the resulting spatial damage over the community when the simulated tornado path strikes the community. Once the intrinsic damage of community components were modeled, a restoration analysis was performed for the cross-dependent networks/sectors until full restoration is achieved for the entire community. For this purpose, Chapter 5 presents the details of the restoration methodology including considering priority rules, resource allocation, mutual aid agreements among utility companies, and the importance of considering cross-dependencies in the community-level analyses.

The results of the restoration analysis for all the networks/sectors in pseudo-Norman were integrated into a proposed socioeconomic resilience metric, i.e., population outmigration, in Chapter 6. This chapter discusses the difference between the definition and formulation of the currently existing population dislocation models and the proposed population outmigration model. Moreover, the importance of cross-dependencies and contribution of different networks/sectors in population outmigration were investigated in this chapter. Beside the community-level resilience metric proposed in Chapter 6, a community-level life-safety metric was proposed for tornado hazard in Chapter 7. This chapter introduces three models for predicting the number of injuries and fatalities after tornadoes of prescribed EF intensity. In this regard, a methodology was presented to combine the existing data from the U.S. tornado database and the U.S. census database in order to develop a dataset that includes the number of people and housing units located in the tornado path along with the other properties (i.e., tornado path width and length, tornado intensity,

property damage, date and time when tornado occurred, etc.) for the recorded tornadoes in the SPC database.

Finally, in Chapter 8, all the models and methodologies proposed in Chapters 2 to 7 were implemented and integrated into a methodology for the community-resilience-based design (CRBD) of the components of the built environment within a community. The CRBD methodology was discussed with an example of the proposed metrics in this dissertation and several recommendations were made to improve this methodology.

CONTRIBUTIONS

Tornado fragility methodology: a methodology was developed in this dissertation to generate tornado fragility curves for individual structures. This mechanics-based fragility methodology proposes two approaches to calculate tornadic wind loads based on the ASCE 7 methodology for straight-line wind loads with certain modifications.

Tornado hazard simulation approach: a statistical simulation approach was proposed to model a tornado path for different intensities in order to conduct community-level analyses. Moreover, the approach was extended to simulate the resulting spatial damage over the community.

Restoration analysis methodology: a restoration methodology was presented to recover the networks/sectors of an affected community, which facilitates the spatial and temporal depiction of the restoration process. This methodology allows consideration of the effect of cascading failures by modeling the dependencies and cross-dependencies across components and networks. Another advantage of this methodology is its flexibility to apply different policies such as priority rules, resource allocation rules, budget constraints, and mutual aid agreement among utility companies.

Community-level socioeconomic resilience metric: population outmigration was defined and quantified in this dissertation as a socioeconomic resilience metric at the community-level. This metric is capable of being used as a community-resilience goal in that it represents coupled physical-socioeconomic aspects of a community with the effects of dependencies and cross-dependencies of the networks making up the community included in the analysis.

Community-level life-safety metric: three models were developed in this dissertation to predict the tornado-induced injuries and fatalities following a tornado within a community. One of these models links the metric to the number of damaged housing units and their level of damage, which makes the model valuable for community-resilience studies. In fact, such a model is linked to other metrics (e.g., population outmigration) that are also a function of the number of damaged housing units and their level of damage. This provides additional information for policymakers and community leaders for decision making.

Community-resilience-based design: a framework was developed in this dissertation to find a set of required performance targets for the specified components of the built environment that satisfy community-level goals including resilience goals. Moreover, the framework can be implemented in analyses that supports risk-informed decision making in order to design master-planned resilient communities as well as upgrade a community's buildings and/or infrastructure to make the community more resilient to future disasters. This could, for example, be used to understand how to better isolate or decouple two or more sectors; establish redundancies; or decide whether to focus on retrofitting schools in the public sector, businesses and residences in the private sector, or (more likely) some combination thereof.

RECOMMENDATIONS

Indirect economic losses: the population outmigration metric derived in this dissertation can be further utilized to assess the indirect economic losses and to formulate a business continuity metric for the community. This is because population outmigration and business continuity have an inverse relationship. In fact, the return of households and businesses are mutually dependent such that the return of households in the market area will increase the chances for businesses to return and vice versa.

Community-level sustainability metric: developing a sustainability metric is a complement for the proposed community-resilience-based design methodology in that it performs as a competing objective against the resilience metric.

Community-resilience goal disaggregation: after developing one or more competing metrics, a multi-objective optimization algorithm can be implemented to disaggregate several community-level goals into a set of performance targets for the components of the built environment. These components can be school buildings in the school network, workplace buildings in the business sector, residential buildings in the residential sector, components in the EPN or WSN, or some combination thereof.

REFERENCES

Adger, W. N. (2000). Social and ecological resilience: are they related?. *Progress in human geography*, *24*(3), 347-364.

Akaike, H. (1974). "A new look at the statistical model identification." *IEEE transactions on automatic control*, 19(6), 716-723.

Alexander, D. E. (2013). "Resilience and disaster risk reduction: an etymological journey." *Natural Hazards and Earth System Sciences*, 13(11), 2707-2716.

Alrasheedi, N. H., and Selvam, R. P. (2011). "Tornado forces on different building sizes using computer modeling." *ASME Early Career Technical Conf.*, Univ. of Arkansas, Fayetteville, AR.

American FactFinder, (2017). <https://factfinder.census.gov/> (April, 2017).

American Society of Civil Engineers (ASCE). Minimum design loads for buildings and other structures, Standard ASCE 7-10. Reston, VA; 2010.

American Society of Civil Engineers (ASCE). Minimum design loads for buildings and other structures, Standard ASCE 7-16. Reston, VA; 2016.

Amini, M. and van de Lindt, J. (2013). "Quantitative Insight into Rational Tornado Design Wind Speeds for Residential Wood-Frame Structures Using Fragility Approach." *J. Struct. Eng.,* 10.1061/(ASCE)ST.1943-541X.0000914, 04014033.

Argyroudis, S., Selva, J., Gehl, P., and Pitilakis, K. (2015). "Systemic seismic risk assessment of road networks considering interactions with the built environment." *Computer-Aided Civil and Infrastructure Engineering*, 30(7), 524-540.

Ashley, W. S. (2007). "Spatial and temporal analysis of tornado fatalities in the United States: 1880–2005." *Weather and Forecasting*, 22(6), 1214-1228.

Attoh-Okine, N. O., Cooper, A. T., and Mensah, S. A. (2009). "Formulation of resilience index of urban infrastructure using belief functions." *IEEE Systems Journal*, 3(2), 147-153.

Ayyub, B. M. (2014). "Systems resilience for multihazard environments: Definition, metrics, and valuation for decision making." *Risk Analysis*, 34(2), 340-355.

Ayyub, B. M. (2015). "Practical resilience metrics for planning, design, and decision-making." *ASCE-ASME Journal of Risk and Uncertainty in Engineering Systems, Part A: Civil Engineering*, 1(3), 04015008.

Baker, E. J. (1991). "Hurricane evacuation behavior." *International Journal of Mass Emergencies and Disasters*, 9(2), 287-310.

Belcher, J. C., and Bates, F. L. (1983). "Aftermath of natural disasters: Coping through residential mobility." *Disasters*, 7(2), 118-128.

Bhamra, R., Dani, S., & Burnard, K. (2011). Resilience: the concept, a literature review and future directions. *International Journal of Production Research*, *49*(18), 5375-5393.

Bluestein, H. B. (2006). *Tornado Alley: Monster Storms of the Great Plains.* Oxford University Press, New York.

Bocchini, P., & Frangopol, D. M. (2010). Optimal resilience-and cost-based postdisaster intervention prioritization for bridges along a highway segment. *Journal of Bridge Engineering*, *17*(1), 117-129.

Boruff, B. J., Easoz, J. A., Jones, S. D., Landry, H. R., Mitchem, J. D., and Cutter, S. L. (2003). "Tornado hazards in the United States." *Climate Research*, *24*(2), 103-117.

Bournonville, M., Dahnke, J., and Darwin, D. (2004). "Statistical analysis of the mechanical properties and weight of reinforcing bars." *University of Kansas Report*.

Brooks, H. E. (2004). "On the relationship of tornado path length and width to intensity." *Weather and Forecasting*, 19(2), 310-319.

Brooks, H. E., and Doswell III, C. A. (2001). "Normalized damage from major tornadoes in the United States: 1890-1999." *Weather and Forecasting*, *16*(1), 168-176.

Brooks, H. E., and Doswell III, C. A. (2002). "Deaths in the 3 May 1999 Oklahoma City tornado from a historical perspective." *Weather and Forecasting*, *17*(3), 354-361.

Bruneau, M., Chang, S. E., Eguchi, R. T., Lee, G. C., O'Rourke, T. D., Reinhorn, A. M., Shinozuka, M., Tierney, K., Wallace, W. A., and von Winterfeldt, D. (2003) "A framework to quantitatively assess and enhance the seismic resilience of communities." *Earthquake spectra*, 19(4), 733-752.

Bruneau, M., and Reinhorn, A. (2007). "Exploring the concept of seismic resilience for acute care facilities." *Earthquake Spectra*, 23(1), 41-62.

Çagnan, Z., and Davidson, R. (2004). "Post-earthquake restoration modeling of electric power systems." In *Proceedings of the 13th World Conference on Earthquake Engineering*.

Cagnan, Z., & Davidson, R. A. (2007). Discrete event simulation of the post-earthquake restoration process for electric power systems. *International Journal of Risk Assessment and Management*, *7*(8), 1138-1156.

Çağnan, Z., Davidson, R. A., & Guikema, S. D. (2006). Post-earthquake restoration planning for Los Angeles electric power. *Earthquake Spectra*, *22*(3), 589-608.

Cameron, A. C., and Trivedi, P. K. (1998). *Regression analysis of count data*. Cambridge university press.

Cavalieri, F., Franchin, P., Gehl, P., & Khazai, B. (2012). Quantitative assessment of social losses based on physical damage and interaction with infrastructural systems. *Earthquake Engineering & Structural Dynamics*, *41*(11), 1569-1589.

Centers for Disease Control and Prevention (CDC), (2017). "1990 Census Data by Zip Code, County, Census Tract and Block Group" <https://www2.cdc.gov/nceh/lead/census90/house11/download.htm> (April, 2017).

Chang, S. E., and Shinozuka, M. (2004). "Measuring improvements in the disaster resilience of communities." *Earthquake Spectra*, 20(3), 739-755.

Chang, S. E., Svekla, W. D., & Shinozuka, M. (2002). Linking infrastructure and urban economy: simulation of water-disruption impacts in earthquakes. *Environment and Planning B: Planning and Design*, *29*(2), 281-301.

Cimellaro, G. P., Reinhorn, A. M., and Bruneau, M. (2010). "Framework for analytical quantification of disaster resilience." *Engineering Structures*, 32(11), 3639-3649.

Cimellaro, G. P., Renschler, C., & Bruneau, M. (2015). Introduction to resilience-based design (RBD). In *Computational Methods, Seismic Protection, Hybrid Testing and Resilience in Earthquake Engineering* (pp. 151-183). Springer International Publishing.

City-Data, (2016). < http://www.city-data.com/city/Norman-Oklahoma.html>.

Cui, X. (2007). "Reliability of Masonry Anchorage." PhD Dissertation, *University of Louisville.*

Cutter, S. L., Barnes, L., Berry, M., Burton, C., Evans, E., Tate, E., & Webb, J. (2008). A place-based model for understanding community resilience to natural disasters. *Global environmental change*, *18*(4), 598-606.

Drabek, T. E., and Key, W. H. (1984). *Conquering disasters: Family recovery and long-term consequences.* New York: Irvington Publishers Inc.

Dessens Jr, J. (1972). Influence of ground roughness on tornadoes: A laboratory simulation. *Journal of Applied Meteorology*, 11(1), 72-75.

Dong, Y., and Frangopol, D. M. (2017). "Probabilistic assessment of an interdependent healthcare–bridge network system under seismic hazard." *Structure and Infrastructure Engineering*, 13(1), 160-170.

Dueñas-Osorio, L., Craig, J. I., & Goodno, B. J. (2007). Seismic response of critical interdependent networks. *Earthquake engineering & structural dynamics*, *36*(2), 285-306.

Ellingwood, B., Rosowsky, D., Li, Y., and Kim, J. (2004). "Fragility Assessment of Light-Frame Wood Construction Subjected to Wind and Earthquake Hazards." *J. Struct. Eng.,* 130(12), 1921–1930.

Ellingwood, B. R., and Tekie, P. B. (1999). "Wind load statistics for probability-based structural design." *Journal of Structural Engineering*, 125(4), 453-463.

Eusgeld, I., Henzi, D., & Kröger, W. (2008). Comparative evaluation of modeling and simulation techniques for interdependent critical infrastructures. *Scientific Report, Laboratory for Safety Analysis, ETH Zurich*, 6-8.

Farmer, R. G., & Allen, E. H. (2006). Power system dynamic performance advancement from history of North American blackouts. In *Power Systems Conference and Exposition, 2006. PSCE'06. 2006 IEEE PES* (pp. 293-300). IEEE.

Federal Emergency Management Agency (FEMA) (2003). "Multi-hazard Loss estimation methodology–Earthquake Model. HAZUS-MH-MR4 Technical Manual." Department Of Homeland Security, Washington, DC.

Federal Emergency Management Agency (FEMA) (2009a). "Tornado Protection- Selecting Refuge Areas in Buildings. FEMA P-431." Second Edition, Department Of Homeland Security, Washington, DC.

Federal Emergency Management Agency (FEMA) (2009b). "Multi-hazard Loss estimation methodology – Hurricane Model. HAZUS-MH-MR4 Technical Manual." Department Of Homeland Security, Washington, DC.

Federal Emergency Management Agency (FEMA) (2010). "Risk Management Series- Design Guide for Improving School Safety in Earthquakes, Floods, and High Winds, FEMA P-424." Department Of Homeland Security, Washington, DC.

Federal Emergency Management Agency (FEMA) (2015). "Safe Rooms for Tornadoes and Hurricanes, FEMA P-361." Third Edition, Department Of Homeland Security, Washington, DC.

Fricker, T., Elsner, J. B., Mesev, V., and Jagger, T. H. (2017). "A dasymetric method to spatially apportion tornado casualty counts." *Geomatics, Natural Hazards and Risk*, 1-15.

Fujita, T. T., (1971). "Proposed characterization of tornadoes and hurricanes by area and intensity." SMRP Research Paper 91, University of Chicago, Chicago, IL, 42 pp.

Gladwin, H. and Peacock, W. G. (1997). "Warning and evacuation: a night for hard houses." in: W. G. Peacock, B. H. Morrow and H. Gladwin (Eds.), *Hurricane Andrew: Ethnicity, Gender, and the Sociology of Disasters*, pp. 52–74. New York: Routledge.

González, A. D., Dueñas-Osorio, L., Sánchez-Silva, M., & Medaglia, A. L. (2016). The interdependent network design problem for optimal infrastructure system restoration. *Computer-Aided Civil and Infrastructure Engineering*, *31*(5), 334-350.

Griot, C. (2010). Modelling and simulation for critical infrastructure interdependency assessment: a meta-review for model characterization. *International Journal of Critical Infrastructures*, 6(4), 363-379.

Guidotti, R., Chmielewski, H., Unnikrishnan, V., Gardoni, P., McAllister, T., & van de Lindt, J. (2016). Modeling the resilience of critical infrastructure: the role of network dependencies. *Sustainable and Resilient Infrastructure*, *1*(3-4), 153-168.

Haan, F., Jr., Balaramudu, V., and Sarkar, P. (2010). "Tornado-Induced Wind Loads on a Low-Rise Building." *J. Struct. Eng.*, 136(1), 106–116.

Haas, C. N. (1999). On modeling correlated random variables in risk assessment. *Risk Analysis*, *19*(6), 1205-1214.

Han, S. R., Guikema, S. D., Quiring, S. M., Lee, K. H., Rosowsky, D., and Davidson, R. A. (2009). "Estimating the spatial distribution of power outages during hurricanes in the Gulf coast region." *Reliability Engineering and System Safety*, 94(2), 199-210.

Heidorn, K. C. (2007). "Tornadoes of Europe." < http://www.islandnet.com/~see/weather/storm/tornadoes-europe.htm> (July 29, 2015).

Henry, D., and Ramirez-Marquez, J. E. (2012). "Generic metrics and quantitative approaches for system resilience as a function of time." *Reliability Engineering & System Safety*, 99, 114-122.

Hill, A. T. (2006). "Material Properties of the Grade 300 and Grade 270 Prestressing Strands and their Impact on the Design of Bridges." Master thesis, *Virginia Polytechnic Institute and State University.*

Hollnagel, E., Woods, D. D., & Leveson, N. (2007). *Resilience engineering: Concepts and precepts*. Ashgate Publishing, Ltd..

Hosseini, S., Barker, K., & Ramirez-Marquez, J. E. (2016). A review of definitions and measures of system resilience. *Reliability Engineering & System Safety*, *145*, 47-61.

Javanbakht, P., and Mohagheghi, S. (2014). "A risk-averse security-constrained optimal power flow for a power grid subject to hurricanes." *Electric Power Systems Research*, 116, 408-418.

Kahan, J. H., Allen, A. C., & George, J. K. (2009). An operational framework for resilience. *Journal of Homeland Security and Emergency Management*, *6*(1).

Keck, M., & Sakdapolrak, P. (2013). What is social resilience? Lessons learned and ways forward. *Erdkunde*, 5-19.

Kikitsu, H., Sarkar, P. P., and Haan, F. L. (2011). "Experimental study on tornado-induced loads of low-rise buildings using a large tornado simulator." In *Proceedings of 13th International Conference on Wind Engineering*.

Kim, Y. S., and Bennett, R. M. (2002). "Flexural Tension in Unreinforced Masonry: Evaluation of Current Specifications." *The Masonry Society Journal*, *20*(1), 23-30.

Koliou, M., Masoomi, H., & van de Lindt, J. W. (2017). Performance assessment of tilt-up big-box buildings subjected to extreme hazards: tornadoes and earthquakes. *Journal of Performance of Constructed Facilities*, 31(5), 04017060.

Koliou, M., van de Lindt, J. W., McAllister, T. P., Ellingwood, B. R., Dillard, M., & Cutler, H. (2018). State of the research in community resilience: progress and challenges. *Sustainable and Resilient Infrastructure*, DOI: 10.1080/23789689.2017.1418547

Lee, K. H., and Rosowsky, D. V. (2005). "Fragility assessment for roof sheathing failure in high wind regions." *Engineering Structures*, *27*(6), 857-868.

Leslie, F. W. (1977). Surface roughness effects on suction vortex formation: A laboratory simulation. *Journal of the Atmospheric Sciences*, 34(7), 1022-1027.

Letchford, C., Levitz, B., and James, D. (2015) Internal Pressure Dynamics in Simulated Tornadoes. *Structures Congress* 2015: pp. 2689-2701.

Limbourg, P., Kochs, H., Echtle, K., and Eusgeld, I. (2007). Reliability prediction in systems with correlated component failures - an approach using copulas. In *Architecture of computing systems (ARCS), 2007 20th international conference on* (pp. 1–8). VDE.

Lin, Y. (2009). "Development of algorithms to estimate post-disaster population dislocation: a research-based approach." Ph.D. dissertation, Office of Graduate Studies, Texas A&M Univ., College Station, TX.

Lin, P., Wang, N., & Ellingwood, B. R. (2016). A risk de-aggregation framework that relates community resilience goals to building performance objectives. *Sustainable and Resilient Infrastructure*, *1*(1-2), 1-13.

Lindell, M. K., Perry, R. W., Prater, C., and Nicholson, W. C. (2006). *Fundamentals of emergency management*. Washington, DC: FEMA.

Lindell, M. K., and Prater, C. S. (2003). "Assessing community impacts of natural disasters." *Natural hazards review*, 4(4), 176-185.

Liu, H., Davidson, R. A., Rosowsky, D. V., and Stedinger, J. R. (2005). "Negative binomial regression of electric power outages in hurricanes." *Journal of infrastructure systems*, 11(4), 258-267.

Liu, Z., and Ishihara, T. (2016). Study of the effects of translation and roughness on tornado-like vortices by large-eddy simulations. *Journal of Wind Engineering and Industrial Aerodynamics*, 151, 1-24.

López, A. L., Rocha, L. E. P., Escobedo, D. L., and Sesma, J. S. (2009). "Reliability and vulnerability analysis of electrical substations and transmission towers for definition of

wind and seismic damage maps for Mexico." In *Proceedings of the 11th Americas Conference on Wind Engineering*, San Juan, Puerto Rico.

Mahmoud, H. and Chulahwat, A. (2017), Spatial and Temporal Quantification of Community Resilience: Gotham City under Attack. *Computer-Aided Civil and Infrastructure Engineering*. doi:10.1111/mice.12318

Martin, R. (2011). Regional economic resilience, hysteresis and recessionary shocks. *Journal of economic geography*, *12*(1), 1-32.

Martin-Breen, P., and Anderies, J. M. (2011). *Resilience: a literature review.* Brighton: Institute of Development Studies.

Masonry Standards Joint Committee (MSJC) (2011). *Building Code Requirements And Specification for Masonry Structures Containing Building Code Requirements for Masonry Structures (TMS 402-11/ACI 530-11/ASCE 5-11), Specification for Masonry Structures (TMS 602-11/ACI 530.1-11/ASCE 6-11) and Companion Commentaries.*

Masoomi, H., and van de Lindt, J.W. (2016). "Tornado fragility and risk assessment of an archetype masonry school building." *Engineering Structures*, 128, 26-43.

Masoomi, H., & van de Lindt, J. W. (2017). Tornado community-level spatial damage prediction including pressure deficit modeling. *Sustainable and Resilient Infrastructure*, *2*(4), 179-193.

Masoomi, H., & van de Lindt, J. W. (2018a). Restoration and functionality assessment of a community subjected to tornado hazard. *Structure and Infrastructure Engineering*, 14(3), 275-291.

Masoomi, H., and van de Lindt, J.W. (2018b). "Fatality and Injury Prediction Model for Tornadoes", accepted, *ASCE Natural Hazards Review*, DOI: 10.1061/(ASCE)NH.1527-6996.0000295

Masoomi, H., Ameri, M.R., and van de Lindt, J.W. (2017a). "Wind performance enhancement strategies for wood-frame buildings." accepted, *Journal of Performance of Constructed Facilities*, DOI: 10.1061/(ASCE)CF.1943-5509.0001172

Masoomi, H., van de Lindt, J.W., and Peek, L., (2017b) "Quantifying Socioeconomic Impact of a Tornado by Estimating Population Outmigration as a Resilience Metric at the Community Level", accepted, *Journal of Structural Engineering*, DOI: 10.1061/(ASCE)ST.1943-541X.0002019

McCarthy, D. W., (2003). "NWS tornado surveys and the impact on the national tornado database." Preprints, *First Symp. on F-scale and Severe Weather Damage Assessment*, Long Beach, CA, Amer. Meteor. Soc., CD-ROM, 3.2.

McDonald, J. R., and Mehta, K. C. (2006). *A recommendation for an Enhanced Fujita scale (EF-Scale)*. Wind Science and Engineering Center, Texas Tech University.

Melchers, R. E. (1999). Structural reliability analysis and prediction, 2nd Ed., Wiley, Chichester, England.

Memari, M., Attary, N., Masoomi, H., Mahmoud, H., van de Lindt, J., Pilkington, S., and Ameri, M. (2017). "Minimal Building Fragility Portfolio for Damage Assessment of Communities Subjected to Tornadoes", accepted, *Journal of Structural Engineering*, DOI: 10.1061/(ASCE)ST.1943-541X.0002047.

Mid-America Earthquake Center (MAEC), (2006). "MAEviz software." <http://mae.cee.illinois.edu/software/software_maeviz.html>.

Mieler, M., Stojadinovic, B., Budnitz, R., Comerio, M., & Mahin, S. (2015). A framework for linking community-resilience goals to specific performance targets for the built environment. *Earthquake Spectra*, *31*(3), 1267-1283.

Miles, S. B., and Chang, S. E., (2003). *Urban Disaster Recovery: A Framework and Simulation Model*, MCEER Technical Report 03-0005, Multidisciplinary Center for Earthquake Engineering Research, Buffalo, NY.

Miles, S. B., & Chang, S. E. (2004, August). Foundations for modeling community recovery from earthquake disasters. In *Proceedings of the 13th World Conference on Earthquake Engineering*.

Miles, S. B., & Chang, S. E. (2006). Modeling community recovery from earthquakes. *Earthquake Spectra*, *22*(2), 439-458.

Minnesota Population Center, (2016). National Historical Geographic Information System: Version 11.0 [Database]. Minneapolis: University of Minnesota. <https://www.nhgis.org/> (April, 2017).

Mitchell, C. M., Esnard, A. M., and Sapat, A. (2011). "Hurricane events, population displacement, and sheltering provision in the United States." *Natural Hazards Review*, 13(2), 150-161.

Nan, C., and Sansavini, G. (2017). "A quantitative method for assessing resilience of interdependent infrastructures." *Reliability Engineering & System Safety*, 157, 35-53.

Natarajan, D., and Hangan, H. (2009). Numerical study on the effects of surface roughness on tornado-like flows. In *11th Americas Conference on Wind Engineering (11ACWE)*.

National Institute of Standards and Technology (NIST) (2016), *Critical Assessment of Lifeline System Performance: Understanding Societal Needs in Disaster Recovery*, NIST CGR 16-917-39 Report, National Institute of Standards and Technology, Gaithersburg, Maryland.

National Oceanic and Atmospheric Administration (NOAA) (2017a). "Natural Hazard Statistics." < http://www.nws.noaa.gov/om/hazstats.shtml> (October, 2017).

National Oceanic and Atmospheric Administration (NOAA) (2017b). "The 10 Costliest U.S. Tornadoes since 1950." <http://www.spc.noaa.gov/faq/tornado/damage$.htm> (April, 2017).

National Oceanic and Atmospheric Administration (NOAA) (2017c). "The 25 Deadliest U.S. Tornadoes." <http://www.spc.noaa.gov/faq/tornado/killers.html> (April, 2017).

National Oceanic and Atmospheric Administration (NOAA) (2017d). "Severe Weather Database Files (1950-2015)." < http://www.spc.noaa.gov/wcm/#data> (April, 2017).

Nedler, J. A., and Wedderburn, R. W. M. (1972). Generalized linear models. *Journal of the Royal Statistical Society, Part A, 135*, Part 3, 370–384.

Noda, S. (1993). Optimum post-earthquake restoration of a telephone system using neural networks. *Journal of natural disaster science*, *15*(1), 91-111.

Nozhati, S., Sarkale, Y., Ellingwood, B., Chong, E. K., and Mahmoud, H. (2018a). "Near-optimal planning using approximate dynamic programming to enhance post-hazard community resilience management." *arXiv preprint arXiv:1803.01451*.

Nozhati, S., Ellingwood, B., Mahmoud, H., and van de Lindt, J. (2018b). "Identifying and analyzing interdependent critical infrastructure in post-earthquake urban reconstruction." In *Proc. of the 11th Nat. Conf. in Earthquake Eng*. Los Angeles, CA: Earthquake Eng. Res. Inst., Jun 2018.

Omer, M., Nilchiani, R., and Mostashari, A. (2009). "Measuring the resilience of the trans-oceanic telecommunication cable system." *IEEE Systems Journal*, 3(3), 295-303.

Ouyang, M. (2014). Review on modeling and simulation of interdependent critical infrastructure systems. *Reliability engineering & System safety*, *121*, 43-60.

Ouyang, M., and Dueñas-Osorio, L. (2014). "Multi-dimensional hurricane resilience assessment of electric power systems." *Structural Safety*, 48, 15-24.

Ouyang, M., Dueñas-Osorio, L., & Min, X. (2012). A three-stage resilience analysis framework for urban infrastructure systems. *Structural safety*, *36*, 23-31.

Pant, R., Barker, K., Ramirez-Marquez, J. E., and Rocco, C. M. (2014). "Stochastic measures of resilience and their application to container terminals." *Computers & Industrial Engineering*, 70, 183-194.

Patterson, E. S., Woods, D. D., Cook, R. I., & Render, M. L. (2007). Collaborative cross-checking to enhance resilience. *Cognition, Technology & Work*, *9*(3), 155-162.

Peacock, W. G., and Girard, C. (1997). "Ethnicity and segregation." in: W. G. Peacock, B. H. Morrow & H. Gladwin (Eds.), *Hurricane Andrew: Ethnicity, gender and the sociology of disaster,* pp. 191-205. New York: Routledge.

Pederson, P., Dudenhoeffer, D., Hartley, S., & Permann, M. (2006). Critical infrastructure interdependency modeling: a survey of US and international research. *Idaho National Laboratory*, *25*, 27.

Pfefferbaum, B. J., Reissman, D. B., Pfefferbaum, R. L., Klomp, R. W., & Gurwitch, R. H. (2008). Building resilience to mass trauma events. In *Handbook of injury and violence prevention* (pp. 347-358). Springer, Boston, MA.

Platt, S., Brown, D., and Hughes, M. (2016). "Measuring resilience and recovery." *International Journal of Disaster Risk Reduction*, 19, 447-460.

Precast/Prestressed Concrete Institute (PCI) (1971). *PCI design handbook: Precast and prestressed concrete,* First Edition, Chicago, IL.

Presidential Policy Directive (PPD), (2013). Critical Infrastructure Security and Resilience. PPD-21, Released February 12, 2013. Available at: http://www.whitehouse.gov/the-press-office/2013/02/12/presidential-policy-directive-critical-infrastructure-security-and-resil, Accessed March 07, 2018.

Prevatt, D. O., Coulbourne, W., Graettinger, A. J., Pei, S., Gupta, R., and Grau, D. (2013). "Joplin, Missouri, tornado of May 22, 2011: Structural damage survey and case for tornado-resilient building codes." *American Society of Civil Engineers*, Reston, Virginia.

Ramachandran, V., Long, S. K., Shoberg, T., Corns, S., and Carlo, H. J. (2015). "Framework for Modeling Urban Restoration Resilience Time in the Aftermath of an Extreme Event." *Natural Hazards Review*, 16(4), 04015005.

Ramseyer, C., Holliday, L., and Floyd, R. (2015). "Enhanced Residential Building Code for Tornado Safety." *J. Perform. Constr. Facil.,* 10.1061/(ASCE)CF.1943-5509.0000832, 04015084.

Reed, D. A., Kapur, K. C., & Christie, R. D. (2009). Methodology for assessing the resilience of networked infrastructure. *IEEE Systems Journal*, *3*(2), 174-180.

Refan, M., Hangan, H., and Wurman, J. (2014). "Reproducing tornadoes in laboratory using proper scaling." *Journal of Wind Engineering and Industrial Aerodynamics*, 135, 136-148.

Reinhold, T. A., and Ellingwood, B. (1982). *Tornado damage risk assessment (No. NUREG/CR-2944; BNL-NUREG-51586).* National Bureau of Standards, Washington, DC (USA). Center for Building Technology.

Reinhorn, A. M., & Cimellaro, G. P. (2014). Consideration of Resilience of Communities in Structural Design. In *Performance-Based Seismic Engineering: Vision for an Earthquake Resilient Society* (pp. 401-421). Springer Netherlands.

Rose, A. (2007). Economic resilience to natural and man-made disasters: Multidisciplinary origins and contextual dimensions. *Environmental Hazards*, *7*(4), 383-398.

Rose, A., & Liao, S. Y. (2005). Modeling regional economic resilience to disasters: A computable general equilibrium analysis of water service disruptions. *Journal of Regional Science*, *45*(1), 75-112.

Roueche, D. B., Prevatt, D. O., Haan, F. L., and Datin, P. L. (2015). An estimate of tornado loads on a wood-frame building using database-assisted design methodology. *Journal of Wind Engineering and Industrial Aerodynamics*, 138, 27-35.

Sabareesh, G. R., Matsui, M., and Tamura, Y. (2012). "Dependence of surface pressures on a cubic building in tornado like flow on building location and ground roughness." *Journal of Wind Engineering and Industrial Aerodynamics*, *103*, 50-59.

Sabareesh, G. R., Matsui, M., and Tamura, Y. (2013). Ground roughness effects on internal pressure characteristics for buildings exposed to tornado-like flow. *Journal of Wind Engineering and Industrial Aerodynamics*, 122, 113-117.

Salem, S., Campidelli, M., El-Dakhakhni, W. W., & Tait, M. J. (2017). Resilience-based design of urban centres: application to blast risk assessment. *Sustainable and Resilient Infrastructure*, 1-18.

Sarkale, Y., Nozhati, S., Chong, E. K., Ellingwood, B., and Mahmoud, H. (2018). "Solving Markov decision processes for network-level post-hazard recovery via simulation optimization and rollout." *arXiv preprint arXiv:1803.04144*.

Satumtira, G., & Dueñas-Osorio, L. (2010). Synthesis of modeling and simulation methods on critical infrastructure interdependencies research. In *Sustainable and resilient critical infrastructure systems* (pp. 1-51). Springer Berlin Heidelberg.

Schaefer, J. T., and Edwards, R. (1999). "The SPC tornado/severe thunderstorm database." In Preprints, *11th Conference on Applied Climatology*, Dallas, TX, Amer. Meteor. Soc., 215-220.

Schaefer, J. T., Kelly, D. L., and Abbey, R. F. (1986). "A minimum assumption tornado-hazard probability model." *Journal of Climate and Applied Meteorology*, 25(12), 1934-1945.

Scherb, A., Garrè, L., and Straub, D. (2015). "Probabilistic risk assessment of infrastructure networks subjected to hurricanes." Paper presented at the *12th International Conference on Applications of Statistics and Probability in Civil Engineering (ICASP12)*, Vancouver, Canada.

Selvam, R. P., and Millett, P. C. (2003). "Computer modeling of tornado forces on a cubic building using large eddy simulation." *J. Arkansas Acad. Sci.,* 57, 140–146.

Sengupta, A., Haan, F. L., Sarkar, P. P., and Balaramudu, V. (2008). "Transient loads on buildings in microburst and tornado winds." *J. Wind Eng. Ind. Aerodynamics,* 96(10–11), 2173–2187.

Shen, G., and Hwang, S. N. (2015). "A spatial risk analysis of tornado-induced human injuries and fatalities in the USA." *Natural Hazards*, 77(2), 1223-1242.

Simiu, E. and Scanlan, R.E. (1996). Wind Effects on Structures, Third edition, John Wiley & Sons, Inc., pp.551- 575.

Simmons, K. M., and Sutter, D. (2008). "Tornado warnings, lead times, and tornado casualties: An empirical investigation." *Weather and Forecasting*, 23(2), 246-258.

Simmons, K. M., and Sutter, D. (2014). "Fatality prediction for the 2011 tornado season based on historical extreme weather data." *Natural Hazards Review*, 15(3), 04014005.

Standohar-Alfano, C. D., and van de Lindt, J. W. (2014). "Empirically based probabilistic tornado hazard analysis of the United States using 1973–2011 data." *Natural Hazards Review*, 16(1), 04014013.

Tabucchi, T., Davidson, R., & Brink, S. (2010). Simulation of post-earthquake water supply system restoration. *Civil Engineering and Environmental Systems*, *27*(4), 263-279.

Topologically Integrated Geographic Encoding and Referencing (TIGER), (2017). "TIGER/Line® with Selected Demographic and Economic Data" <https://www.census.gov/geo/maps-data/data/tiger-data.html> (April, 2017).

Unanwa, C. and Mahan, M. (2014). "Statistical Analysis of Concrete Compressive Strengths for California Highway Bridges." *J. Perform. Constr. Facil.* 28, SPECIAL SECTION: Performance of Bridges under Critical Natural Hazards, 157–167.

United States Census Bureau, (2017). <https://www.census.gov/> (April, 2017).

Unnikrishnan, V. U., & van de Lindt, J. W. (2016). Probabilistic framework for performance assessment of electrical power networks to tornadoes. *Sustainable and Resilient Infrastructure*, *1*(3-4), 137-152.

van de Lindt, J., Amini, M. O., Standohar-Alfano, C., and Dao, T. (2012). "Systematic study of the failure of a light-frame wood roof in a tornado." *Buildings*, *2*(4), 519-533.

van de Lindt, J., Graettinger, A., Gupta, R., Skaggs, T., Pryor, S., and Fridley, K. (2007). "Performance of Wood-Frame Structures during Hurricane Katrina." *J. Perform. Constr. Facil.,* 10.1061/(ASCE)0887-3828(2007)21:2(108), 108-116.

van de Lindt, J., Pei, S., Dao, T., Graettinger, A., Prevatt, D., Gupta, R., and Coulbourne, W. (2013). "Dual-Objective-Based Tornado Design Philosophy." *J. Struct. Eng*., 139(2), 251–263.

Vann, W. P., and McDonald, J. R. (1978). *An Engineering Analysis: Mobile Homes in a Windstorm*. Institute for Disaster Research, College of Engineering, Texas Tech University.

Vlacheas, P., Stavroulaki, V., Demestichas, P., Cadzow, S., Ikonomou, D., & Gorniak, S. (2013). Towards end-to-end network resilience. *International Journal of Critical Infrastructure Protection*, *6*(3), 159-178.

Vogus, T. J., & Sutcliffe, K. M. (2007, October). Organizational resilience: towards a theory and research agenda. In *Systems, Man and Cybernetics, 2007. ISIC. IEEE International Conference on* (pp. 3418-3422). IEEE.

Wang, S., Sarker, B. R., Mann, L., & Triantaphyllou, E. (2004). Resource planning and a depot location model for electric power restoration. *European Journal of Operational Research*, *155*(1), 22-43.

Wang, Y., Wang, N., Lin, P., Ellingwood, B., Mahmoud, H., & Maloney, T. (2018). De-aggregation of community resilience goals to obtain minimum performance objectives for buildings under tornado hazards. *Structural Safety*, 70, 82-92.

Weber, L. and Peek, L. (2012). *Displaced: Life in the Katrina Diaspora.* Austin: University of Texas Press.

Whitehead, J. C. (2005). "Environmental risk and averting behavior: Predictive validity of jointly estimated revealed and stated behavior data." *Environmental and Resource Economics*, 32(3), 301-316.

Whitehead, J. C., Edwards, B., Van Willigen, M., Maiolo, J. R., Wilson, K., and Smith, K. T. (2000). "Heading for higher ground: factors affecting real and hypothetical hurricane evacuation behavior." *Global Environmental Change Part B: Environmental Hazards*, 2(4), 133-142.

Xiao, Y., and Van Zandt, S. (2012). "Building community resiliency: Spatial links between household and business post-disaster return." *Urban Studies*, 49(11), 2523-2542.

Xu, N., Guikema, S. D., Davidson, R. A., Nozick, L. K., Çağnan, Z., & Vaziri, K. (2007). Optimizing scheduling of post-earthquake electric power restoration tasks. *Earthquake engineering & structural dynamics*, *36*(2), 265-284.

Youn, B. D., Hu, C., & Wang, P. (2011). Resilience-driven system design of complex engineered systems. *Journal of Mechanical Design*, *133*(10), 101011.

Zhang, X., Mahadevan, S., Sankararaman, S., & Goebel, K. (2018). Resilience-based network design under uncertainty. *Reliability Engineering & System Safety*, *169*, 364-379.

Zhang, Y., Yang, N., and Lall, U. (2016). "Modeling and simulation of the vulnerability of interdependent power-water infrastructure networks to cascading failures." *Journal of Systems Science and Systems Engineering*, 25(1), 102-118.